INFORMATION TO USERS

This manuscript has been reproduced from the microfilm master. UMI films the text directly from the original or copy submitted. Thus, some thesis and dissertation copies are in typewriter face, while others may be from any type of computer printer.

The quality of this reproduction is dependent upon the quality of the copy submitted. Broken or indistinct print, colored or poor quality illustrations and photographs, print bleedthrough, substandard margins, and improper alignment can adversely affect reproduction.

In the unlikely event that the author did not send UMI a complete manuscript and there are missing pages, these will be noted. Also, if unauthorized copyright material had to be removed, a note will indicate the deletion.

Oversize materials (e.g., maps, drawings, charts) are reproduced by sectioning the original, beginning at the upper left-hand corner and continuing from left to right in equal sections with small overlaps.

Photographs included in the original manuscript have been reproduced xerographically in this copy. Higher quality 6" x 9" black and white photographic prints are available for any photographs or illustrations appearing in this copy for an additional charge. Contact UMI directly to order.

Bell & Howell Information and Learning
300 North Zeeb Road, Ann Arbor, MI 48106-1346 USA
800-521-0600

UMI®

ARTIFICIAL INTELLIGENCE TECHNIQUES FOR RELIABILITY ASSESSMENT OF NONLINEAR BRIDGE SYSTEMS

By

Linzhong Deng

A dissertation submitted to the Graduate Faculty in Engineering in partial fulfillment of the requirements for the degree of Doctor of Philosophy, The City University of New York

2000

This manuscript has been read and accepted for the Graduate Faculty in Engineering in satisfaction of the dissertation requirement for the degree of Doctor of Philosophy.

September 6, 2000
Date

Professor Michel Ghosn
Chair of Examining Committee

September 6, 2000
Date

Professor Mumtaz K. kassir
Executive Officer

Professor John Fillos, Department Chairman

Professor George Mylonakis

Professor Anil Agrawal

Dr. Shaowen Shao, Risk Analyst

The City University of New York

ABSTRACT

ARTIFICIAL INTELLIGENCE TECHNIQUES FOR RELIABILITY ASSESSMENT OF NONLINEAR BRIDGE SYSTEMS

By

Linzhong Deng

Advisor: Professor Michel Ghosn

Artificial Intelligence techniques are used to develop simulation-based methods for the reliability evaluation of complex and large structural systems with application to highway bridge structures.

Load intensity, bridge response, and structural capacity are uncertain in nature. The object of structural reliability theory is to account for the uncertainties encountered during the load capacity evaluation of structural components and systems, and to account for these uncertainties during the calibration of safety factors for design codes. In order to perform a reliability analysis, two tools are required: the first tool is an accurate nonlinear analysis program capable of analyzing the behavior of structural systems for a specific (deterministic) set of loading conditions and material properties. The second tool is a systematic search algorithm that will identify the probabilistically dominant failure modes accounting for the randomness in applied loading and material properties.

The purpose of this study is to develop the two tools necessary to evaluate the safety of bridge structural systems. The first tool consists of new analysis models for steel and prestressed concrete highway bridges that are implemented in a modified version of the program NONBAN. The new models accurately represent the nonlinear behavior of bridge members using empirically derived information from moment-rotation curves and plastic hinge length equations. The second tool consists of a new Shredding Genetic Algorithm (SGA) that is designed to efficiently identify dominant failure modes of bridge structural systems. SGA improves the traditional genetic algorithm by interfering with the natural selection process and filtering out the weakest and unhealthy offsprings using the principle of elitism.

To improve the efficiency of the analysis process, a new solver, referred to as the pseudoforce method, is derived based on the Sherman-Morrison-Woodburg formula. By combining SGA with the pseudoforce solver, the reliability analysis of bridge systems is reduced by a factor of 4 compared to classical search methods in combination with traditional analysis techniques. The proposed techniques will eventually lead to better control of the safety of bridge structural systems and improve the reliability of structural designs. Examples are provided to demonstrate the efficiency and applicability of the proposed models.

In memory of my mother:

CHUNHUA ZHANG

怀念亲爱的妈妈
张春花 女士

ACKNOWLEDGEMENTS

My heart felt deepest gratitude goes to Prof. Michel Ghosn, my mentor, for all the guidance and help he has extended to me. In the past five years, he guided me academically and showed me the truths of life and the world, which, I believe, are the best possible things that a student can learn from his advisor. Without his help, my task would have been insurmountable. I also want to thank and acknowledge Dr. Shaowen Shao for her time, advice and support during the course of my work on this dissertation. Thanks also go to Prof. George Mylonakis for his suggestions and advise on this work. Thanks also go to Mr. Ales Znidaric at ZAG in Slovenia for providing the experimental results of the Slovenia girders and bridge.

I am also unconditionally grateful to my wife, Haiying Ma, and my parents for their support and encouragement during my study period in the USA.

CONTENTS

LIST OF TABLES

LIST OF FIGURES

CHAPTER 1

INTRODUCTION

1.1 GENERAL BACKGROUND

In the most general sense, the reliability of a structure defines its ability to fulfill its design purpose for a specified period of time. For example, will a bridge built today be able to safely carry traffic loads for its intended 75-year service life? In a narrow sense, structural reliability is the probability that a structure does not attain a given limit state (ultimate capacity or serviceability) during a specified reference period. In this sense, one could say that the probability that a bridge built today will collapse before the end of its 75-year design life is around 0.28×10^{-6} (Nowak, A., 1993). The bridge reliability is then 99.999972% ($1.00-0.28 \times 10^{-6}$). The mathematical definition of reliability reflects the fact that structural safety is not absolute i.e. no matter how careful a structural designer is, there is always some chance that the structure will not adequately serve its intended purpose. This is because all the quantities (except physical and mathematical constants) that enter into the structural analysis and safety evaluation process are random variables associated with varying degrees of uncertainty. Such quantities include the capacity of each of the system's structural members and components (e.g. beams, struts, connections), geometric dimensions and properties (e.g. plate thickness, moment of inertia), dead loads, live loads, material deterioration, etc. (Heller and Thangjutham, 1993). For example, there is always a possibility that the bridge will be subjected to a

previously unforeseen load that will cause it to fail. The purpose of the structural design process is then to ensure the safety of the bridge under certain reasonable loading conditions while realizing that our ability to estimate the structural capacity of the system is limited. Structural reliability analysis is concerned with the rational treatment of the uncertainties encountered during the structural analysis and evaluation process. This is achieved by developing mathematical tools that help engineers devise consistent decision making strategies related to the safety of structural systems (Thoft-Christensen, and Baker 1982; Thoft-Christensen, Murotsu 1986; Frangopol, 1999). In recent years, reliability concepts have been implemented in the design and analysis specifications of all types of structural systems including bridges, buildings, etc. (AASHTO LRFD 1994; AISC LRFD 1994, ACI 1995). One difficulty observed during the practical implementation of the reliability theory is the lack of sufficiently accurate statistical database. In addition, the uncertainties inherent in structural discretization and structural modeling are very difficult to estimate. These types of uncertainties are usually known as model uncertainties and should normally be included into the final estimate of the reliability index and the probability of failure. Because of the modeling uncertainties, the probability of failure values, calculated through classical reliability methods, are often used only as notional measures of risk rather than as actuarial values. Nevertheless, it has been shown that these measures will still provide robust and consistent safety factors when used to calibrate new design codes and specifications (Moses & Ghosn, 1985). Also, they provide a means to compare the safety of alternative designs.

Traditional methods for evaluating the reliability of bridges, like traditional methods for the design and analysis of bridge systems, are based on linear elastic structural analysis although structural members may be selected based on their ultimate capacity (AASHTO, 1994). During the design process, the safety of each member is considered separately. Load and resistance factors are used to account for the uncertainties encountered during the analysis of the structure and when estimating the capacity of each member. This traditional approach, that has been successfully used for generations, does not accurately model the true behavior of the bridge and consequently does not give a true representation of the actual safety of the complete structural system (Thoft-Christensen & Murotsu 1986). For this reason, changes have been recently introduced in the AASHTO LRFD specifications to improve the bridge design and analysis process. This is achieved by encouraging the use of better analysis tools and by calibrating the safety factors based on formal reliability methods (AASHTO 1994; Zokaie, Osterkamp, and Imbsen 1991; Nowak 1995; Ghosn 1998). In addition, in order to account for the system performance rather than simply deal with individual members, recent studies have proposed to include system factors during the member design process (Ghosn and Moses 1997).

To account for the large level of uncertainty encountered while predicting bridge system performance, the calibration of the system factors has also been based on structural reliability concepts. These factors were calibrated by checking the single most likely failure mode of the system. In reality, bridge structures have high levels of redundancy and multiple load paths, which produce numerous possible failure modes. Identifying

these failure modes is an important part of an accurate reliability analysis of any structural system (Murotsu, Okada & Shao 1993).

Bridge system failure modes depend on the possible combination and points of application of the applied loads, and are related to the geometric configurations of the structure, its material properties, and member ductility. Thus, it is often difficult to enumerate all possible failure modes or even to predetermine the dominant ones. For this reason, failure mode analysis forms one of the most important tasks in the system reliability evaluation of structures in general and bridges in particular. From a system point of view, only some of the failure modes have high probability of occurring. These "important" failure modes affect the probability of system failure significantly. On the other hand, most modes are not so important and can be neglected during the evaluation of the performance of the system.

In order to identify the dominant failure modes of bridge systems, two tools are generally required: The first tool is an accurate nonlinear structural analysis program capable of analyzing the behavior of the bridge system for a specific (deterministic) set of loading conditions and material properties. The second tool is a systematic search algorithm that will determine the probabilistically dominant failure modes accounting for the randomness in the applied loading and material properties.

The object of this dissertation is to propose two new tools for the system reliability analysis of highway girder-bridges. The structural analysis tool consists of an improved

version of the program NONBAN (NONlinear Bridge ANalysis). The modal search tool proposed in this study is an improved Genetic Search strategy for modal identification using a Shredding Genetic Algorithm (SGA). This Chapter will present a brief review of the background of these tools and the objectives of the dissertation. More details on the proposed work will be provided in the following Chapters.

1.2 PROGRAM NONBAN

The original version of the program NONBAN was developed during a series of projects on Redundancy in Highway Bridge Superstructures supported by the National Cooperative Highway Research Program and the Transportation Research Board of the National Research Council (Ghosn, Casas, & Xu; 1996, Ghosn, & Moses, 1997, Ghosn, Deng, Xu, Liu & Moses, 1997). The program uses a grillage (grid) analysis method to perform the linear and nonlinear analysis of highway bridge structural systems. Two methods are normally used to extend the traditional linear elastic grillage analysis method to the nonlinear range: The first consists of using a nonlinear element stiffness matrix derived from the stress-strain or the moment-curvature relationships of each beam's section properties (Razaqpur & Nofal, 1988). The other method consists of accounting for the nonlinear behavior by introducing rotational springs or rigid-plastic hinges at the ends of each beam element and including the stiffnesses of the rotational springs or the subhinges in the element stiffness matrices (Livesey, 1970; Pail & Buckle, 1970; Ricles, & Popov, 1994).

In the first method, the moment-curvature relationship is normally obtained analytically and thus may not accurately model the true behavior of bridge sections as it cannot easily account for secondary effects such as residual stresses, lateral-torsional buckling, local buckling, and other factors that depend on the specific loading or boundary and support conditions. These secondary effects are significant for composite steel-girder bridge members particularly for continuous bridges that often have non-compact sections in regions of negative bending. For example, experimental investigations have shown that the yielding strength of a composite steel girder section is 20% of the yielding strength obtained analytically even in positive bending (Schilling, 1989). This difference is due to the effects of residual stresses, the deformations of shear studs, the behavior of the concrete deck, etc. In concrete members the difficulty arises from the lack of available models that can accurately predicted the extent of the plastic zones wherever they may concentrate.

To better account for secondary effects and extent of plastification, many researchers have used experimental results to complement the analytical models. This is often achieved by dividing bridge members into finite beam elements and assuming that the nonlinear effects are concentrated at the end nodes of each element while the rest of the element remains elastic. The nonlinear effects are modeled by nonlinear rotational springs or rigid-plastic hinges. The traditional beam element stiffness matrix is then adjusted to account for the effects of the rotational springs. Thus, each spring's rotation will be a function of the plastic zone in each member and the plastic curvature. The

spring coefficients may then be calculated from the member's moment-curvature relationship if the extent of the plastic zone in an element is known. This approach has produced improved results over the purely analytical representation described above. However, a number of problems remain unresolved. The first problem is the predetermination of the extent of the plastic zone in each beam element. For concrete bridges, the plastic zone is often defined in terms of the length of the plastic hinge L_p. For steel bridges, the extent of plastification is calculated from the bending moment diagrams.

Many research studies have attempted to find empirical methods to predetermine the extent of plastification for concrete members (Baker, 1956; Corley, 1966; Sawyer, 1964). But, the accuracy of the results obtained using empirical L_p values are highly dependent on the structure's mesh size and the boundary conditions. In addition, even if L_p is known, the accuracy of analytical moment-curvature relationships is questionable. An alternative approach consists of calculating a spring's moment-rotation relationship (spring stiffness) from experimental data, thus avoiding the need to explicitly calculate L_p. This also helps reduce the gap between analytical results and observed actual behavior. But experimental moment-rotation curves are only available for specific beam types subjected to specific loading and support conditions. These conditions are often different from those encountered in practice, and methods need to be devised to utilize these limited available experimental results for studying a range of typical bridge configurations subjected to various loading conditions.

To help improve the capability of NONBAN and overcome the above-mentioned deficiencies, this dissertation proposes a method that would generalize the applicability of available experimental moment-rotation relationships to cover a wide range of bridge configurations and loading conditions. The proposed method assumes a linear variation of curvature along finite lengths of a bridge's members. Using this assumption with the experimental results of typical steel bridge beams, an empirical relationship between the moments and curvatures of bridge elements is obtained and used as input for the grillage analysis. Similarly, for concrete members, a transfer model is developed to generalize the empirical results available from experiments using particular loading conditions. Thus, the proposed procedures join the benefits of using experimental data on the behavior of individual girders to the simplicity of using a stiffness matrix formulation that accounts for the nonlinear behavior through rotational springs. This dissertation will demonstrate that the results obtained from the nonlinear grillage analysis of bridge systems using the proposed methods are in excellent agreement with laboratory experimental results as well as field tests on full-scale bridge systems.

Another problem, encountered while performing a nonlinear analysis of large-scale structural models, is the large number of iterations needed for the program to converge to the ultimate system capacity. Each iteration requires the assembly and the defactorization of a global stiffness matrix that models the effects of every member in the system. In addition, the reliability analysis requires repeating the calculations for a large number of realizations for each random variable. With today's capabilities, this computational effort would then require days of computer time. Thus, the development of efficient nonlinear

algorithms and efficient methods to assemble and solve the stiffness matrices becomes a critical issue for the practical implementation of structural reliability tools to real-size problems.

One classical method used for solving nonlinear systems of equations is the Newton-Raphson algorithm (Bathe 1996). To improve the efficiency of the Newton-Raphson algorithm, various methods (e.g. Initial stress method, Modified Newton-Raphson method (Bathe 1996; Zienkiewicz & Taylor 1994) have been developed. These modified methods were observed to sometimes have convergence problems for complicated systems. In addition, the Newton-Raphson algorithm requires a significant computational effort mostly spent on assembling and de-factorizing the global stiffness matrix at every iteration step. To avoid these repetitious processes, a class of new methods, known as matrix updating methods or quasi-Newton methods, has been developed (Dennis1976). The BFGS (Broyden-Fletcher-Goldfarb-Shanno) method is one typical method in this large family which is suitable for application in nonlinear structural analysis programs (Matthies & Strang 1979; Bathe and Cimento 1980).

Because most available improved nonlinear solvers are not accurate, this dissertation will present a new solver derived from the Sherman-Morrison-Woodburg formula. The solver is then incorporated into the incremental loading algorithm of NONBAN to calculate the ultimate capacity of bridge systems. This dissertation will prove that the proposed method improves the efficiency of the computational algorithm such that the total computational time required to solve the nonlinear structural analysis problem is no

harder than the time required to invert the global stiffness matrix. Compared to other methods, the proposed method will improve the computing efficiency of NONBAN in proportions of the square root of the number of degrees of freedom, DOF.

1.3 GENETIC SEARCH ALGORITHM

For large structural systems such as realistic models of bridges and buildings, finding the dominant failure modes is a difficult undertaking because of the random nature of the loading process and the uncertainties associated with predicting the structural response. Several probabilistic and deterministic/heuristic strategies for identifying the dominant failure modes of structural systems have been developed in the last two decades (Goldburg 1989; Robinson, & Toussaint 1993; Shao, & Murotsu 1999, Moses 1990, Wang, Corotis & Ramirez 1995, Frangopol 1999, Nowak 1995). But, these traditional methods have their limitations when it comes to working with realistic structural systems formed by a large number of members of different levels of ductility, different levels of statistical correlation, and different possible combinations of loads.

Traditional failure mode identification methods can be generally classified into two categories: a) Methods based on probabilistic techniques such as the branch-and-bound technique and different simulation-based procedures that are theoretically rigorous but require too much computation time. b) Deterministic search methods that include the incremental loading technique, plastic mechanism analysis, and other heuristic strategies

(Moses, 1982; Thoft-Christensen & Murotsu 1986; Karamchandani 1987). The deterministic search methods are usually faster than probabilistic search strategies but may sometimes miss important failure modes.

On the other hand, recent advances in artificial life theory and its application have led to the development of very efficient and comprehensive search algorithms which lend themselves to immediate use in structural applications. For example, Shao, & Murotsu, (1999) successfully applied a Genetic Search Algorithm to obtain the failure modes of typical structural configurations. By their very nature, GAs include intelligent optimization mechanisms that guide a random search into the most interesting (critical) region(s) of the pertinent domain. Shao's algorithm is based on generating search directions in the space formed by the random variables affecting the reliability of a structural system. By tracing failure path(s) in each direction and evaluating the corresponding reliability, the genetic algorithm is able to gradually narrow down the search directions to the most likely failure region(s), and thus identify the dominant failure modes. This method can be considered as a compromise between the probabilistic and the deterministic strategies. It includes the advantages of both traditional search strategies and aims to reach an acceptable level of accuracy and efficiency.

Shao & Murotsu, (1999) showed that their Genetic Search Algorithm can be easily coupled with deterministic analysis programs such as NONBAN to accurately model the nonlinear behavior of bridge structures during the search process. One drawback observed during the use of Shao's approach was the excessive number of iterations

required for the algorithm to converge to the most dominant modes. In addition, the algorithm is programmed to search within pre-set directions and the final results may give a good approximation of the final failure modes but not necessarily the exact expressions.

To overcome some of the drawbacks of the Genetic Algorithm as used by Shao, this dissertation reviews the historic development and the original logic behind the algorithm. In biology, decoding of genes is known to be a very demanding and time consuming task. In the original years of genetic decoding research, even the most advanced research laboratories needed over one year to decode a single chromosome (Thompson 1999). To improve the efficiency of the search, scientists have developed a splitting technique that shreds a chromosome into many small fragments (Lemonick & Thompson 1999). Then, a gene mapping procedure is used to identify the fragmented chromosomes. By following this shredding procedure, scientists found that their decoding efficiency improved by orders of magnitudes. Following this general approach, this dissertation proposes to improve the efficiency of Shao's GA, by developing a new method herein called the Shredding Genetic Algorithm (SGA). This will be effected by dissecting a chromosome, which represents a possible failure direction pointing toward a potential failure mode, into pairs of genes and forming a fitness index matrix that quantifies the importance of each pair to the whole genome of failure modes. This shredding algorithm simulates the interference of breeders into the natural evolutionary selection process by filtering the weak offsprings from the pool of genes available for reproduction. This thesis will show

that the proposed filtration operator will help improve the efficiency of the genetic search strategy without losing its robustness.

1.4 RESEARCH OBJECTIVE AND DISSERTATION OUTLINE

The objective of this dissertation is to develop an efficient method for obtaining the reliability of bridge structural systems. Two tools will be developed to achieve the objective. The first tool will consist of an improved version of the program NONBAN that will use new member behavior models to better represent the nonlinear response of typical steel and concrete bridge members. These models will be based on a combination of experimental and analytical concepts and will be shown to vastly improve the accuracy of the program. In addition, the efficiency of the nonlinear program and its convergence will be improved by developing a new solver that will not require the assembly or decomposition of the global stiffness matrix at every load increment.

The second tool is the shredding genetic search algorithm, SGA, that will identify the dominant failure modes of bridge systems. The proposed SGA will incorporate an expert system that will help improve the efficiency of the search strategy. It will also utilize a new filtration operator that will select the best chromosome based on a fitness index matrix.

To achieve the goals of this study, the following research tasks will be performed:

1. Study the behavior of steel bridge members and develop a model to incorporate experimental findings on member behavior to improve the accuracy of NONBAN.
2. Study the behavior of prestressed-concrete bridge members and develop a L_p transfer model that will accurately represent the behavior of members subjected to various loading schemes and boundary conditions.
3. Improve the efficiency of structural nonlinear analysis programs by developing the pseudoforce algorithm that will reduce computational effort during the assembly and the solution of the global stiffness matrix.
4. Develop the Shredding Genetic Algorithm to efficiently identify the dominant failure modes of bridge structural systems.
5. Test the accuracy, efficiency and applicability of the proposed methods and demonstrate their applicability for the reliability analysis of bridge structural systems.

A detailed description of this research work and findings is provided in the following chapters. Chapter 1 provides an introduction to the problem at hand and reviews the background. Chapter 2 studies the nonlinear behavior of steel bridge members. Chapter 3 discusses the behavior of prestressed concrete members. Chapter 4 develops the proposed pseudoforce nonlinear structural analysis solver. Chapter 5 outlines the proposed Shredding Genetic Algorithm for the reliability analysis of structural systems.

Chapter 6 demonstrates the application of the proposed models for the reliability analysis of highway bridge systems. Chapter 7 summarizes the conclusions of this study and proposes ideas for further research.

CHAPTER 2

NONLINEAR ANALYSIS OF COMPOSITE STEEL GIRDER BRIDGES

This chapter describes a procedure for the nonlinear analysis of composite steel girder highway bridges. The procedure uses a modified grillage (grid) analysis method where material nonlinearity is modeled by empirically derived moment-curvature relationships. These are obtained from experimental data on the behavior of typical composite steel girder bridges. A linear variation of plastic curvature along the length of each beam element is assumed. An equivalent grid plastic hinge length, L_{gp}, is used to simulate the extent of plastification over the whole length of a grid element. The procedure can account for span continuity by including a negative bending moment-curvature relationship. Numerical investigations verify the proposed method's validity by comparing the analytical results with those of in-situ and laboratory full-scale and model-scale bridge tests. This chapter also demonstrates that the proposed nonlinear analysis method provides a simple tool that can be used to obtain reasonably accurate representations of the nonlinear behavior of composite steel girder bridges. The method uses a grillage discretization technique whose results are relatively insensitive to variations in the mesh size. The proposed method has a high potential for use in engineering practice because of the simple input requirements and its reasonable level of accuracy.

2.1 INTRODUCTION

The stiffness matrix method, and particularly the grillage analysis approach, has been widely used for several decades to perform the linear–elastic structural analysis of buildings and bridge systems. The grillage method is currently the most widely used approach in bridge engineering practice. For example, the AASHTO-LRFD Specifications (1994) propose a set of empirical equations for calculating the girder distribution factors. These equations were obtained based on the grillage analysis of typical bridge configurations (Zokaie, Osterkamp, Imbsen 1991). In addition, the Specifications recommend that engineers perform their own analyses using either the grillage method or more refined finite element methods to obtain more accurate results. In Europe, where bridge design specifications do not provide load distribution factors, bridge engineers often perform grillage-type analyses to predict the distribution of the applied forces to individual bridge members and to evaluate the safety of their designs (Hambly 1991).

Traditional grillage analysis consists of modeling a bridge superstructure as a grid formed by linear elastic beam elements. The longitudinal members of the bridge system are modeled as longitudinal beam elements along the main axis of the bridge, while the slab and diaphragms are modeled as transverse beams. This approach is used for slab bridges, composite and non-composite slab on girder bridges as well as spread box beam bridges and multi-cell box bridges (Hambly 1991).

Most applications of the grillage method in bridge analysis are based on the linear elastic stiffness matrix approach although researchers have adopted it to nonlinear analysis by updating the stiffness matrix at every load increment to reflect the reduced stiffness that occurs when portions of a beam plasticize. Another method assumes that the plastic zone is concentrated at the ends of each beam element where plastic hinges would form (Livesley 1970). The typical application of this method for the nonlinear analysis of bridge systems has been described by Ghosn, Casas and Xu (1996) and Ricles and Popov (1994). In the latter reference, the hinge at each end of the beam element is divided into a series of subhinges as illustrated in Figure 2.1. The formulation of the nonlinear stiffness matrix of a beam element is based on the assumption that the linear elastic section of the beam is in series with the nonlinear hinge at each of its ends (nodes I and J, as shown in Fig. 2.1). Inelastic flexural and shear deformations developed in the flexural and shear subhinges, in addition to the elastic flexural and shear deformations of the beam itself, give the total deformation of the nonlinear beam. Each hinge is of zero length, and consists of a number of subhinges (for example, 8 subhinges are shown in Figure 2.1). Hence most of the beam remains in the elastic range. Each subhinge has a rigid-plastic force-deformation relationship. In the linear elastic range, the subhinges at the ends of the beam are rigid (have an infinite stiffness). Therefore, the element stiffness is that of the elastic beam alone. As the loads applied on the structure increase beyond the elastic limit, the subhinges yield one by one. A reduction in the total element stiffness occurs due to the softening of the stiffnesses of the subhinges. The relationship between the deformations of each hinge (the assembly of the subhinges) and the element's end generalized forces (shear forces and moments) can be represented by multi-linear curves

as shown in Figure 2.2. The focus of this chapter is on the nonlinear behavior in bending although the nonlinear behavior of beam elements under shear deformations can also be included as demonstrated by Ricles & Popov, (1994) and Ghosn, Casas & Xu (1996).

The effect of the plastic subhinges is modeled as rotational springs connected to the ends of the elastic beams. Details on the derivation of the stiffness matrix of beam elements with ends connected to plastic rotational springs are given by Livesley (1970), Ghosn, Casas and Xu (1996) and Ricles, J.M., Yang, Y.S., and Priestley (1998). As an example, the grillage element stiffness matrix for the element shown in Figure 2.1 can be expressed as shown in Figure 2.3. The stiffness matrix shown in Figure 2.3 assumes uncoupling between the torsional stiffness and the bending stiffness of the beam element at all load levels and assumes a linear elastic behavior in torsion. The nonlinear effects are represented by the slopes of the plastic M-θ curve for each element. These curves model the nonlinear behavior of composite steel members as explained in the next section.

2.2 MODELING THE NONLINEAR BEHAVIOR OF COMPOSITE STEEL MEMBERS

The factors affecting the nonlinear behavior of composite steel members are complex and intricately interrelated. Local flange, local web and lateral-torsional distortions interact and tend to build up gradually. Experimental investigations have shown that composite sections begin to exhibit nonlinear behavior at a relatively small load that is about 20% of

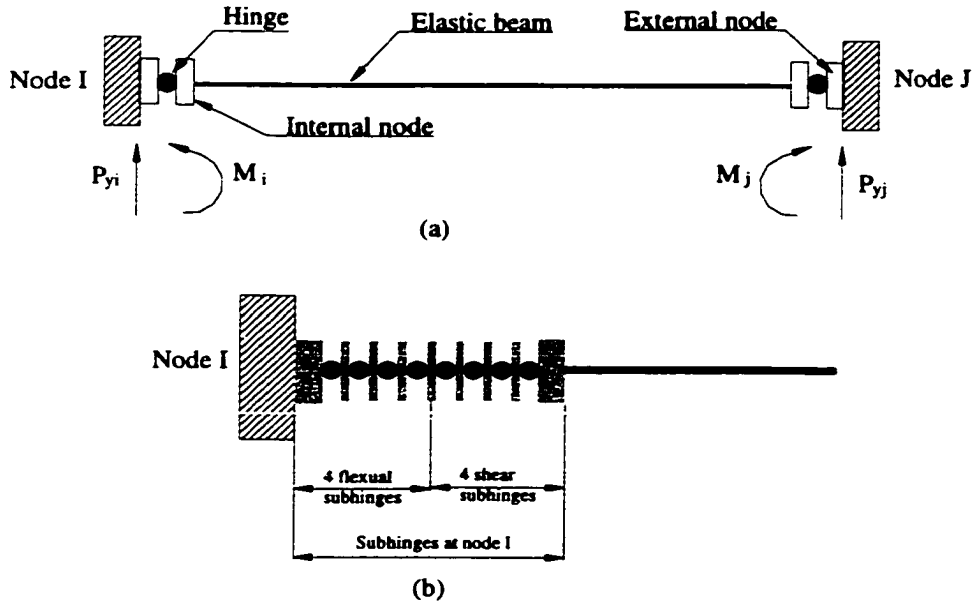

Figure 2.1. Nonlinear representation of bridge beam elements.

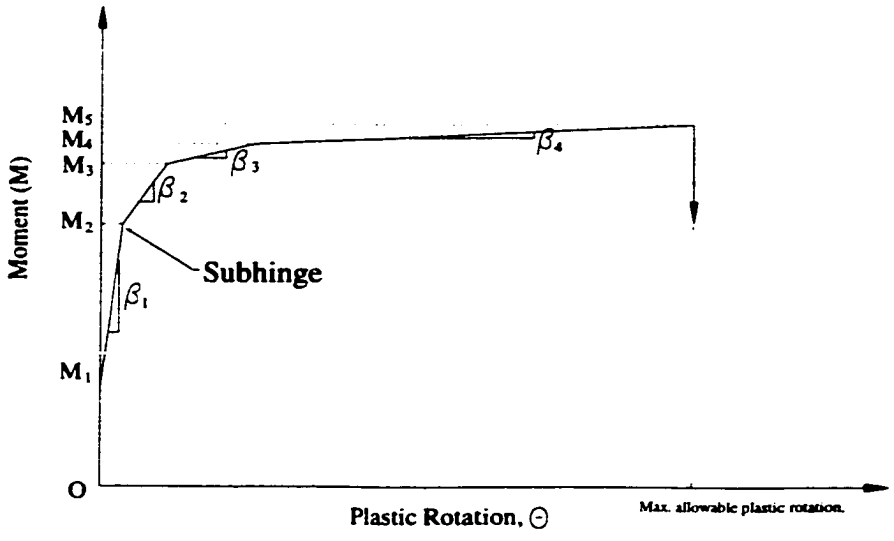

(a)

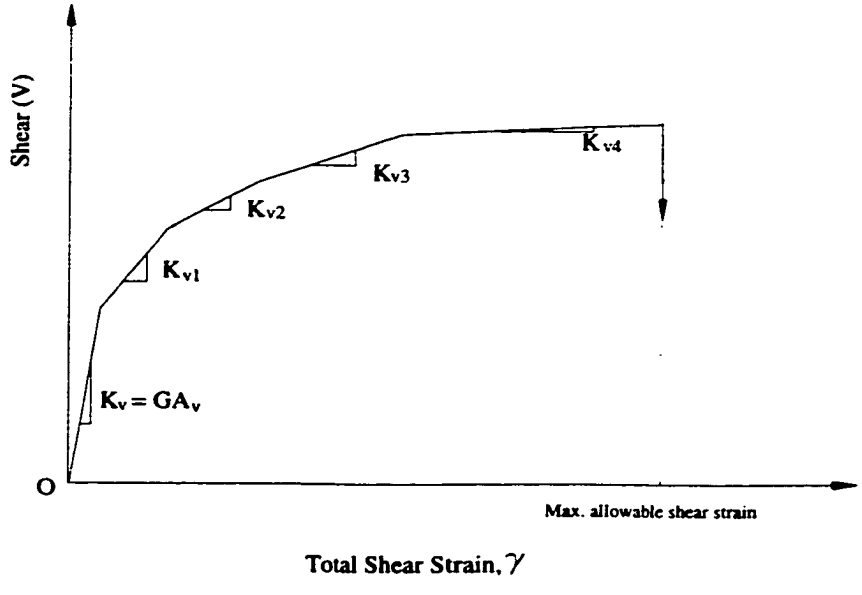

(b)

Figure 2.2. Idealized Force-Deformation Relationships of Nonlinear Hinges.

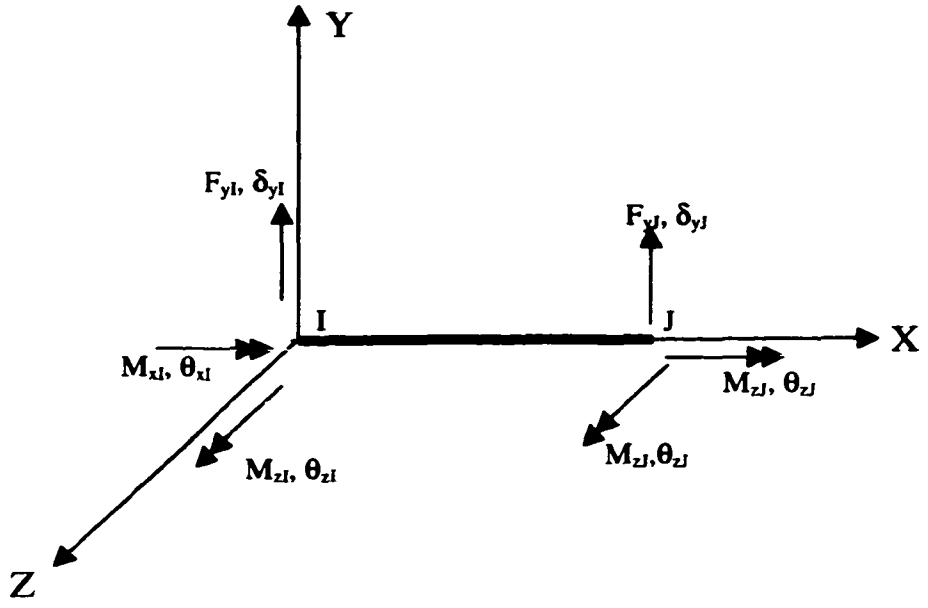

(a), Local coordinate system.

$$\begin{bmatrix} F_{yI} \\ M_{xI} \\ M_{zI} \\ F_{yJ} \\ M_{xJ} \\ M_{zJ} \end{bmatrix} = \begin{bmatrix} K_{1,1} & 0 & K_{1,3} & K_{1,4} & 0 & K_{1,6} \\ 0 & K_{2,2} & 0 & 0 & K_{2,5} & 0 \\ K_{3,1} & 0 & K_{3,3} & K_{3,4} & 0 & K_{3,6} \\ K_{4,1} & 0 & K_{4,3} & K_{4,4} & 0 & K_{4,6} \\ 0 & K_{5,2} & 0 & 0 & K_{5,5} & 0 \\ K_{6,1} & 0 & K_{6,3} & K_{6,4} & 0 & K_{6,6} \end{bmatrix} \begin{bmatrix} \delta_{xI} \\ \theta_{xI} \\ \theta_{zI} \\ \delta_{yJ} \\ \theta_{xJ} \\ \theta_{zJ} \end{bmatrix}$$

(b), Stiffness matrix of a single beam element.

$$K(1,1) = K(4,4) = 6*\left[-1+\frac{3(2+C_1)(2+C_2)}{C_1(4+C_2)+4(3+C_2)}\right]\frac{EI_z}{L^3}$$

$$K(1,3) = K(3,1) = \frac{6(2+C_2)}{C_1(4+C_2)+4(3+C_2)}\frac{\beta_1}{L}$$

$$K(1,4) = K(4,1) = 6*\left[1-\frac{3(2+C_1)(2+C_2)}{C_1(4+C_2)+4(3+C_2)}\right]\frac{EI_z}{L^3}$$

$$K(1,6) = K(6,1) = \frac{6C_2(2+C_1)}{C_1(4+C_2)+4(3+C_2)}\frac{EI_z}{L^2}$$

$$K(3,3) = \frac{4(3+C_2)\beta_1}{C_1(4+C_2)+4(3+C_2)}$$

$$K(3,4) = K(4,3) = \frac{-6C_1(2+C_2)}{C_1(4+C_2)+4(3+C_2)}\frac{EI_z}{L^2}$$

$$K(4,6) = K(6,4) = -K(1,6)$$

$$K(3,6) = K(6,3) = \frac{2C_1C_2}{C_1(4+C_2)+4(3+C_2)}\frac{EI_z}{L}$$

$$K(6,6) = \frac{4(3+C_1)\beta_2}{C_1(4+C_2)+4(3+C_2)}$$

$$K(2,2) = K(5,5) = -K(2,5) = -K(5,2) = \frac{GJ_x}{L}$$

Where: $C_1 = \frac{\beta_i L}{EI_z}; C_2 = \frac{\beta_j L}{EI_z}$

β_i = slope of plastic M-θ curve for end I.
β_j = slope of plastic M-θ curve for end J.
J_x = torsional moment of inertia about x axis.
I_z = moment of inertia about z axis.
L = element length.
E = elastic modulus.
G = shearing modulus.

Figure 2.3. Stiffness Matrix of Bridge Beam Element.

the ultimate capacity. This is believed to be due to the residual stresses in the beams, the effect of the shear connectors, the nonlinear properties of the concrete and the reinforcing steel. Beyond this range, strain hardening and instability work against each other and tend to balance out (Schilling and Morcos 1988, and Vasseghi and Frank 1987).

Several researchers have attempted to develop analytical models to study the general behavior of composite steel girder bridges (Razaqpur and Nofal 1988; Komatsu, Moriwaki, Fujino, and Takimoto, 1984; Idriss, and White, 1991; Hall and Kostem 1981). Other researchers gave special attention to the particular factors influencing the behavior of composite steel sections. For example, Keuser and Mehlborn (1987) developed a model that considers the effect of reinforcement bonding. Razaqpur and Nofal (1988), Kullman and Hosain, (1985), Hawkin and Mitchell (1984) presented models to describe the effects of shear connectors. Nagarajarao, Estuar, and Tall (1964) gave models for the residual stresses in steel members. Bazant and Byung (1983) studied the effect of concrete cracking. These models can then be included in a detailed finite element analysis to study the behavior of composite steel bridges. However, these methods are difficult to use in practice because they either require large computational effort or demand detailed data that is often hard to obtain as many of the required parameters need to be determined on a case-by-case basis. For these reasons, developing a simple yet accurate method that can be applied on a routine basis is deemed to be of utmost importance.

This chapter proposes a method to represent the nonlinear behavior of bridge elements by evenly spreading the effects of nonlinearity over an equivalent grid element plastic hinge length, L_{gp}. The proposed method is empirical in the sense that it requires the availability of a "representative" Moment-Rotation curve. Such curves have been obtained through previous research studies at AISI (American Iron & Steel Institute) and the University of Texas (Vasseghi and Frank 1987). The research sponsored by AISI has concluded that the nonlinear behavior of typical steel bridge sections can be modeled by moment versus plastic rotation curves similar to the Texas curve shown in Figure 2.4 (Schilling & Morcos, 1988). The Texas curve, obtained experimentally, is normalized as a function of the ultimate plastic moment capacity, M_p. It describes the behavior of composite girders in positive bending. Other curves for negative bending of beams with different section slenderness ratios are also available in the literature (Schilling, 1989). To obtain the curve of Figure 2.4, a 40-ft simple span beam was loaded by one concentrated force at the center. A portion of the total load was applied to the steel section before the slab hardened. Although the curve was obtained from a 40-ft beam, researchers at the University of Texas and AISI have shown that this curve models the behavior of most typical bridge sections for all span lengths (Vasseghi and Frank 1987).

The Texas curve accounts for all the important factors that affect a composite steel section's nonlinear behavior including the effects of residual stresses, strain hardening, flexibility of shear connectors, effective slab width, effect of the slab's reinforcing steel and the cracking of concrete slab. This curve will be used in the rest of this chapter as the basic tool to describe any composite section's nonlinear properties in positive bending.

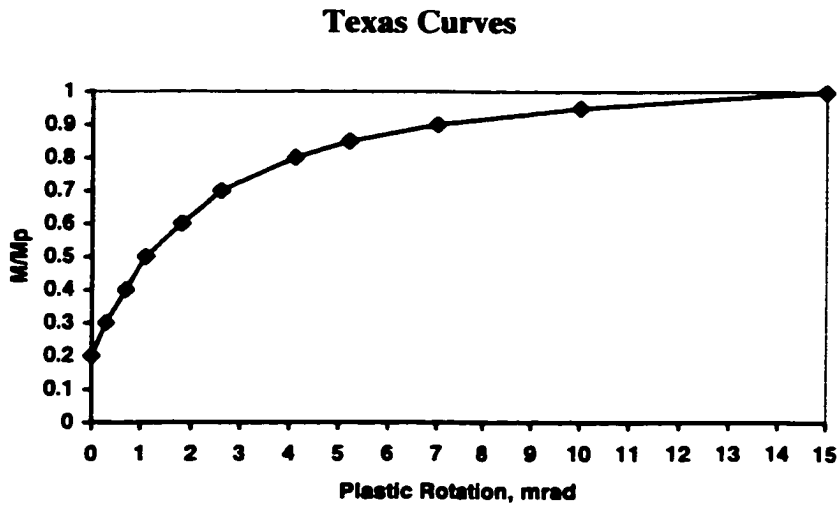

Figure 2.4. Texas Moment-Rotation Curve.

2.3 M-φ CURVE FOR POSITIVE BENDING OF STEEL BEAM SECTIONS

To execute the nonlinear grillage analysis, the stiffness matrix shown in Figure 2.3 must be evaluated at every load increment. In addition to the linear elastic properties of each beam element (moment of inertia I_z, elastic modulus E, rotational inertia J_x and shear modulus G), assembling the stiffness matrix requires the determination of the element's rotational stiffnesses at both ends. These rotational stiffnesses are labeled, β_I and β_J, for ends I and J respectively. The Texas curve cannot be directly used because the loading conditions and the support conditions of each element are different than those used to develop the Texas M-θ curve. However, the experimental curve contains the necessary information that can be utilized to obtain the required β_I and β_J coefficients. The procedure used in this study to obtain these coefficients consists of three steps: 1) Derive the moment-curvature relationship implicit in the Texas M-θ curve. 2) Discretize any other loaded beam into a number of elements and calculate the plastic rotation in the beam through a numerical integration of the curvature equation derived in step 1. 3) Calculate the plastic hinge stiffnesses β_I and β_J. These steps are further described in the next sections.

2.3.1 Derivation of Moment-curvature Relationship.

The end rotations of a beam element are related to the curvatures along the length of the element. These curvatures are themselves related to the internal bending moments. Therefore, determining the appropriate moment-curvature, M-φ, relationship is a very important factor for producing accurate results for the nonlinear behavior of bridge systems.

It is assumed that each composite steel section's plastic moment curvature relationship (M-φ curve) can be represented by a multilinear curve. It is also assumed that a typical loaded beam element IJ can be represented as shown in Figure 2.5 where θ_{TI} is the total rotation of the beam at end I and θ_{TJ} is the total rotation at end J, and L is the element length.

The method assumes that the function describing the relationship between φ (plastic section curvature) and M (moment) is monotonously increasing. By assuming that this function is valid for all sections of the beam element, the total rotation of this element can be calculated by:

$$\theta_{TI} + \theta_{TJ} = \int_0^L \varphi_T \, dx \qquad \text{(Eq. 2.1)}$$

θ_{TI} and θ_{TJ} are the total rotations at ends I and J, φ_T is the total section curvature, and L is the length of the element. The total section curvature consists of the summation of the elastic curvature, φ_e, and the plastic curvature, φ, such that:

$$\varphi_T = \varphi_e + \varphi \qquad \text{(Eq. 2.1.a)}$$

Similarly, the total rotation consists of the summation of the elastic rotation, θ_e, and the plastic rotation,θ:

$$\theta_T = \theta_e + \theta, \qquad \text{(Eq. 2.1.b)}$$

By separating the plastic rotation θ from the elastic rotation, equation (2.1) becomes:

$$\theta = \theta_I + \theta_J = \int_0^L \varphi \, dx \qquad \text{(Eq. 2.2)}$$

φ represents the plastic curvature, and θ_I and θ_J are the plastic rotations at ends I and J.

The step function χ (M_i,M_j) is defined as:

$$\chi(M_i, M_j) = \begin{cases} 1 & M_i \le x \le M_j \\ 0 & otherwise. \end{cases} \qquad \text{(Eq. 2.3)}$$

The relationship between M and θ shown in Figure 2.2a can then be expressed as:

$$\theta = \sum_{i=1}^{n} (a_i + b_i M)\chi(M_{i-1}, M_i) \qquad \text{(Eq. 2.4)}$$

n is the total number of linear segments used to model the moment-rotation relationship. Thus, if ten segments are used to model the Texas curve, it can be represented by an expression of the form:

$$\begin{aligned}\theta = {} & (3M-0.6)\chi(0.2,0.3)+(4M-0.9)\chi(0.3,0.4) \\ & +(4M-0.9)\chi(0.4,0.5)+(7M-2.4)\chi(0.5,0.6) \\ & +(8M-3.0)\chi(0.6,0.7)+(15M-7.9)\chi(0.7,0.8) \\ & +(18M-10.3)\chi(0.8,0.85)+(36M-25.4)\chi(0.85,0.9) \\ & +(60M-47)\chi(0.9,0.95)+(100M-85)\chi(0.95,1.0)\end{aligned} \qquad \text{(Eq. 2.5)}$$

The following three observations were made by researchers during the conduct of the experiments that produced the Texas curve of Figure 2.4 (Vasseghi and Frank 1987; Schilling 1989):

- Plastic behavior begins at a moment level on the order of 20 percent of the plastic moment capacity (0.2 Mp).
- A plane section remains plane throughout the whole loading process.
- The Texas curve can be used to describe most typical girders for different span lengths and for different composite steel girder sections.

These three observations will be used as postulates during the derivations of the end stiffnesses for beam elements under nonlinear bending.

The experimental setup used to generate the Texas curve and the corresponding bending moment diagram are modeled as shown in Figure 2.6. In Figure 2.6, the following symbols are used: x gives the location of the section under consideration. x_1 is the coordinate of the point where the plastic zone begins and x_2 is the coordinate of the point where the plastic zone ends. M_p is the ultimate capacity of a section. M is the moment at midspan ($0.2M_p<M<M_p$). m is the moment at point x.

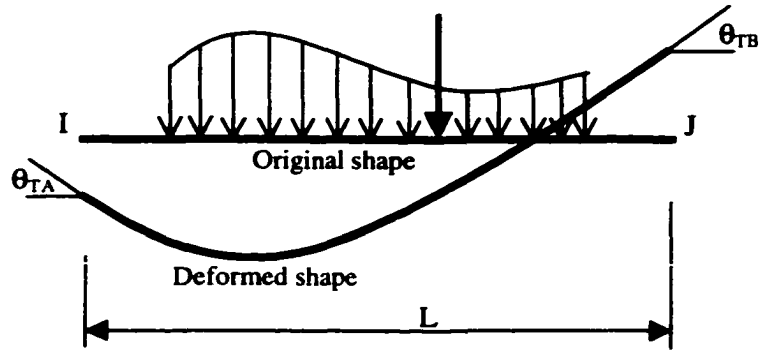

Figure 2.5. Idealized Deformation of a Typical Beam Element.

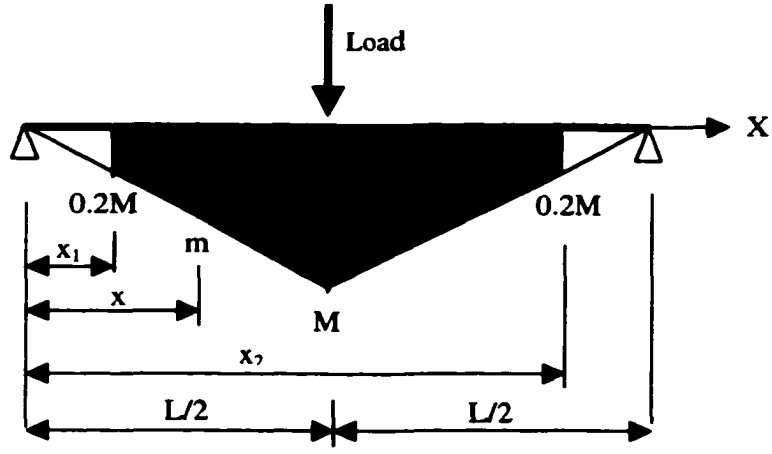

Figure 2.6. Moment Diagram for the Texas Experiment set-up.

According to Figure 2.6, equation (2.2) and the third postulate made above, this beam's plastic rotation θ can be expressed as a function of the section's plastic curvature, φ through an equation of the form:

$$\theta = \int_{x1}^{x2} \varphi dx, \qquad \text{or, using symmetry:} \quad \theta = 2\int_{x1}^{L/2} \varphi \, dx \qquad \text{(Eq. 2.6)}$$

Knowing that the nonlinear range begins at a moment level equal to 0.2 M_p through the first postulate, and given a linear moment diagram, the x_1 and x_2 coordinates can be calculated as:

$$x_1 = \frac{0.2M_p}{M}\frac{L}{2}, \quad \text{and by symmetry:} \qquad x_2 = L - x_1. \qquad \text{(Eq. 2.7)}$$

Substituting the expressions for x_1 and x_2 and Equation (2.3) into Equation (2.6), we obtain:

$$2\int_{\frac{0.2M_p}{M}\frac{L}{2}}^{\frac{L}{2}} \varphi \, dx = \sum_{i=1}^{n} (a_i + b_i M)\chi(M_{i-1}, M_i) \qquad \text{(Eq. 2.8)}$$

The curvature, φ, is a function of the moment, m. From Figure 2.6, we know that:

$$x = \frac{L}{2}\frac{m}{M} \qquad \text{(Eq. 2.9)}$$

and

$$dx = \frac{L}{2}\frac{dm}{M} \qquad \text{(Eq. 2.10)}$$

Substituting equations 2.9 and 2.10 into equation 2.8, we obtain:

$$\int_{0.2M_p}^{M} \varphi(m)dm = \frac{M}{L}\sum_{i=1}^{n}(a_i + b_i M)\chi(M_{i-1}, M_i) \qquad \text{(Eq. 2.11)}$$

Taking the derivatives of both sides of equation (2.11), the following expression for the curvature is obtained:

$$\begin{aligned}\varphi(M) &= \frac{1}{L}\sum_{i=1}^{n}(a_i + 2b_i M)\chi(M_{i-1}, M_i) \\ &+ \frac{1}{L}\sum_{i=1}^{n}\left[(a_i M_{i-1} + b_i M_{i-1}^2)\delta(M - M_{i-1}) - (a_i M_i + b_i M_i^2)\delta(M - M_i)\right]\end{aligned} \qquad \text{(Eq. 2.12)}$$

For the example where the Texas moment rotation curve was represented by 10 linear segments, (n=10) Eq. 2.12 is expressed as:

$$\begin{aligned}\varphi(M) = \frac{1}{L}[\ &(6M - 0.6)\chi(0.2,0.3) + (8M - 0.9)\chi(0.3,0.4) \\ &+ (8M - 0.9)\chi(0.4,0.5) + (14M - 2.4)\chi(0.5,0.6) \\ &+ (16M - 3.0)\chi(0.6,0.7) + (30M - 7.9)\chi(0.7,0.8) \\ &+ (36M - 10.3)\chi(0.8,0.85) + (72M - 25.4)\chi(0.85,0.9) \\ &+ (120M - 47)\chi(0.9,0.95) + (200M - 95)\chi(0.95,1.0)\ ] \\ &+ \frac{1}{L}\sum_{i=1}^{n}\left[(a_i M_{i-1} + b_i M_{i-1}^2)\delta(M - M_{i-1}) - (a_i M_i + b_i M_i^2)\delta(M - M_i)\right]\end{aligned} \qquad \text{(Eq.2.13)}$$

The function $\delta(M-M_i)$ is the dirac delta function defined as:

$$\delta(M - M_i) = \begin{cases} undefined\ when\ M = M_i \\ = 0 \qquad when\ M \neq M_i \end{cases} \qquad and \qquad \int_{-\infty}^{\infty} \delta(M - M_i)dM = 1 \qquad \text{(Eq.2.14)}$$

The curvature expression of Eq. (2.13) can be graphed as shown in Figure 2.7.

For simplicity, we can reduce the number of linear segments from 10 to 4 using a regression analysis through the points of Figure 2.7. The following expression for M-φ is thus obtained:

$$\begin{aligned} \varphi(M) &= \frac{1}{L}\sum_{i=1}^{3}(c_i + d_i M)\chi(-M_{i-1}, M_i) \\ &= \frac{1}{L}\left[\left(\frac{M}{120} - 0.001\right)\chi(0.2,0.5) + \left(\frac{M}{23} - 0.0186\right)\chi(0.5,0.8) \right. \\ &\left. + \left(\frac{M}{2} - 0.3839\right)\chi(0.8,1.0) \right] \end{aligned} \qquad \text{(Eq. 2.15)}$$

This expression may be represented as shown in Figure 2.8.

Following the third postulate made from the results of the Texas experiment, we assume that the M-φ curve described in Figure 2.8 can be used to describe the behavior of most typical composite steel girder sections.

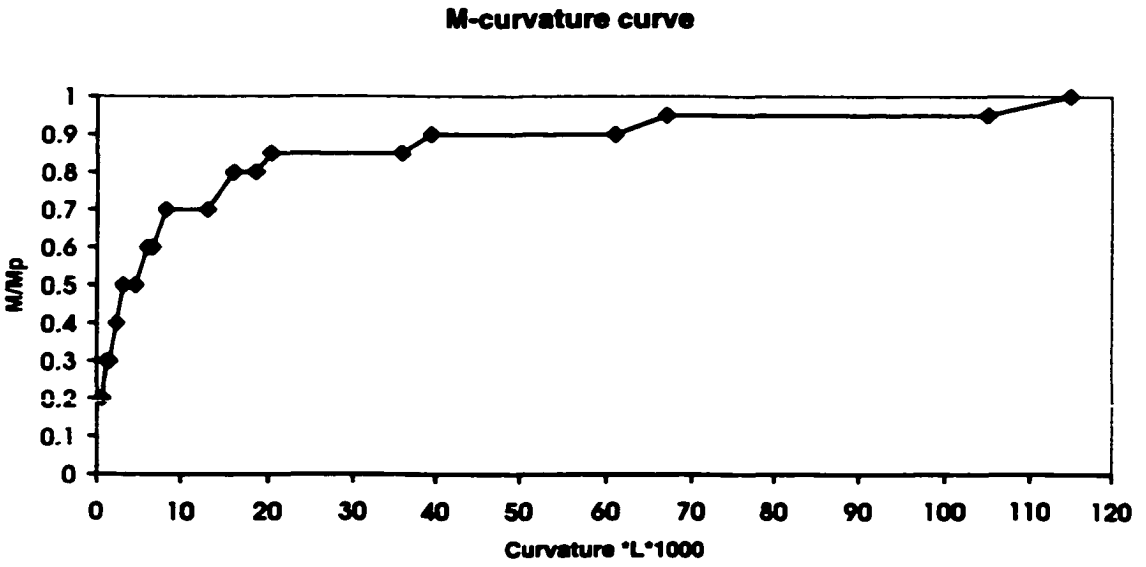

Figure 2.7. Plot of the calculated moment-plastic curvature relationship.

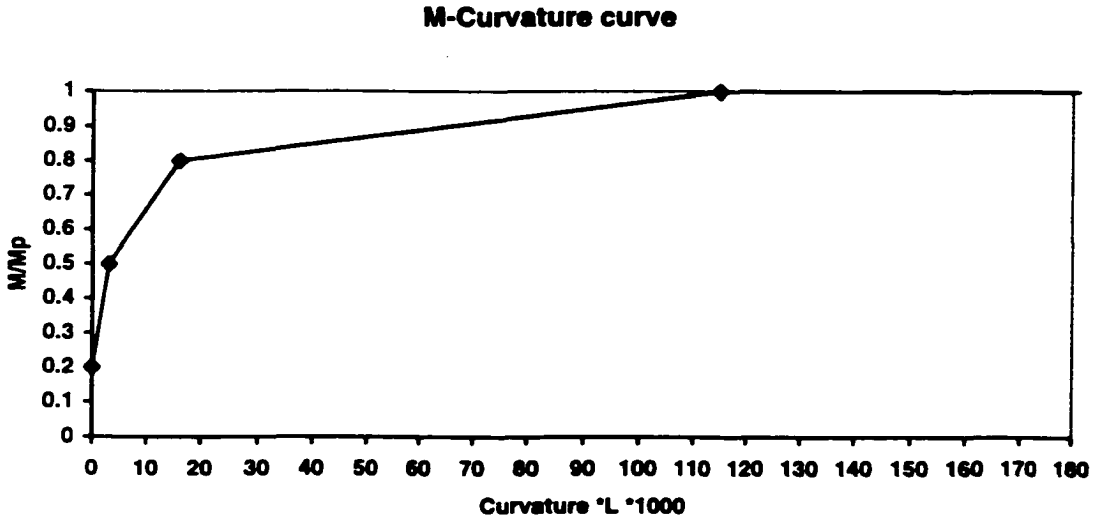

Figure 2.8. Idealized moment-curvature relationship using 4 linear segments.

2.3.2 Calculation of plastic rotations at beam element's ends.

The distribution of the plastic curvature φ along the length, L, of a beam element may be represented as a multi-linear curve as shown in Figure 2.9. The amplitude of the curvature depends on the element's moment distribution following the expression of Equation 2.15.

In Figure 2.9, φ_i, is the plastic curvature at point i, i=0,...,k, where i=0 at end I and i=k at end J, L_j, j=1, 2, ...k, is the length of segment j. Based on Figure 2.9, the plastic rotation θ of a beam segment of length L ($L = \sum L_j$) is:

$$\theta = \theta_I + \theta_J = \sum_{i=1}^{k} \int_0^{L_i} (\varphi_{i-1} + \frac{\varphi_i - \varphi_{i-1}}{L_i} x) dx = \sum_{i=1}^{k} (\varphi_{i-1} + \varphi_i) \frac{L_i}{2} \qquad \text{(Eq. 2.16)}$$

θ_I is the plastic rotation at end I, and θ_J is the plastic rotation at end J. For simplification and without losing generality, we can assume that the rotation at end I is related to the curvature at point I and the plastic rotation ($\theta_I + \theta_J$) of the beam by:

$$\theta_I = \frac{\varphi_I}{\varphi_I + \varphi_J} (\theta_I + \theta_J) = \frac{\varphi_I}{\varphi_I + \varphi_J} \sum_{i=1}^{k} (\varphi_{i-1} + \varphi_i) \frac{L_i}{2} \qquad \text{(Eq. 2.17)}$$

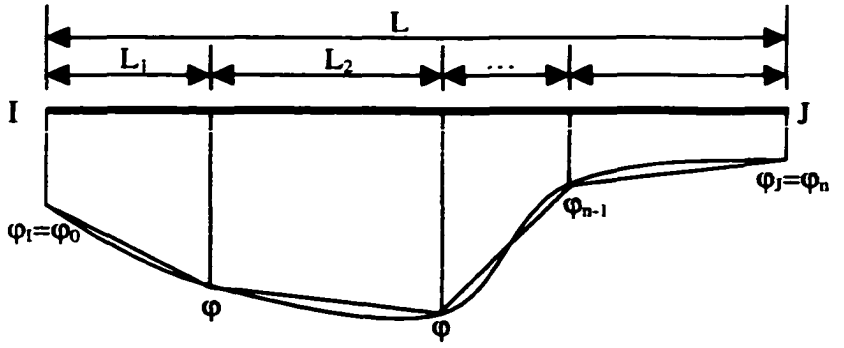

Figure 2.9. Multi-linear representation of a beam element's curvature.

Similarly, the rotation at end J is related to the total rotation and the curvature at J by:

$$\theta_J = \frac{\varphi_J}{\varphi_I + \varphi_J}(\theta_I + \theta_J) = \frac{\varphi_J}{\varphi_I + \varphi_J}\sum_{i=1}^{k}(\varphi_{i-1} + \varphi_i)\frac{L_i}{2} \qquad \text{(Eq. 2.18)}$$

If for simplicity we assume that φ varies linearly along the element's length i.e. there is only one linear segment between points I and J. By letting k=1 in equations 2.17 and equation 2.18, we get:

$$\theta_I = \varphi_I \frac{L}{2}$$
$$\theta_J = \varphi_J \frac{L}{2} \qquad \text{(Eq. 2.19)}$$

When the beam element is long, or when the moment diagram within one element has large levels of fluctuations, the assumption that the curvature varies linearly is not valid as this assumption would result in a stiff beam element that will underestimate the "true" deformations. However, by refining the mesh and increasing the number of elements used to model the bridge superstructure, the results obtained will approach the actual results. Hence, assuming a linear variation of curvature along an element length is consistent with the finite element methodology.

2.3.3 Calculation of the plastic hinge stiffness coefficients, β_I and β_J.

In this study we assume that the rotations at ends I and J of a beam element are related to the moments at these ends by the stiffness coefficients β_I and β_J. From Figure 2.2 and knowing θ_I and θ_J, from Eq. 2.19, the stiffness coefficients β_I and β_J can be calculated as:

$$\beta_I = \frac{\Delta\theta_I}{\Delta M_I}, \qquad \beta_J = \frac{\Delta\theta_J}{\Delta M_J} \qquad \text{(Eq. 2.20)}$$

θ_I and θ_J are the end rotations calculated as shown in Equation 2.19 from the moment-curvature relationship of Equation 2.15. The rotational spring stiffness coefficients β_I and β_J are used as input to the stiffness matrices described in Figure 2.3.

2.4 IMPLEMENTATION

The program NONBAN (NONlinear Bridge ANalysis) was written to perform the nonlinear analysis of bridge systems using the grillage analysis method described in this chapter. NONBAN also uses an incremental loading technique to simulate the nonlinear structural behavior of a girder bridge under applied vehicular loads. The objective of NONBAN is to describe the failure path of composite steel girder bridges. To use NONBAN, the bridge should be discretized as a plane grid (grillage model) with composite (or noncomposite) longitudinal elements representing the main girders and

transverse beam elements representing the slab and diaphragms that contribute to the lateral distribution of the load to the longitudinal members.

Nonlinear member properties are considered for bending about the main axis of each element and for shear deformations in the vertical direction. The nonlinear behavior of each element is modeled by a multilinear moment versus plastic rotation (M-θ) curve and a multilinear shear deformation (V-γ) curve as shown in Fig. 2.2. The slopes of the moment versus plastic rotation curve are calculated as described in the previous section. For typical steel bridges, the shear deformations are negligible and may be ignored. The rest of the input is similar to the input required for any linear elastic analysis of composite steel frames. A full description of the linear-elastic properties required to perform the grillage analysis is given by Hambly (1991) and Zokaie et. al. (1991). The input consists of the moments of inertia for every beam element (including polar moment of inertia to account for the torsional effects), the elastic and shearing modulii as well as the distributed dead load and the nodal location of the applied live load. In NONBAN, the live load is automatically incremented throughout the linear and nonlinear ranges until failure is reached. Failure is defined as the formation of a mechanism (instability of the system) or as the load at which a maximum deflection or maximum beam rotation is reached. The output of the program includes the deflections, the total rotations at each node, and the moments and forces at the ends of each beam element. The output also consists of a plot giving the load factor versus deformation curve that describes the relationship between the amplitude of the applied live load and the maximum vertical displacement of the bridge. A complete user manual and a listing of the program are

provided in the Appendix to NCHRP Report 12-36 (Ghosn, Deng, Xu, Liu and Moses 1997). The program was found to provide acceptable agreements with the results of experimental tests on full-scale and model-scale composite steel girder bridges as will be discussed in the next section.

2.5 MODEL VERIFICATION.

The verification of the program NONBAN and the modeling scheme proposed in this chapter to study steel I-beam bridges is accomplished by comparing the results of NONBAN to those of a full-scale laboratory test and a model-scale test. The full-scale test was performed in the Laboratory of the University of Nebraska (Kathol, Azizinamini and Luedke 1995) while the model test was performed in Canada (Razaqpur and Nofal 1988).

2.5.1 Nebraska's Full Scale Bridge Test

The bridge was designed, constructed and tested in the Structural Laboratory of the University of Nebraska-Lincoln for a project sponsored by the Nebraska Department of Roads (Kathol, Azizinamini, and Luedke 1995). The test was performed on a full-scale bridge model having a span of 70 feet and is 26 feet wide. The superstructure consists of three welded plate girders built compositely with a 7 1/2 in reinforced concrete deck. The girders are spaced 10 feet on center and the reinforced concrete deck has a 3-ft overhang.

Figure 2.10 shows this bridge's cross section. The plates forming the girders consist of a 9"x ¾" top flange, a 54" x $^{3}/_{8}$ " web, a 14" x 1 ¼" center bottom flange, and 14"x ¾" end bottom flange. Intermediate web stiffeners consist of a total of 4 5/16 in thick plates spaced at 39.5 inches and 10 plates at 67.2 inches. Shear studs 7/8 in diameter and 5 inches tall are spaced 18 at 7 inches, 14 at 9 inches, and 16 at 10 3/16 inches from left to right. The studs are placed symmetrically about the girder centerline.

During bridge construction cross-frames ("K-Frame" type) were placed at 11.2 feet spacings. For the ultimate load test, the cross frames were removed and the bridge was loaded in both lanes simultaneously until failure. The bridge failed when shear punching occurred under one loading point in the slab. Figure 2.11 shows the loading configuration used by Kathol, Azizinamini & Luedke (1995). These loads simulate two side-by-side vehicles having configurations similar to one HS-20 truck in each lane.

To obtain the material properties, strength tests were performed on steel samples and concrete cylinders. The average results of these tests are summarized in Table 2.1 which is adapted from the reference by Kathol, Azizinamini & Luedke (1995).

To perform the structural analysis using the approach proposed in this study, the bridge is modeled as a grid as shown in Figure 2.12. Each longitudinal girder is divided into 10 equal elements. The contribution of the slab to the longitudinal strength and stiffness is considered by using the properties of the composite section. The contribution of the slab to the transverse distribution of the load is effected by 11 transverse beams. The points

of application of the wheel loads are represented by the symbol "□" in Figure 2.12. Since these points do not correspond to actual nodes on the grid model, nominal (artificial) elastic beams with negligible stiffness are used to connect these points to the adjacent nodes.

Elastic and inelastic member properties are calculated for all beam sections. The longitudinal girders' composite moment of inertia is found to be 66955 in^4. The ultimate moment capacity is 77493 kip-in for positive bending. The bare steel section produces a moment of inertia of 21332 in^4 and the ultimate moment capacity is 35988 kip-in. The middle transverse beam representing the contribution of an 83 in wide portion of the slab has a moment of inertia equal to 2980 in^4, the torsion coefficient, J_x, is 5840 in^4 (from $J_x=bt^3/6$ as proposed by Hambly, 1991) and the ultimate moment capacity is 746 kip-in. The end transverse beams have moments of inertia and ultimate moment capacity equal to1/2 those of the middle beams. The moment curvature relation of the concrete transverse beams are obtained using concrete beam theory.

The dead load is divided into a permanent dead load and a superimposed load. The permanent dead load applied on the bare section is equal to 0.092 kip/in. The superimposed dead load applied on the composite girders is 0.023 kip/in.

Tests to determine the ultimate load capacity of the bridge were performed by applying various levels of loads through hydraulic jacks (Kathol, Azizinamini, and Luedke 1995). The loads were increased until punching shear failure occurred in the slab under one of

the load pads. The researchers observed that: "The girders remained elastic until a load level equal to 12 times the weight of HS-20 trucks... The location of the neutral axis did not change throughout the loading process indicating that composite action remained at very high load levels..." Punching shear failure in the slab occurred at a load level corresponding to 16 times HS-20 trucks. The deflection at that load level was measured to be approximately 7.1 in. Although the load deflection curve was beginning to flatten out at that point, it was evident that the ultimate capacity of the main girders was not reached (Kathol, Azizinamini and Luedke 1995).

The program NONBAN is run assuming that the sections are composite and accounting for the different properties of the edge beams and interior beams. For the edge beams however, the effect of the railings was ignored. Since the middle diaphragms were removed before the ultimate load test, the NONBAN model ignored their presence. Also, the model ignored the presence of the edge diaphragms since their contribution at this point is mainly for stability of the loaded structure. NONBAN used the Texas curve to model the behavior of the composite compact sections in positive bending (Equation 2.15 and Figure 2.8).

Figure 2.13 shows a comparison between the laboratory results (Kathol, Azizinamini, & Luedke, 1995) and the results of NONBAN. Reasonably good agreement is observed in the figure for the whole range of the loading process including the prediction of the yielding load and the nonlinear loading path. The results show that the ultimate capacity was not reached in the test but that the slab punching shear failure occurred at a load level

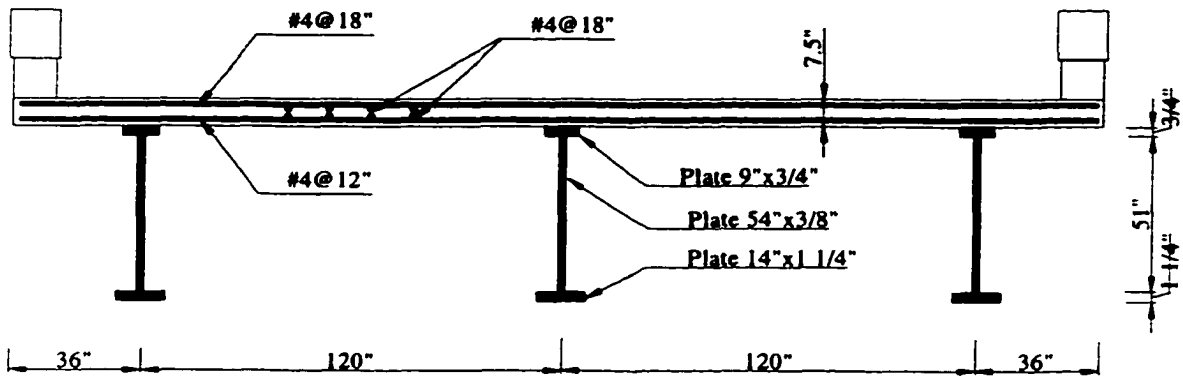

Figure 2.10. Cross section of Nebraska bridge.

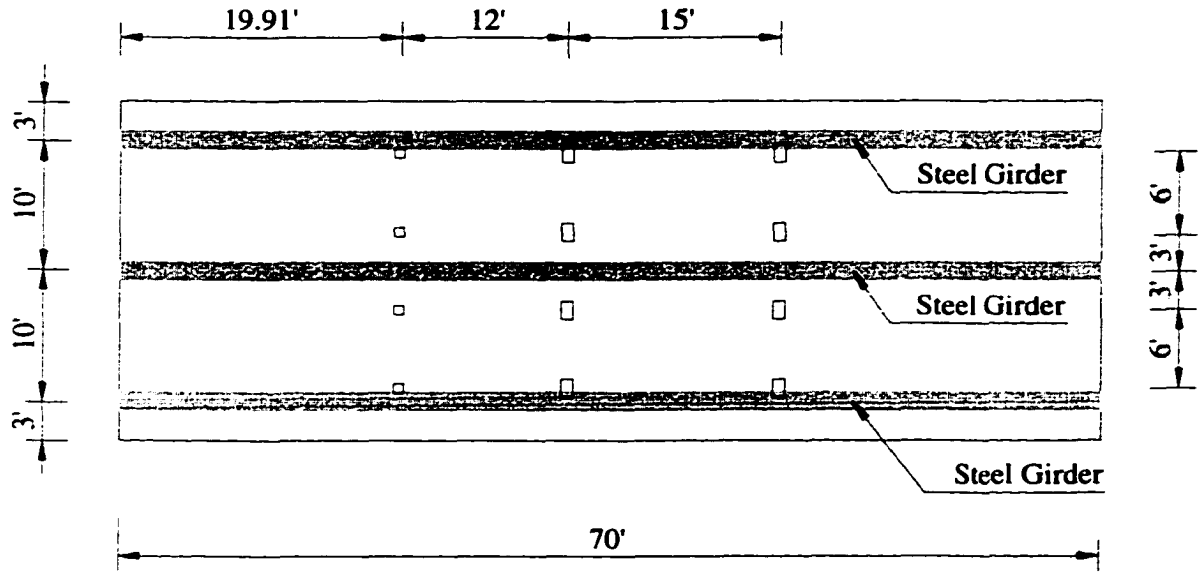

Figure 2.11. Loading configuration simulating two H20 trucks in each lane.

Table 2.1. Summary of material strengths for Nebraska bridge.

Material	Yield Strength f_y (ksi)	Ultimate Strength f_u (ksi)	Young's Modulus E (ksi)
Structural Steel	41.73	65.56	27,600
Rebar	72.6	119.35	27,550
Concrete		6.151	4,470

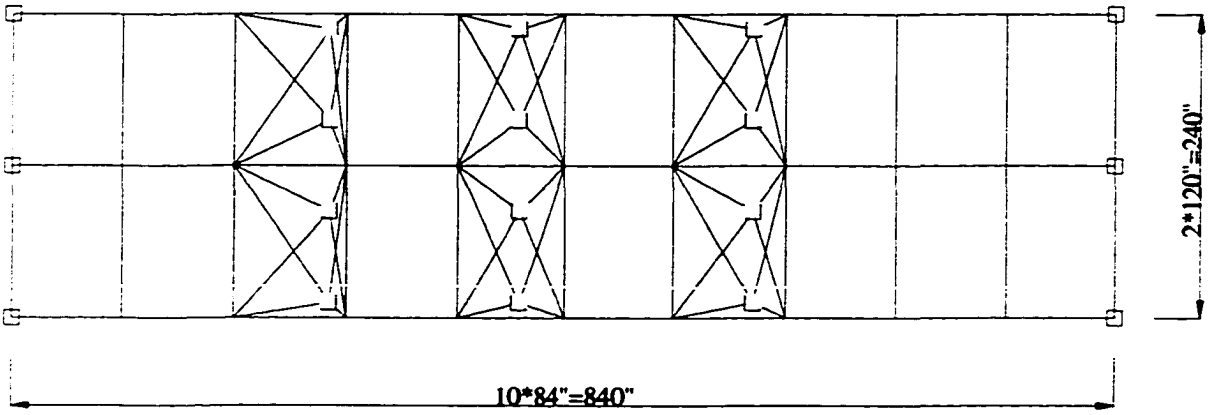

Figure 2.12. Grid mesh used to model the Nebraska bridge.

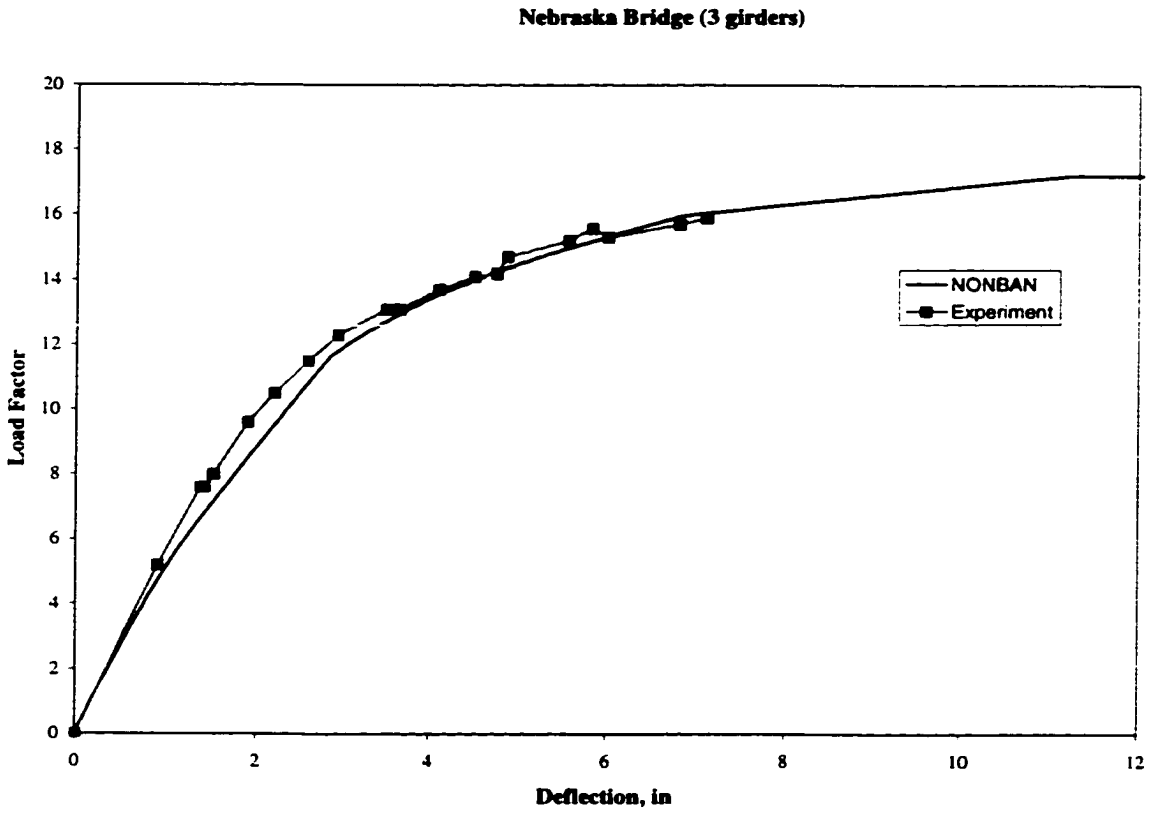

Figure 2.13. Comparison of results between NONBAN and the experiment for Nebraska bridge.

slightly lower than ultimate. Because accurate models to predict the punching shear capacity of bridge decks were not available, NONBAN was run without considering the possibility of punching shear failures. If no limits on member ductility are assumed and ignoring shearing failures, NONBAN predicted that the ultimate load would be reached at a load factor corresponding to 17.21 times the two HS-20 trucks. This corresponds to the formation of a mechanism which is manifested by obtaining large levels of deformation for a very small increment of load.

2.5.2 Canada's Bridge Model Test

The Canadian laboratory test (Razaqpur and Nofal 1988) was performed on a model of a simple span bridge with a span length equal to 6m. The bridge consists of three steel W250xs9 rolled I-beams with 6000 mm span supporting a 70 mm deck slab as shown in Figure 2.14. Core samples were used to estimate the strength of the concrete in the deck and the steel of the beams. The beams and the slab were built to act as composite sections. The bridge model did not have any midspan cross frames or diaphragms. The material properties are given in Table 2.2.

Tests to determine the ultimate load capacity of the bridge were performed using an actuator. The loads simulated a three-axle truck configuration. The loads were applied at three points above the middle girder as described by Razaqpur & Nofal (1988) and shown in Figure 2.15. The loads were then increased until the ultimate capacity was reached. To prepare the mesh for the NONBAN analysis, the length of the bridge is again divided into

ten equal segments. The longitudinal beams are connected by eleven transverse beams representing the transverse capacity of the slab.

Figure 2.16 shows a comparison between the laboratory results published by Razaqpur, & Nofal (1988), and the results of NONBAN. Reasonably good agreement is observed in the figure for the whole range of loading including the prediction of the yielding load and the maximum load. It is observed that the NONBAN results produced an ultimate load of 719.5 kN. This value is similar to the maximum load measured in the laboratory, which is equal to 720 kN. This example gives an illustration of the validity of the program NONBAN and the proposed method to model the nonlinear behavior of steel members.

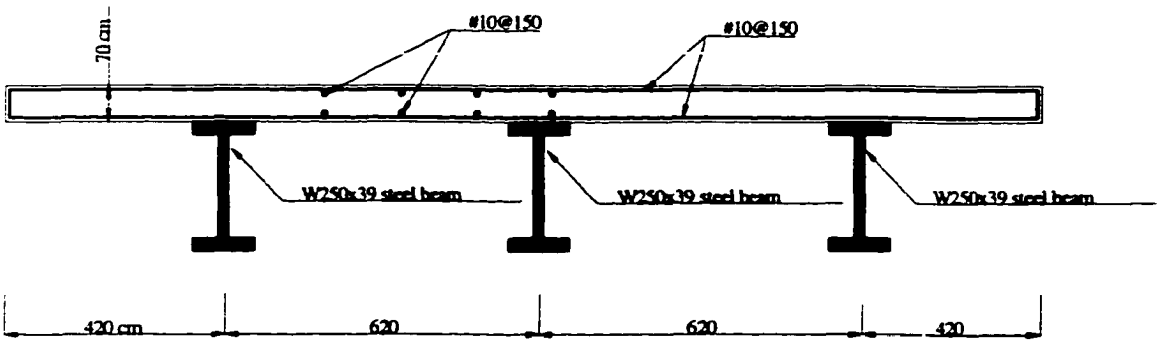

Figure 2.14. Cross section of Canada's bridge model.

Table 2.2. Material properties for Canada bridge.

Material	f_c (kPa)	f_t (kPa)	σ_y (kPa)	ε_y	ε_u	E (GPa)
Concrete	42.1	3.5		0.0005	0.0045	31
Reinforcing bar			400	0.002	0.02	200
Structural steel			300	0.002	0.02	150

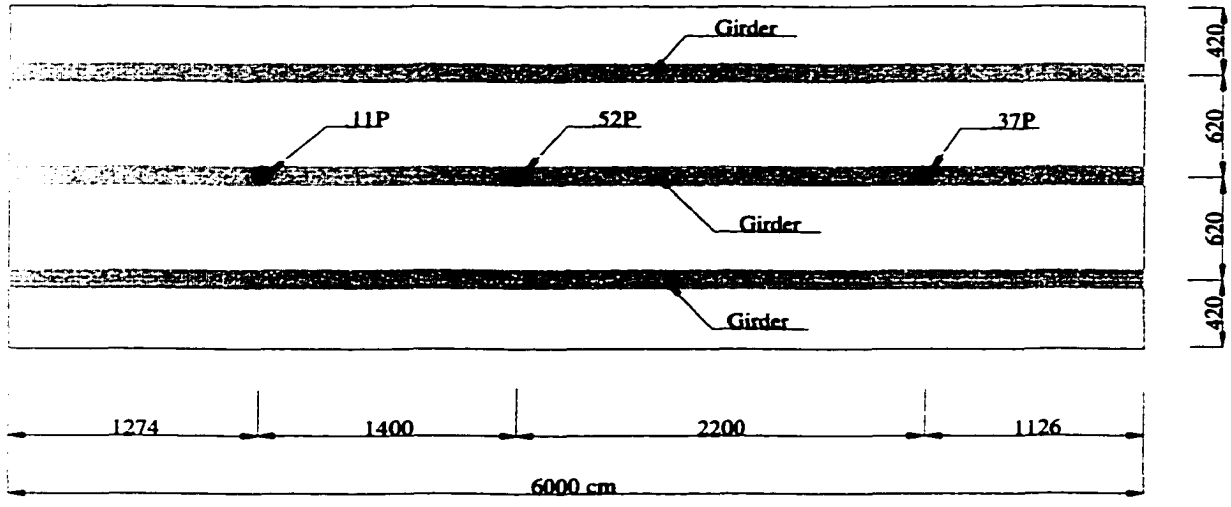

Figure 2.15. Load Positions used in ultimate capacity testing.

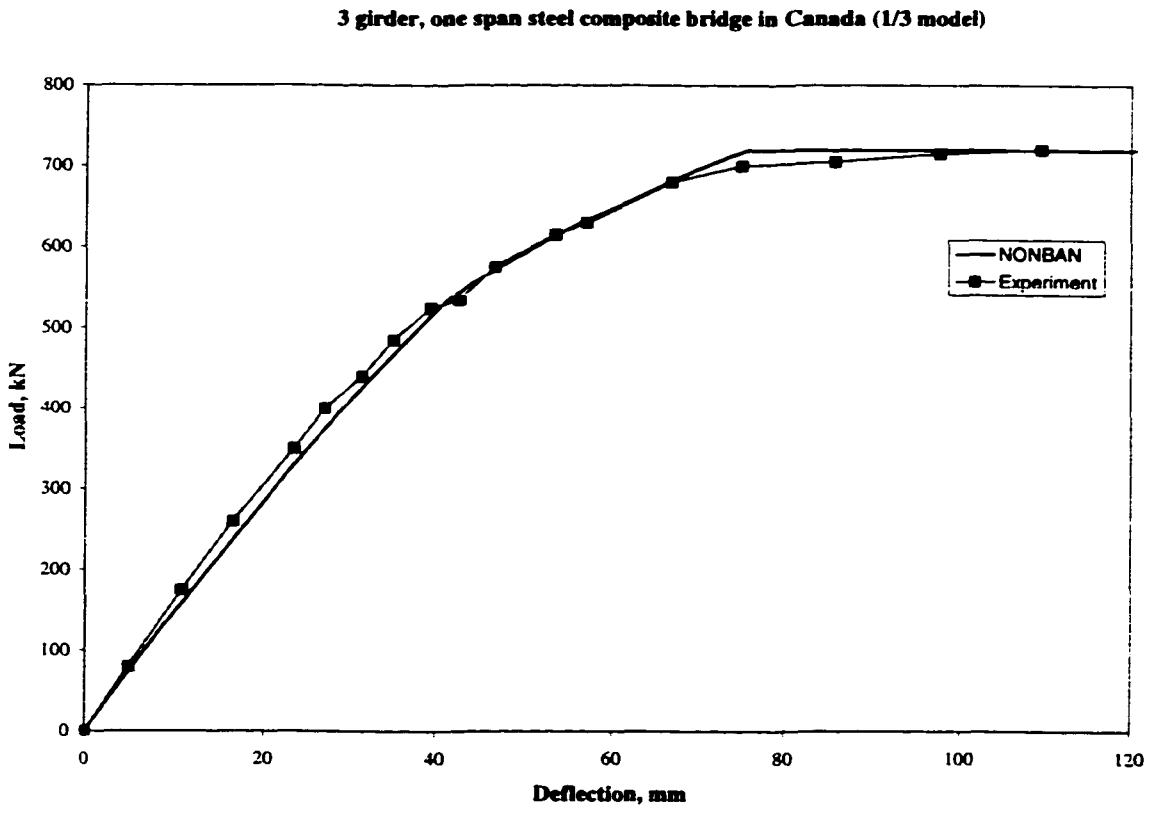

Figure 2.16. Comparison of NONBAN results to experiment results of Canada bridge.

2.6 SENSITIVITY OF RESULTS TO MESH-SIZE.

From experimentation with the grid method it has been observed that there are two factors that may affect the results of the nonlinear analysis. The first one is the stopping criterion (i.e. the definition of failure). The second one is the stability of the mesh size. Several stopping criteria have been used with NONBAN. These include: 1) The formation of a plastic hinge mechanism; 2) A large level of deflection rendering the bridge non-functional; 3) A maximum plastic hinge rotation in a beam element causing the element to unload; 4) Punching shear failures. In many practical situations Criteria 2) 3) and 4) may occur before a mechanism forms. Criterion 2) implies a certain level of subjective judgement in order to define the level of displacement that would render a bridge nonfunctional. Ghosn & Moses (1998) have used a maximum deflection of span length/100 to define the functionality limit state. In addition, most experimental investigations on bridge structures have shown that punching shear failures normally occur in secondary members (e.g. slab), thus eliminating the need to use Criterion 4) for most practical situations as this implies a local failure rather than the collapse of the bridge. Criterion 3) implies that a bridge is considered to have failed when the plastic rotation in a main load-carrying member reaches a limiting value. The limiting rotation value is normally obtained from experimental results depending on the materials properties (e.g. for composite member failure occurs when the strain in concrete reaches its ultimate value causing the crushing of concrete or when the steel fractures as it reaches its tensile capacity). For example, Schilling & Morcos (1987) have shown that

steel composite girders in positive bending have very high ductility levels. This would justify the unlimited ductility assumption used during the analyses of the two simple span bridges mentioned above although NONBAN can accept any limits that the operator chooses to use.

Based on their experience with the grillage analysis of elastic bridges, Hambly (1991) and Zokaie et. al. (1991) have recommended to discretize bridges into 10 equal elements in the longitudinal direction to obtain good results during the linear elastic analysis. The experience of the writers confirm this recommendation even for the nonlinear analysis as long as the moment rotation relationship used during the analysis is obtained from experimental results and is used as recommended in this chapter. This recommendation is made based on several successful comparisons between the results of NONBAN and those of published experimental tests. As an illustration of the robustness of the proposed mesh discretization procedure, the results obtained by NONBAN for different mesh sizes are compared to those of the experimental data for the bridge test performed in Nebraska. Figure 2.12 shows the mesh of the base case that divided the longitudinal girders into ten equal beam elements. The results obtained show good agreement with the test results as illustrated in Figure 2.13. If the mesh size is changed such that the longitudinal girders are divided into 5, 20, or 40 equal elements, the final results are as good as those of the base case as shown in Figure 2.17. It is noted however, that the change in the mesh size did produce some difference in the final failure point. The cause of this difference is in the approximation involving the derivation of equation 2.19. This difference is

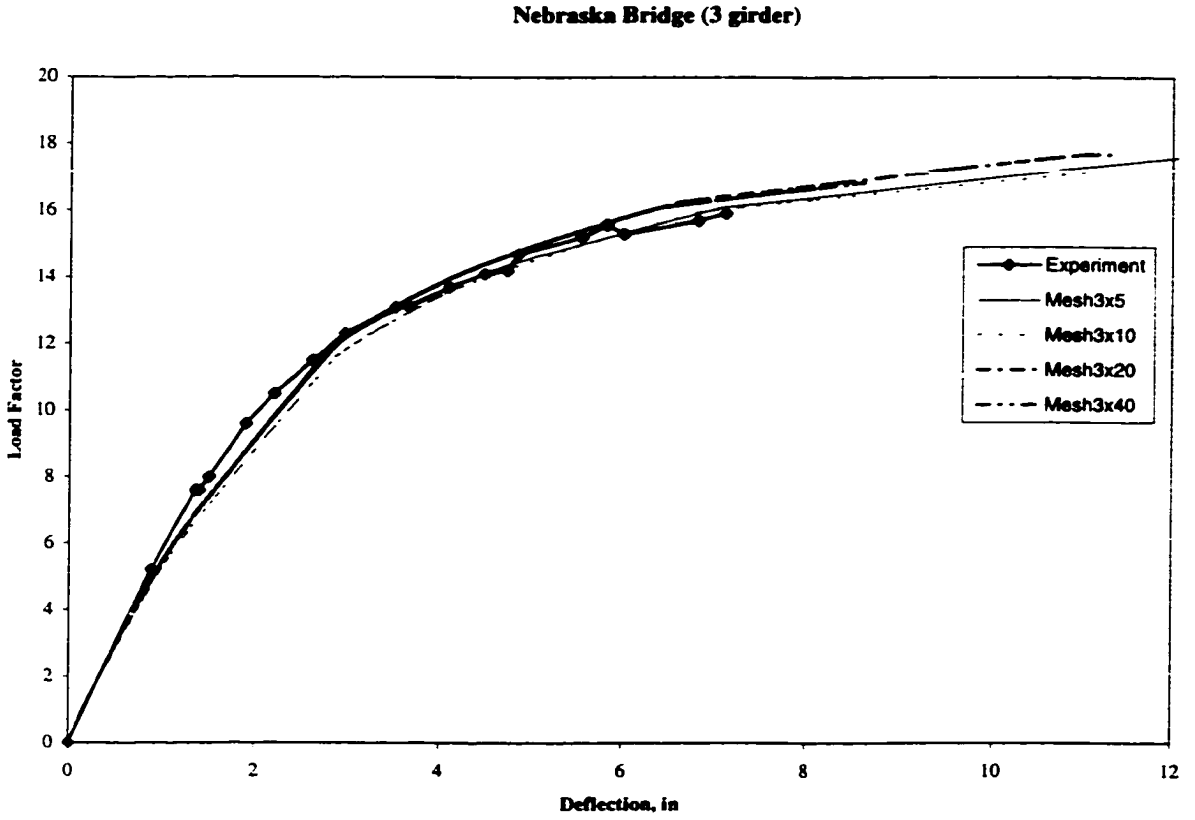

Figure 2.17. Results of Nebraska bridge for different mesh sizes compared to experiment results.

manifested by having different displacements at failure while the ultimate loads obtained from the different meshes show negligible differences.

2.7 CONTINUOUS STEEL BRIDGES

Continuous steel bridges whose members exhibit both positive as well as negative bending can be analyzed using the same approach described above. The negative bending moment-curvature relationship, M-φ curve, can be obtained from experimental moment-plastic rotation, M-θ, curves using the same steps of Equations 2.5 to 2.15. Experimental M-θ curves for compact, ultracompact and noncompact sections in negative bending are available in the literature. For example, Schilling (1989) provides such curves for different section slenderness ratios. For low slenderness ratio, the experimental curve may be represented as shown in Figure 2.18.

Using the same definitions given above, the curve in Figure 2.18 can be expressed as:

$$\theta = (16.67M - 11.67)\chi(0.7,1.0) \qquad \text{(Eq. 2.21)}$$

Resulting in the following expression for the plastic curvature:

$$\varphi(M) = \frac{1}{L}(33.33M - 11.67)\chi(0.7,1.0) \qquad \text{(Eq. 2.22)}$$

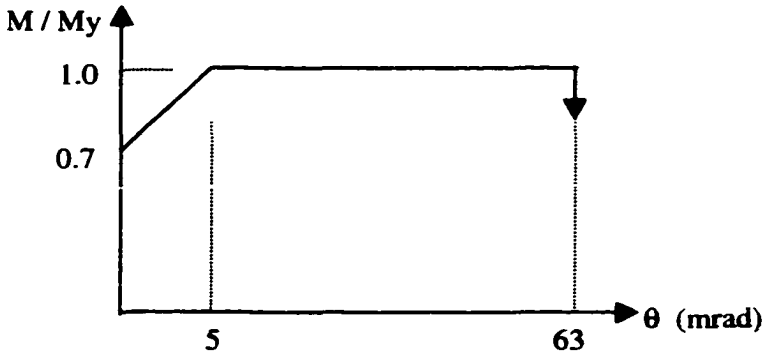

Figure 2.18. M-θ curve for negative bending moment.

Given the moment-curvature expression of Equation 2.15 and Equation 2.22, the standard analysis procedure developed above can be used to analyze continuous steel girder bridges. The validity of the approach is demonstrated using the results of the Tennessee field test (Burdette & Goodpasture, 1971).

2.7.1 Tennessee Field Test

The Tennessee field test was performed by Burdette & Goodpasture (1971) on a four-span continuous bridge with span lengths of 70ft, 90ft, 90ft and 70ft. The bridge consists of four steel W36x170 rolled I-beams at 8.25 ft spacing supporting a 7 in deck slab. Sections over the piers are W36x160 with 10 ½ "x 1" cover plates at the bottom. The loads were placed to simulate an HS truck in each lane of the second span. Burdette & Goodpasture (1971) give a more complete description of the tested bridge. Core samples were used to estimate the strength of the concrete in the deck and the steel of the beams. The beams and the slab were built to act as composite sections.

Tests to determine the ultimate load capacity of the bridge were performed by anchoring a rod into the rock below the bridge and jacking. The loads were then increased until the ultimate capacity is reached. The researchers observed that: "The first evidence of distress was related to the diaphragms when a noticeable and audible slip occurred between the diaphragm and the steel girders... The behavior of the bridge was almost linear elastic up to yielding of the section under the applied loads... At a load of about 650 kips, a crack occurred between the curb and slab near the first pier and tension cracks

were visible in the deck over the pier... After yielding, the bridge "lifted off" the abutment... Eventually, plastic hinges developed near the center pier and the web of the exterior girder buckled at the formation of the hinge..." Shortly after, compression failure occurred at one of the curbs and the test was terminated at a load of 125 kips.

The program NONBAN was run assuming that the contribution of the curbs and overhang to the properties of the longitudinal edge beams is similar to the effect of half the slab in the interior beams. Thus, all four longitudinal girders are assumed to have the same properties. Since the diaphragms broke early in the loading process, and since no information was provided about the properties of the diaphragms, the NONBAN model ignored their presence. For cases where the diaphragms are important, NONBAN can account for the their nonlinear behavior all the way until failure. To prepare the mesh for the NONBAN analysis, each span is divided into ten equal segments. The NONBAN analysis used the composite properties of the longitudinal beams for regions of positive bending. In the negative bending regions, the beam properties assume non-composite action but include the effect of the cover plates and the reinforcing steel of the slab. Since the amount of reinforcing steel was not provided in the reference, typical values were used. In this case it is assumed that the area of reinforcing steel is 3226 mm^2. The longitudinal beams are connected by forty-one transverse beams representing the transverse capacity of the slab. The possibility of having shear failures in the slab is not considered in this example.

Figure 2.19 shows a comparison between the field results published by Burdette & Goodpasture, (1971) and the results of NONBAN. Excellent agreement is observed in the figure for the whole range of the loading process. This includes the prediction of the yielding loads and the ultimate load. In this analysis, bridge members are assumed to have an infinite level of ductility. Thus, the ultimate capacity is reached when a mechanism forms which is manifested by obtaining large levels of deformation for a very small increment of load. This example demonstrates the validity of the proposed model and the program NONBAN to perform the nonlinear analysis of typical continuous steel bridges as well as simple span bridges. The method requires a valid moment-curvature relationship that accurately represents the behavior of the girders of the bridges being analyzed. For bridges with unusual designs, the Texas and Shilling curves used in this chapter may not be applicable, and additional research may be required to verify these curves' validity for such cases before applying them in conjunction with the model proposed in this chapter.

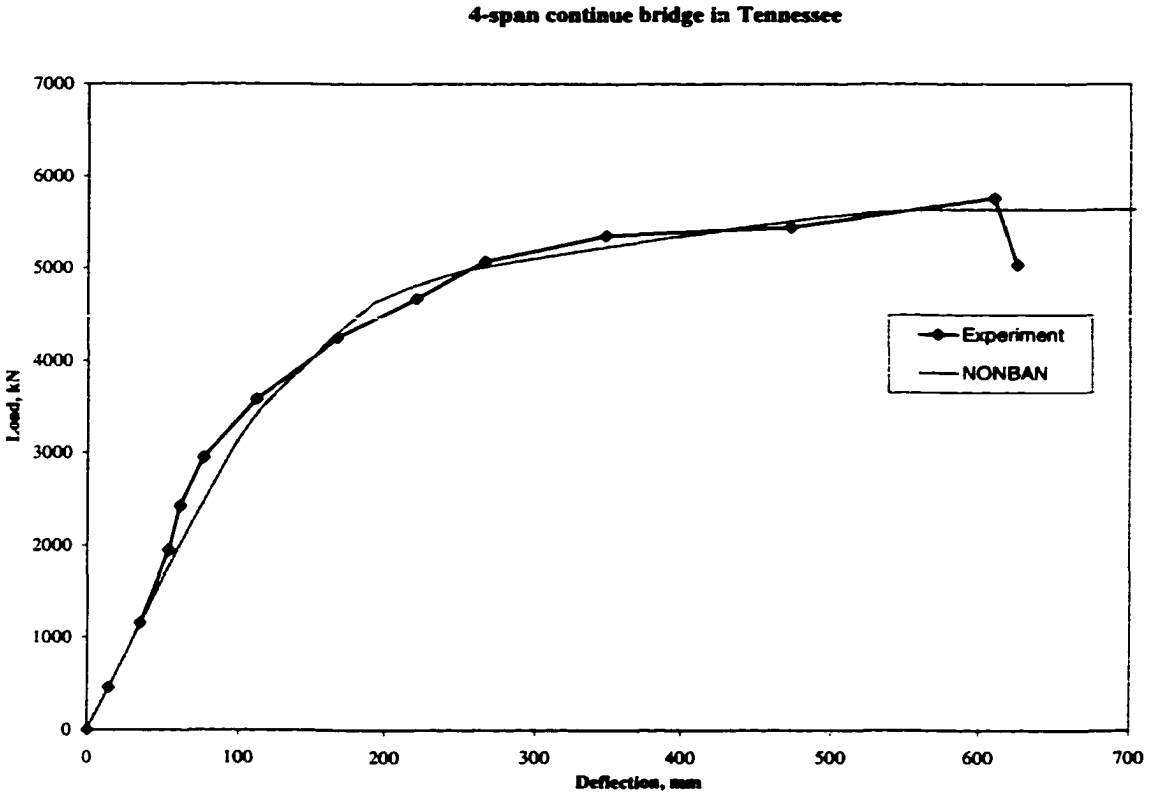

Figure 2.19. Comparison of experimental and NONBAN results for 4-Span continuous bridge in Tennessee.

2.8 SUMMARY

This chapter described a method to analyze the nonlinear response of steel girder bridges. The method has the following features:

- It is based on a nonlinear grillage analysis using an incremental loading technique to derive a complete load versus deflection curve.
- The input data is similar to that required for the linear analysis of bridges. This data consists of the bridge geometry (mesh) as well as the linear elastic properties of the members (moments of inertia, modulus of elasticity, etc.). The only additional input data required is the ultimate moment capacity of each section M_p and shear capacity as well as the moment versus curvature, and shear versus shearing strain relationships.
- The method can predict the load path realistically both for simple-support and continuous bridges. Particularly, reasonably accurate results are obtained when the moment curvature relationship is derived from experimental steel beam tests such as the ones conducted at the University of Texas.
- The method provides a simple tool that can be used to obtain detailed descriptions of the nonlinear behavior and ultimate capacity of highway bridges.
- The validity of the model was verified by comparing the results to those from in-situ experimental tests and from full scale and model scale laboratory tests.

- The model proposed in this chapter can be used to predict the complete nonlinear behavior of straight steel I-girder bridges. Such information may be useful for designing new bridges for ultimate limit states and for the rating of existing bridges. Using the complete nonlinear behavior of bridges in the rating process may result in a reduction in the retrofitting needs.
- Because the model produces a complete load versus deformation curve for each bridge structure, the bridge designer (or rater) would be able to check the deflection of a bridge at different load levels to ensure that the bridge remains functional at high live load levels. It is also recognized that serviceability criteria should be independently checked.

CHAPTER 3

NONLINEAR FLEXURAL BEHAVIOR OF PRESTRESSED CONCRETE GIRDER BRIDGES

This chapter presents a procedure to improve the accuracy of the classical grillage method for the nonlinear analysis of concrete girder bridges. The procedure uses equivalent element plastic hinge lengths that account for the actual mesh size instead of using a mesh-independent global plastic hinge length. A thorough review of the results of tests conducted on two 1/3 model prestressed concrete girders and a 1/3 model prestressed concrete girder bridge is undertaken in order to model the nonlinear properties of prestressed concrete girder bridges. The purpose of this review is to study the extent of plastification and plastic hinge length development as well as the evaluation of the validity of the grillage method for the nonlinear analysis of girder bridges. A L_p-transfer model is used to calculate the plastic hinge length for every beam element of the grillage based on the results from the experiments and other empirical models. The L_p-transfer model allows the use of empirical data obtained from tests on individual girders to model the response of a variety of bridge configurations subjected to different loading conditions. The equivalent grillage element plastic hinge length, L_{gp}, is calculated as a function of the grillage mesh size. A number of examples are presented to demonstrate the validity of the proposed method by comparing the analytical results of grillage analysis using the L_p transfer model with those of laboratory and in-situ experimental tests of full scale and model scale prestressed concrete bridges. The proposed approach

has a high potential for use in engineering practice because of the simple input requirement and improved accuracy.

3.1 INTRODUCTION

The stiffness matrix method, and particularly the grillage analysis approach, is widely used to perform the linear–elastic structural analysis of bridge systems. For example, the AASHTO-LRFD (1994) Specifications propose a set of empirical equations for calculating the girder distribution factors that were obtained based on the grillage analysis of typical bridge configurations (Zokaie, Osterkamp & Imbsen, 1991). In addition, the Specifications encourage engineers to perform their own analyses using either the grillage approach or more refined finite element methods to obtain more accurate results. In Europe, where bridge design specifications do not provide load distribution factors, bridge engineers rely on structural analyses to predict the distribution of the applied forces to individual bridge members. In most instances, engineers use a grillage type analysis to study the load distribution to individual members and to evaluate the safety of their designs. (Hambly, 1991).

The traditional grillage analysis method consists of modeling a bridge superstructure as a grid formed by linear elastic beam elements. The main members of the bridge system are modeled as longitudinal (composite or noncomposite with the slab) beam elements along the main axis of the bridge. The lateral distribution of the load to the longitudinal members, effected by the slab and diaphragms, is modeled by a number of transverse

beams. This approach is used for slab bridges, slab on girder bridges, as well as spread box beam bridges and multi-cell box girder bridges (Hambly,1991).

Most applications of the grillage method in bridge analysis are based on the linear elastic stiffness matrix approach. Researchers have adopted the grillage method to perform nonlinear analyses by updating the element stiffness matrices at every load increment to reflect the reduced stiffnesses that occur when portions of the elements (longitudinal or transverse beams) plasticize (Razaqpur & Nofal, 1988). A second approach assumes that plastic zones concentrate at the ends of each beam element where plastic hinges would form. The effect of the plastic zone is modeled through springs that connect the elastic portions of the elements to the end nodes (Livesley, 1970). The typical application of the second method for the nonlinear analysis of bridge systems has been described in several publications (Ghosn, Casas & Xu,1996 and Ricles & Popov, 1994). The model implies that the elastic parts of adjacent beam elements are joined at the nodes by means of flexible connections. These flexible connections are modeled as rotational springs (or hinges). When members are still in the linear elastic range, the stiffnesses of the connections are infinitely high. As the plastification (or nonlinearity) caused by bending stresses spreads, the connections become more flexible. The relationships between the moments in the beam elements and the rotations of the plasticized connections are represented by the stiffnesses of the rotational springs. Although these stiffnesses are not necessarily linear, they can be assumed to be piecewise linear. Hence, this model can be used in an incremental nonlinear structural analysis. The effect of shear nonlinearity can

also be considered by using displacement springs. This model can be represented as shown in Figure 3.1 (Ghosn & Casas, 1996).

The formulation of the nonlinear stiffness matrix of a beam element is based on the assumption that the linear elastic section of the beam is in series with nonlinear springs at each of its ends (nodes I and J, as shown in Fig. 3.1). Inelastic flexural and shear deformations developed in these nonlinear springs, in addition to the elastic flexural and shear deformations, give the total deformation of the nonlinear beam. The relationship between the deformations of each hinge and the element's end generalized forces (forces and moments) can be represented by multi-linear curves as shown in Figure 3.2. The derivation of the stiffness matrix of a beam with ends connected to rotational springs is given by Livesley (1970) or Ghosn, Casas, & Xu (1996). As an example, the element stiffness matrix for the element shown in Figure 3.1 can be expressed as shown in Figure 3.3 neglecting the effect of shearing deformations. The stiffness matrix shown in Figure 3.3 assumes uncoupling between the torsional stiffness and the bending stiffness of the beam element at all load levels and assumes a linear elastic behavior in torsion. The nonlinear flexural effects are represented by the slopes of the plastic M-θ (moment-rotation) curve which can be derived from the M-φ (moment-curvature) relationship of each element as will be discussed further below.

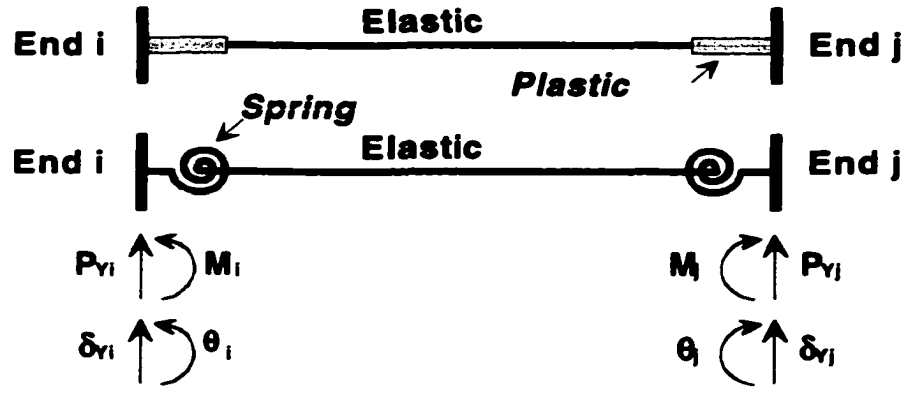

Figure 3.1. Plastic hinge model for nonlinear analysis of bridge members.

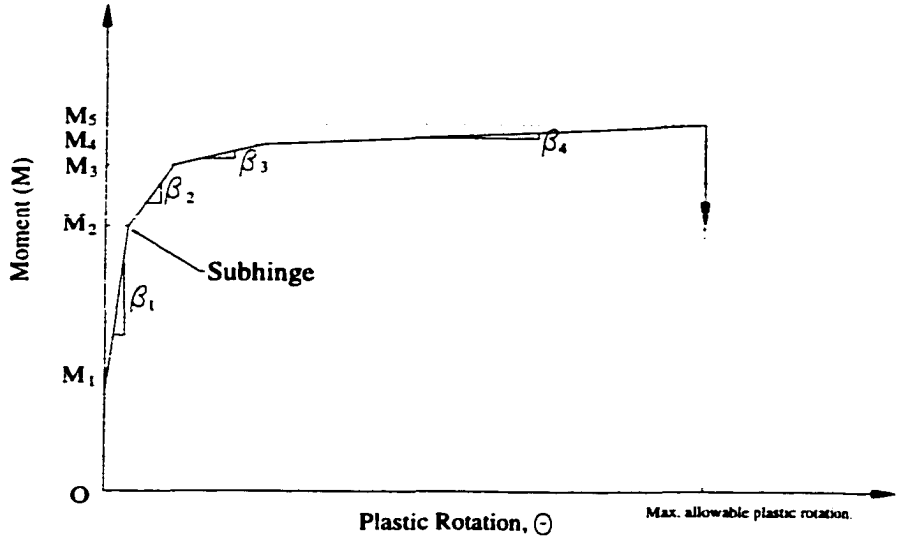

(a) Moment-plastic rotation curve

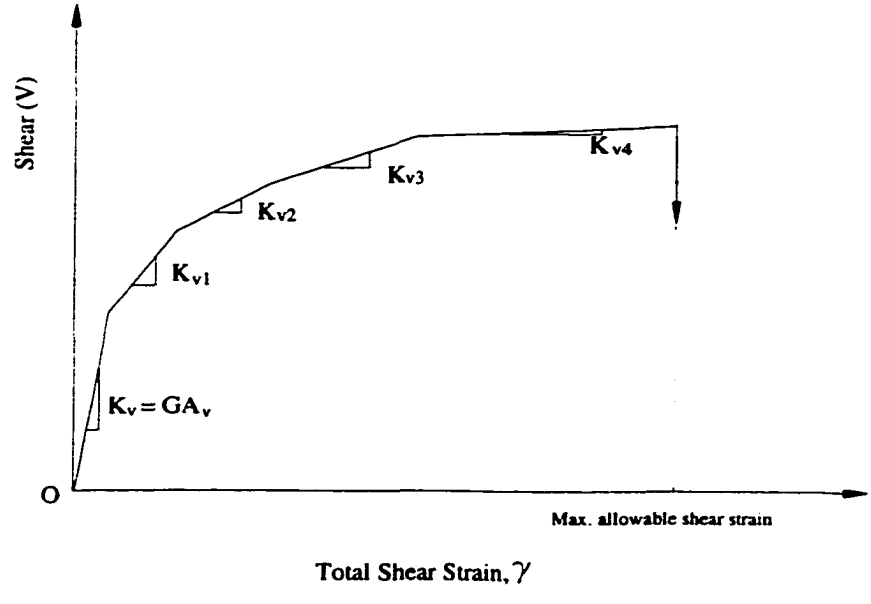

(b) Shearing force-shearing strain curve

Figure 3.2. Idealized load-deformation relationships of nonlinear springs.

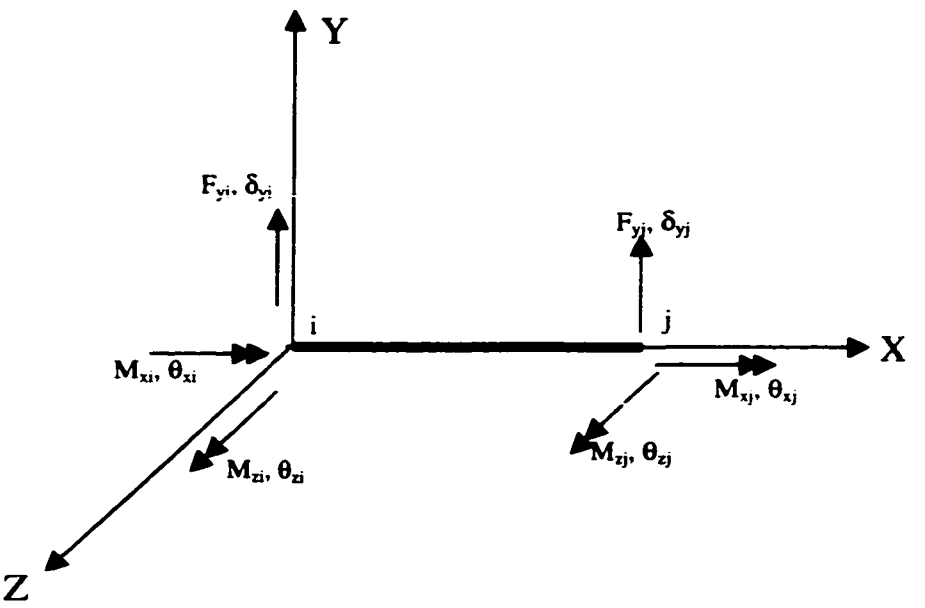

(a) Local coordinates system.

$$\begin{bmatrix} F_{yi} \\ M_{xi} \\ M_{zi} \\ F_{yj} \\ M_{xj} \\ M_{zj} \end{bmatrix} = \begin{bmatrix} K_{1,1} & 0 & K_{1,3} & K_{1,4} & 0 & K_{1,6} \\ 0 & K_{2,2} & 0 & 0 & K_{2,5} & 0 \\ K_{3,1} & 0 & K_{3,3} & K_{3,4} & 0 & K_{3,6} \\ K_{4,1} & 0 & K_{4,3} & K_{4,4} & 0 & K_{4,6} \\ 0 & K_{5,2} & 0 & 0 & K_{5,5} & 0 \\ K_{6,1} & 0 & K_{6,3} & K_{6,4} & 0 & K_{6,6} \end{bmatrix} \begin{bmatrix} \delta_{xi} \\ \theta_{xi} \\ \theta_{zi} \\ \delta_{yj} \\ \theta_{xj} \\ \theta_{zj} \end{bmatrix}$$

(b) Stiffness matrix of one beam element.

$$K(1,1) = K(4,4) = 6*\left[-1+\frac{3(2+C_1)(2+C_2)}{C_1(4+C_2)+4(3+C_2)}\right]\frac{EI_z}{L^3}$$

$$K(1,3) = K(3,1) = \frac{6(2+C_2)}{C_1(4+C_2)+4(3+C_2)}\frac{\beta_1}{L}$$

$$K(1,4) = K(4,1) = 6*\left[1-\frac{3(2+C_1)(2+C_2)}{C_1(4+C_2)+4(3+C_2)}\right]\frac{EI_z}{L^3}$$

$$K(1,6) = K(6,1) = \frac{6C_2(2+C_1)}{C_1(4+C_2)+4(3+C_2)}\frac{EI_z}{L^2}$$

$$K(3,3) = \frac{4(3+C_2)\beta_1}{C_1(4+C_2)+4(3+C_2)}$$

$$K(3,4) = K(4,3) = \frac{-6C_1(2+C_2)}{C_1(4+C_2)+4(3+C_2)}\frac{EI_z}{L^2}$$

$$K(4,6) = K(6,4) = -K(1,6)$$

$$K(3,6) = K(6,3) = \frac{2C_1C_2}{C_1(4+C_2)+4(3+C_2)}\frac{EI_z}{L}$$

$$K(6,6) = \frac{4(3+C_1)\beta_2}{C_1(4+C_2)+4(3+C_2)}$$

$$K(2,2) = K(5,5) = -K(2,5) = -K(5,2) = \frac{GJ_x}{L}$$

Where: $C_1 = \frac{\beta_i L}{EI_z}; C_2 = \frac{\beta_j L}{EI_z}$

β_i = slope of plastic M-θ curve for end i.
β_j = slope of plastic M-θ curve for end j.
J_x = torsional inertia about x axis.
I_z = moment of inertia about z axis.
L = element length.
E = elastic modulus.
G = shearing modulus.

Figure 3.3. Stiffness matrix of bridge beam element.

3.2 DETERMINATION OF PLASTIC HINGE LENGTH L_P

Performing the nonlinear finite element analysis procedure described above requires the availability of the spring constants β_I and β_J (slopes of M-θ curves) for each end of the discrete element in function of the end rotations θ_I and θ_J. This information is needed to assemble the stiffness matrix. Traditionally, in the grillage analysis method, the spring constants are calculated from the combination of moment versus plastic curvature relationships and the plastic hinge length L_p. The relationship between the moment diagram and the curvature of a concrete beam is described in Figure 3.4 which shows a segment of a reinforced concrete flexural member that has reached its ultimate curvature and bending moment at the critical section. End A of the member is the free end of a cantilever or a point of contraflexure. End B is a column face or the point of maximum moment. The distribution of curvature along the member may be generally described as shown in Figure 3.4.c where the region of inelastic curvature is spread over a segment of the beam length. Along the length of the beam and particularly in the plasticized region, the curvature fluctuates because of the variability in the section properties due to the presence of cracks. The actual curvature distribution at ultimate can be idealized as the summation of an elastic region shown in light gray and a plastic region shown in dark gray in Figure 3.4.c. M_u as shown in Figure 3.4.b is the ultimate moment capacity of the girder. φ_u and φ_u, shown in Figure 3.4.c, are, respectively, the curvature at ultimate and at first yielding.

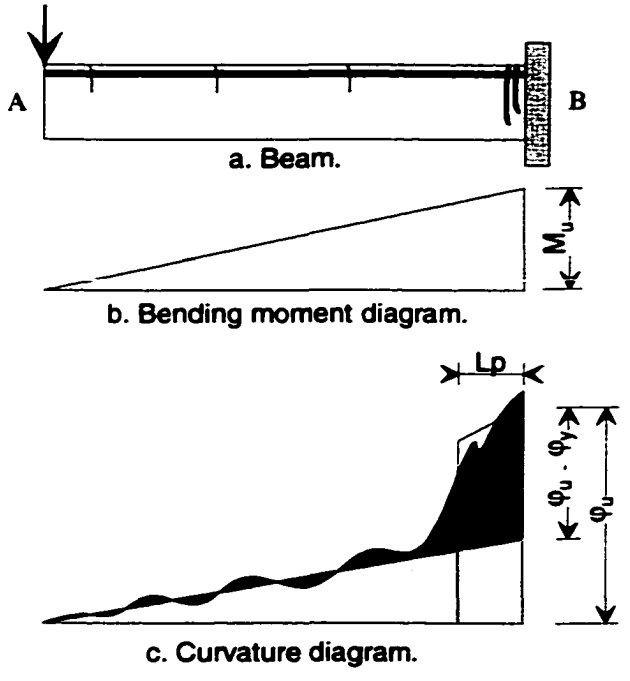

Figure 3.4. Curvature distribution along beam length at ultimate moment.

The contribution of the elastic curvature to the total rotation over the full length of the member is given by:

$$\theta_e = \int_A^B \frac{M}{EI} dx \qquad \text{(Eq. 3.1)}$$

Where EI is the elastic flexural rigidity, θ_e is the elastic rotation over AB, M is the expression for the moment along the length of the beam.

If a fully cracked section is assumed for the elastic part over the full length of the member, EI is given by $EI_{CR}=M_Y/\varphi_y$, where EI_{CR} is the flexural rigidity of the beam's cracked section, M_Y is the moment where the nonlinear range is first reached, and φ_y is the curvature where the nonlinear range is first reached (yield). More accurate expressions for EI that account for partial cracking along the length of the beam are provided by Park and Pauley (1975).

When the beam undergoes nonlinear deformations, its rotation can be calculated by assuming that plasticity is uniformly spread over a length L_p. For example, the dark area of Figure 3.4.c represents the inelastic curvature that develops in the "plastic hinge" region. The curvature for the inelastic zone could be replaced by an equivalent rectangular area of height φ_u-φ_y and length L_p, where φ_u and φ_y are respectively the curvature at ultimate and the curvature when nonlinearity is first reached. This rectangle has the same area as the actual inelastic curvature distribution, as shown in Figure 3.4.c.

L_p is the equivalent length over which the nonlinear curvature is considered to be constant and it is known as the plastic hinge length. Hence, the maximum plastic hinge rotation θ_{max} on one side of the critical section (end B) may be written as:

$$\theta_{max} = (\varphi_u - \varphi_y)L_p \qquad \text{(Eq. 3.2.a)}$$

$$\theta_{max} \approx \varphi_u L_p \qquad \text{(Eq. 3.2.b)}$$

Equation (3.2.b) gives an approximation to (3.2.a) by ignoring the effect of φ_y because the value of φ_y is usually much smaller than φ_u.

The curvatures at ultimate, φ_u, and at first "yield", φ_y, are related to the shape of the cross section and the stress-strain, σ-ε, relationships of the concrete and reinforcing steel. φ_u and φ_y can be determined from basic principles of equilibrium and from general mechanics of materials models for the deformation of beam sections subjected to bending moments . If the σ-ε relationships for steel and concrete are represented by multi-linear curves, then, the resulting M-φ curve can also be represented as a multi-linear curve.

The plastic hinge length, L_p, is affected by many factors, including the applied loading conditions and the shape of the bending moment and shearing force diagrams, the cross section geometry, materials' nonlinear properties, creep, and cracking. L_p is difficult to obtain in closed form. Therefore, various empirical models have been proposed by several researchers to estimate the length of the plastic hinge L_p (Baker,1956; Corley

1966; Mattock, 1967, Sawyer, 1964). In particular Baker (1956) provides two formulas one for members with unconfined concrete, the other is for members confined by transverse steel. Corley (1966) provides a statistically based formula from the work of several international research groups. Mattock's (1967) formula modifies Corley's (1966) model to give better correlation with experimental data and is easier to use. Sawyer's (1964) formula assumes that the ratio of the moment at first yielding to the ultimate M_y/M_u is approximately equal to 0.85, and that the total plastic zone is spread over ¼ the span length.

For common values of span to effective depth ratios, L/d, normally encountered in bridge engineering practice, the values of L_p calculated from the formulas provided by the different researchers are extremely inconsistent. For example, when using L/d = 8 to 25, L_p calculated by Baker's formula lies in the range 0.4d to 2.4d, L_p calculated by Corley's and Mattock's formulas lies in the range between 0.7d to 1.125d and L_p calculated by Sawyer's formula lies in the range between .55d to 1.19d. Because of the large differences and uncertainties observed in the various formulas, many practicing engineers use simple approximations to find L_p as a function of the effective depth of the cross section. For example, Skogman, Tadros, & Grasmick (1988) assume that L_p = d. Others (e.g. Mattcok, 1965) use L_p=0.5 d.

The ultimate concrete strain ε_c is an important parameter that controls the maximum plastic rotation. Baker's formula for unconfined concrete assumes ε_c = 0.0035. Other researchers developed formulas applicable to different values of ultimate strain, ε_c,

varying between 0.004 and 0.01 that are valid for common beam configurations (Baker,1956; Corley 1966; Mattock, 1967, Sawyer, 1964).

Current prestressed bridges are built to maintain composite action between the deck slab and the prestressed beams. Normal construction procedures for concrete decks do not require large levels of transverse reinforcement. Also, the reinforcing steel grid spacing is large compared to the deck thickness. Usually, in properly designed beams, the effective flange width is much larger than the width of the prestressed beam and the neutral axis lies within the flange. In addition, the relatively small width of the girders relative to the effective deck width precludes any confining action in the deck that may be provided by the girders. Thus, even-though large confinement ratios may be present in the girder itself, the concrete in the deck is unaffected by this confinement and the compression zone may be considered to be unconfined. Therefore, Baker's formula for members with unconfined concrete may be used to predict L_p for composite prestressed bridge girders. This formula is given as:

$$L_p = k_1 k_2 k_3 \left(\frac{z}{d}\right)^{\frac{1}{4}} d \qquad \text{(Eq. 3.3)}$$

$$\varepsilon_c = 0.0035$$

Where

- k_1=0.7 for mild steel or 0.9 for cold-worked steel,
- k_2=1+0.5P_u/P_0, where P_u = axial compressive force in the member, and P_0 = axial compressive strength of member without bending moment.

- k_3 = 0.6 when f_c'= 35 MPa (5100 psi) or 0.9 when f_c'=12 MPa (1700 psi); where f_c'=0.85*cube strength of concrete.
- z = distance between critical section and the point of contraflexure.
- d = effective depth of member.
- ε_c = concrete's ultimate strain.

The applicability of Baker's formula for prestressed concrete bridge members is verified by the experimental results performed through the US-Slovene research project DOT 95-200 "Redundancy of prestressed parallel beam superstructures". This verification is undertaken in the following section.

3.3 RESULTS OF INDIVIDUAL BEAM TESTS

Two 1/3 scale composite prestressed concrete girders and a 1/3 scale three-girder prestressed concrete bridge are constructed and tested to investigate their behavior under increasing vertical loads and to verify the proposed analysis model (Znidaric, 1998). The prestressed concrete I girders are each constructed to act compositely with a 1100 mm × 80 mm concrete slab section. The girders are 9.98 m long, spanning 9.68 m between the centers of supports as shown in Figure 3.5. Regular Φ6 mm steel bars are chosen for the main longitudinal reinforcement and Φ3.8 mm smooth steel wires for the stirrups and secondary longitudinal reinforcement. Three grouted 15.24 mm (0.6 in) tendons, each composed of 7 wires of 5.08 mm diameter, are used for post-tensioning of each girder. The effective prestressing force is 127.3 kN per tendon

The σ-ε relationships for the steel bars and tendons are provided in Figure 3.6. Nine 15-cm concrete cubes were taken for each beam during the construction process. Such cubes are used in Europe instead of the standard 150mm (6in) diameter cylinders used in US. Mean values of compressive strength after 28 days were respectively 52.4 and 55.0 MPa for each beam. The concrete σ-ε relations are assumed to be as shown in Figure 3.7 based on projections from typical concrete σ-ε relationships.

Figure 3.8 shows the laboratory set-up of the composite girder tests. A total of 9 strain gauges are attached to the tendons at midspan, at ¼ and ¾ of the span. Twenty-four gauges are attached to the reinforcing steel in each girder and several more onto the reinforcement of the slab and in the concrete. More than 20 strain and displacement transducers are attached to the surface of each girder. Five point loads are applied through two displacement-controlled actuators. The loading scheme simulates the configuration of the presently used Slovenian live load model.

The only difference between the two composite girders was the slight variation in the concrete strength. Girder 1 had a concrete strength=55 MPa. Girder 2 had a concrete strength=52 MPa. Both girders collapsed due to the failure of one of their tendons. The measured strains on the upper side of the concrete slab at failure are 0.00266 for girder 1 and 0.00149 for girder 2. In both cases, cracks in the concrete ended approximately 2 cm from the upper edge of the slab. Figure 3.9 presents the recorded load/displacement

response at the midspan of girders 1 and 2. Figure 3.10 presents the relationships between moments at midspan and the end rotations.

L_p can be calculated for each girder from equation 3.2.b if φ_u and the corresponding θ_{max} are known. Knowing the stress-strain relationships for all the materials forming a section, the relationship between internal bending moment applied on the section and the curvature can be calculated from the basic principles of equilibrium and the section geometry. Given the stress vs. strain curves for concrete, prestressing tendons, and reinforcing steel shown in Figures 3.6 and 3.7, the moment vs. curvature curve for a section at the midspan of girders 1 and 2 are derived as shown in Figure 3.11.

According to Figure 3.11, the maximum curvature φ_u that girder 1 can take before breaking is 0.113 1/m, corresponding to a theoretically calculated moment M_u equal to 523 KNm. Figure 3.10 shows that the maximum rotation, θ_{max} of girder1 is 0.0399 rad when the applied M_u' is equal to 527 KNm. It is noted that the difference between the measured maximum moment M_u' and the calculated M_u is less than 1%. By interpolation, the maximum rotation when M_u=523 kNm is calculated to be 0.0376. Thus, we can approximately calculate the length of the plastic hinge, L_p, of girder 1 for the breaking point from Equation 3.2.b as:

$$L_p = \frac{\theta_{max}}{\varphi_u} = \frac{0.0376}{0.113} = 0.333m = 0.582d$$

Given that the effective depth, d=0.5725m, we observe that 0.333m is equal to 0.582d. Similarly, according to figure 3.11, φ_u of girder 2 is 0.115, when the ultimate moment M_u is equal to 502 KNm. In Figure 3.10, θ_{max} of girder 2 is 0.0333, when the applied moment M_u' is equal to 499.5 KNm. Thus, by interpolation, L_p for girder 2, and using Equation 3.2.b, L_p is calculated as:

$$L_p = \frac{\theta_{max}}{\varphi_u} = \frac{0.0339}{0.102} = 0.332m = 0.580d$$

For an effective depth d=0.5725m, it is observed that L_p=0.580 d.

Using Baker's formula for L_p, Equation 3.3 gives:

$L_p = 0.9*1*0.384(9.69/2/.5725)^{1/4}*0.5725 = 0.337$ m $= 0.589$d.

This value shows that Baker's formula works reasonably well for the two girders described herein with a difference of less than 2%. This small difference is exceptionally good and is not expected to be typical for other test results. It is also noted that the strains in the concrete when the two girders failed due to the rupture of the tendons are: 0.00266 for girder 1, and 0.00149 for girder 2 which are well below the maximum values of 0.0035 assumed by Baker for unconfined concrete. Nevertheless it seems that Baker's formula is reasonable for the analysis of composite prestressed I-girders used in typical bridge configurations.

Although the use of Baker's equation seems to provide accurate estimates for L_p, the formula requires the knowledge of the moment distribution along the length of the girder. In particular it requires as input the location of the points of contraflexure as expressed in terms of z. These are easy to find for isolated simply supported girders such as the ones described in this section. However, girders within a structural system behave in a different manner than isolated girders in an experimental set up. The complexity of the system behavior makes it difficult to exactly predetermine the location of the maximum moments, the location of the plastic hinges and the points of contraflexure. In bridge systems, girders are connected by slabs and diaphragms that allow for the redistribution of the loads so that the whole bridge may continue to support additional loading even after individual members reach their limit capacities. Also, L_p as calculated by Baker is applicable only at the ultimate moment and is not valid throughout the nonlinear loading process and different values have to be used for every loading step. For these reasons, calculating L_p during the nonlinear analysis of a bridge system is found to be a daunting task. To avoid the need to explicitly calculate L_p, an L_p transfer model is developed in the next section.

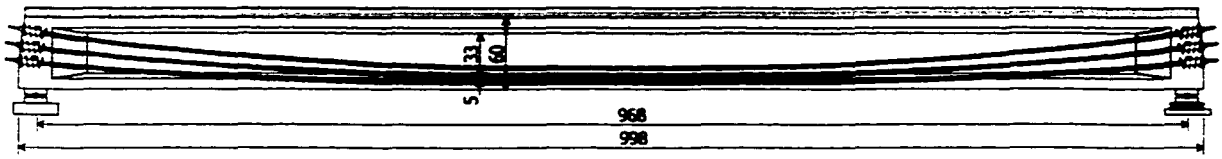

(a) Girder profile

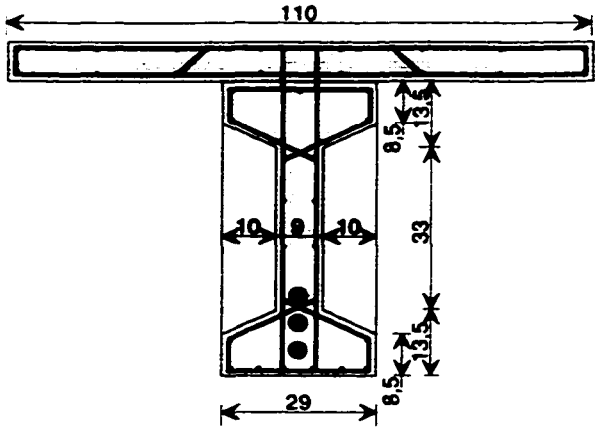

(b). Girder cross section.

Figure 3.5. Elevation and cross section of Slovenia girder 1.

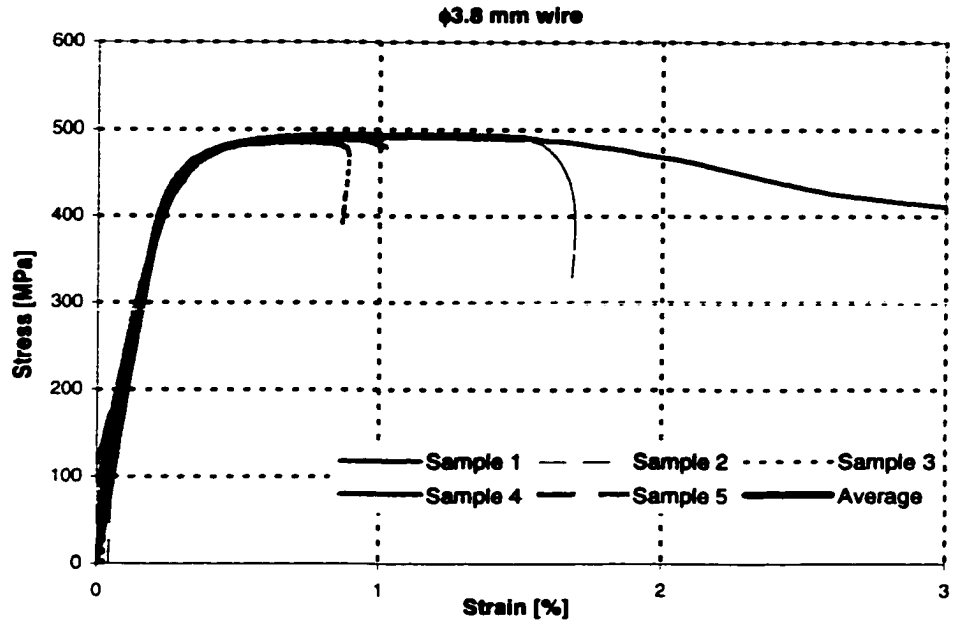

Figure 3.6(a)

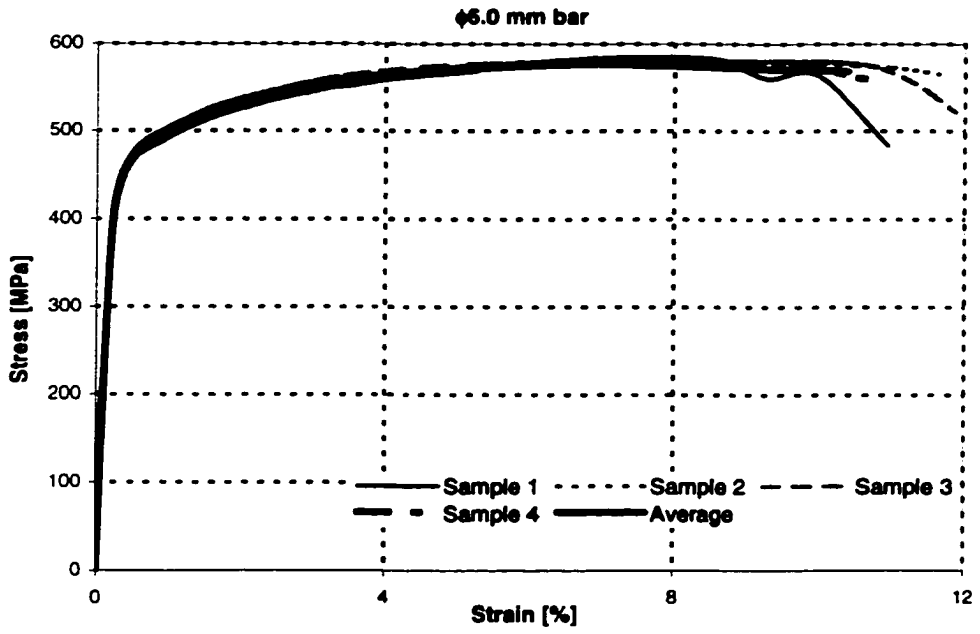

Figure 3.6(b)

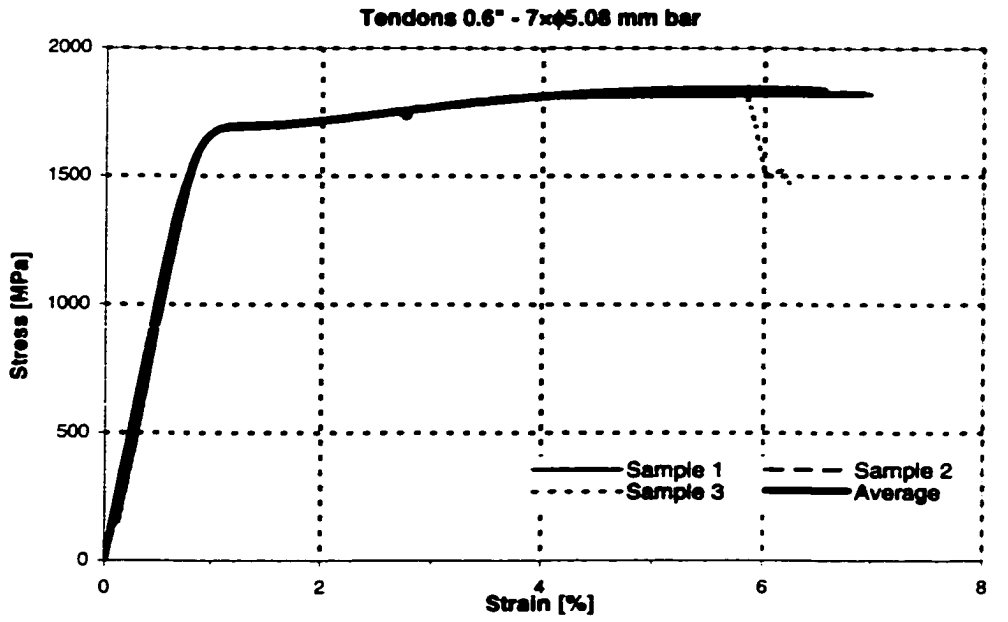

Figure 3.6(c)

Figure 3.6. Stress-strain relationships for steel bars and tendons.

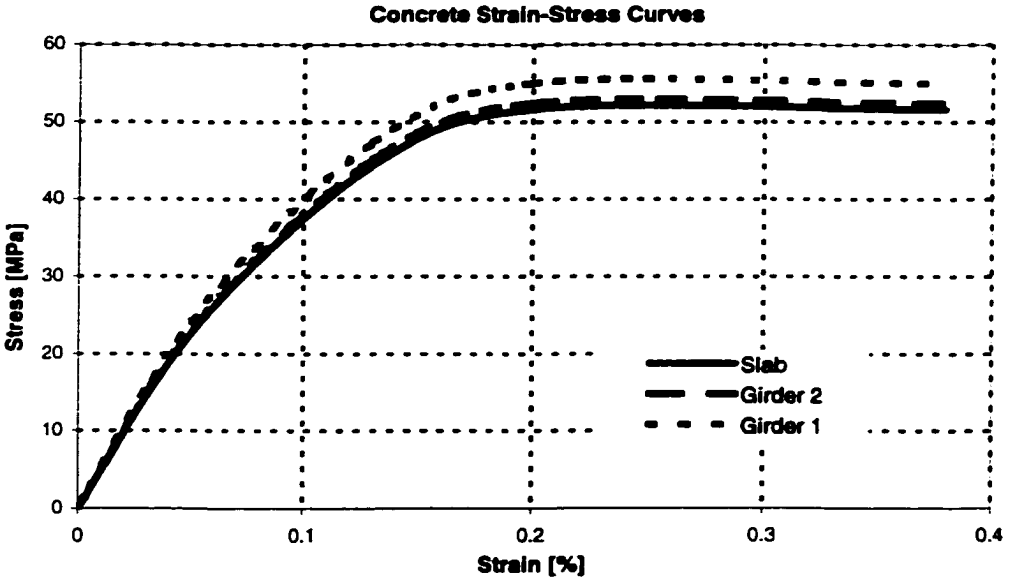

Figure 3.7. Concrete stress-strain relationship for Girders 1, 2 and slab.

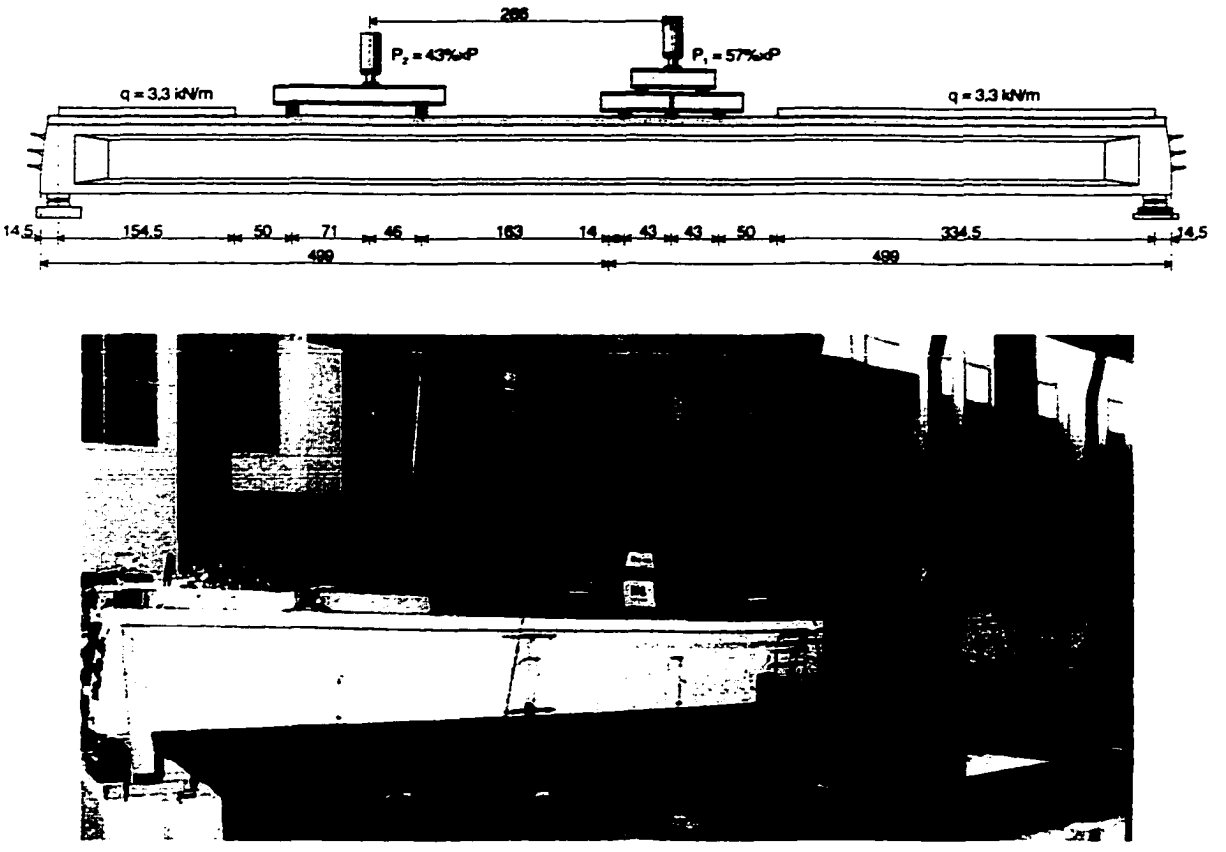

Figure 3.8. Test setup for girder 1 in Slovenia.

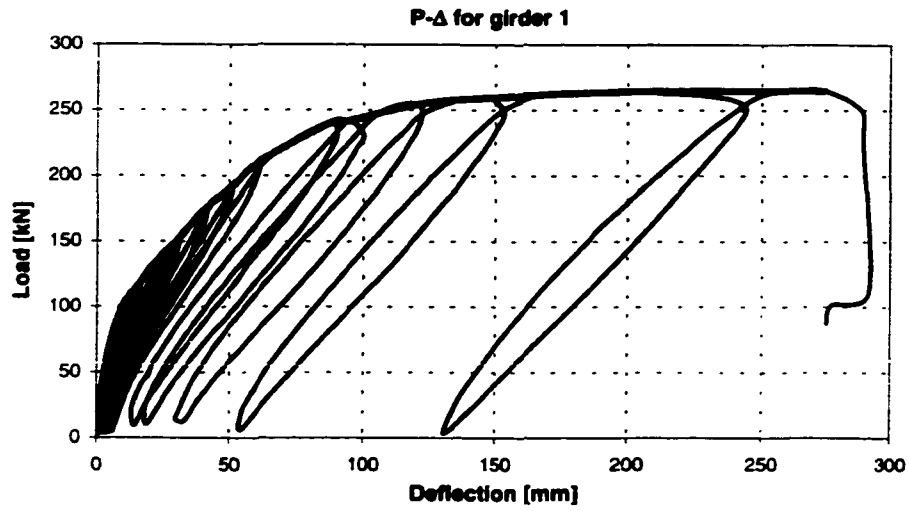

a). Load-deflection response at the midspan of girder 1.

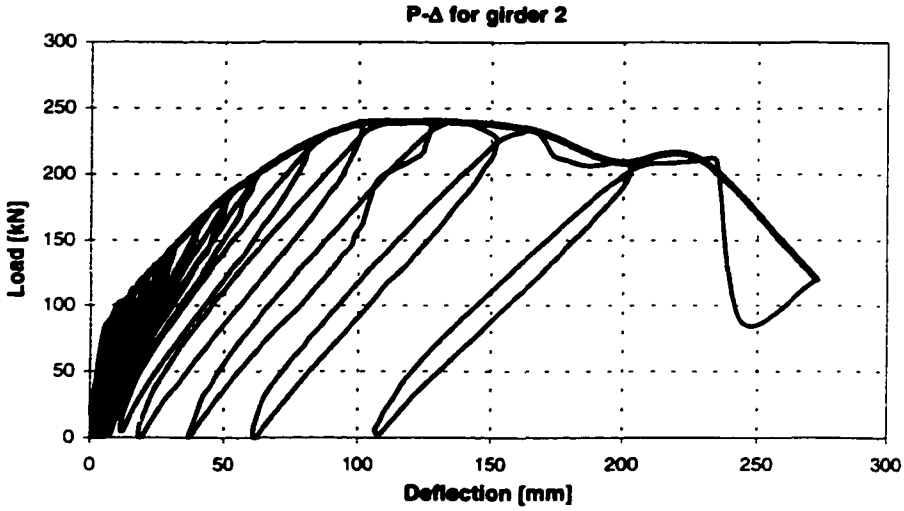

b). Load-deflection response at midspan of girder 2.

Figure 3.9. Load-deflection response at midspan of girders 1 and 2.

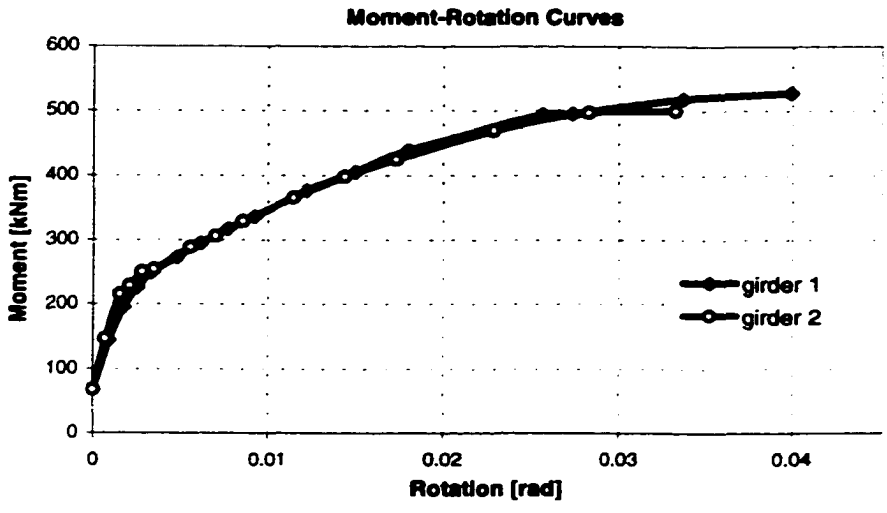

Figure 3.10. Moment-plastic rotation curve of girders 1 and 2.

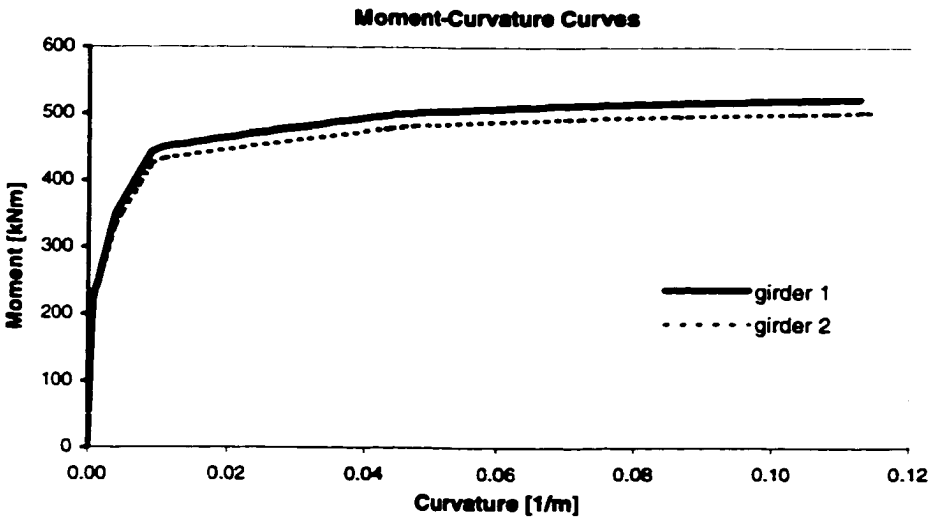

Figure 3.11. Moment-curvature curve of girders 1 and 2.

3.4 DEVELOPMENT OF L_p TRANSFER MODEL

For illustration, let us consider a simple-span concrete girder loaded as shown in Figure 3.12.a. The girder is loaded up to the point when the ultimate moment capacity is reached at the middle of the span. The moment at the end of the plastic zone is equal to M_y as shown in Figure 3.12.b. If we also assume a moment-curvature diagram as shown in Figure 3.12.c, the curvature diagram along the length of the girder can be represented as shown in Figure 3.12.d.

To perform the analysis, this girder, is divided into 20 girder elements. We assume that each girder element's rotation is decomposed into an elastic rotation and a plastic rotation. The effect of the element plastic rotation, θ_{gp}, can be modeled through springs attached to the end of each girder element. This model for element rotations is similar to the model used in Figure 3.1.

Let us isolate one girder element and assume that its curvature diagram is idealized as shown in Figure 3.13. The plastic curvature of the element can be represented as two rectangles with areas equal to $\theta_{gpi} = \varphi_i L_{gp}$ and $\theta_{gpj} = \varphi_j L_{gp}$. θ_{gpi} and θ_{gpj} represent the plastic rotations at ends i and j respectively where φ_i is the plastic curvature at end i of the element, φ_j is plastic curvature at end j, and L_{gp} is the plastic hinge length of the grillage element. Thus, the total plastic rotation of this element, θ_{gp}, is:

$$\theta_{gp} = \varphi_i L_{gp} + \varphi_j L_{gp} = (\varphi_i + \varphi_j) L_{gp} \qquad \text{(Eq. 3.4)}$$

By assuming that L_{gp} is the same for all the elements of a girder, the total plastic rotation of the whole girder, which is discretized as n girder elements, can be calculated by superposition of all the elements' plastic rotations:

$$\theta = \sum_{i=1}^{n} (\varphi_i + \varphi_{i+1}) L_{gp} \qquad \text{(Eq. 3.5)}$$

For the girder, shown in Figure 3.12.a with the curvature diagram shown in Figure 3.12.c discretized into n= 20 elements, only 4 elements out of the 20 are in the plastic range. Thus, the plastic rotation can be calculated as:

$$\theta = \sum_{i=1}^{n} (\varphi_i + \varphi_{i+1}) L_{gp} = 2\left(\left(0 + \frac{7}{3}\right) L_{gp} + \left(\frac{7}{3} + 7\right) L_{gp}\right) = \frac{70}{3} L_{gp} \qquad \text{(Eq. 3.6)}$$

From empirical Equation (3.2.a) and Figure 3.12.c, the total plastic rotation of the whole girder should be:

$$\theta = 2\theta_{max} = 2(\varphi_u - \varphi_y) L_p = 2 * 7 L_p = 14 L_p \qquad \text{(Eq. 3.7)}$$

where θ is the total rotation for the whole beam and θ_{max} is the plastic hinge rotation between the critical section and the point of contraflexure. Hence, to solve for L_{gp} it

would be sufficient to set equation (3.5) equal to Equation (3.2) which for this example gives:

$$L_{gp} = \frac{14L_p}{70/3} = 0.60L_p \qquad \text{(Eq. 3.8)}$$

If the girder is divided into 10 elements rather than the 20 elements used above, we will obtain $L_{gp}=1.0L_p$.

To solve a nonlinear structural analysis problem, the structure may be discretized into girder elements with various possible mesh sizes. The girder geometry, section properties, loading conditions and material properties are known for each element. The moment-curvature relationship of these elements can be obtained from the section dimensions and stress-strain relationships. However, The bending-moment diagram is not known before the analysis is performed and thus L_{gp} cannot be determined before the analysis is actually undertaken. On the other hand, L_{gp} can be calculated following the same steps described above to simulate the behavior of a particular girder with a known loading condition, known moment diagram, and known value of L_p. Once L_{gp} is calculated, it is assumed to be valid for more complicated configurations under the effect of different loading conditions. This method will be referred to as "L_p transfer model". The method also requires that the actual girder have the same mesh element size as the transfer girder used to find L_{gp} but the loading and boundary conditions do not necessarily have to be the same.

In summary, to analyze a bridge system using the L_p transfer model, we can follow the steps outlined in Figure 3.14. These steps are:

- Discretize the bridge system into a mesh of girder elements as shown in Figure 3.14.a
- Build the L_p transfer model for each girder using the same mesh size as that used in the original bridge girder. The transfer model is a simply supported girder with one point load at midspan as shown in 14.b.
- Calculate the Moment-Curvature diagram of the transfer model according to the properties of the girder's section as shown in 14.c.
- Calculate L_p for the transfer model from Baker's formula as shown in 14.d and obtain the total plastic rotation of the transfer girder from empirical Equation 3.2 as: $\theta = 2\theta_{max} = 2\varphi_u L_p$
- Draw the moment diagram for L_p-transfer girder as shown in 14.e.
- Calculate the plastic curvature diagram as shown in Figure 3.14.f. The total plastic rotation is given in function of L_{gp} as:

  $\theta = \sum_{i=1}^{n} (\varphi_i + \varphi_{i+1}) L_{gp}$, where n is the total number of nodes.

- Setting the plastic rotation calculated using Baker's empirical formula to be equal to the plastic rotation calculated from the transfer girder element, then as shown in Figure 3.14.g, L_{gp} for each element becomes:

$$L_{gp} = \frac{2 * \varphi_u}{\sum_{i=1}^{n} (\varphi_i + \varphi_{i+1})} L_p \qquad \text{(Eq. 3.9)}$$

- Repeat the above steps to find L_{gp} for all girders as shown in Figure 3.14.h.

- These L_{gp} values represent the plastic zones of each element of the discretized girders in the original bridge system. The L_{gp}'s are used to perform the nonlinear analysis of the bridge system using the standard grillage method (Figure 3.14.i).

The approach described above can be used to find the effective plastic hinge length L_{gp} in each plasticized girder. Different girders may have different L_{gp} values. But every element of one girder must have the same element length (equal mesh size) and must have the same L_{gp}.

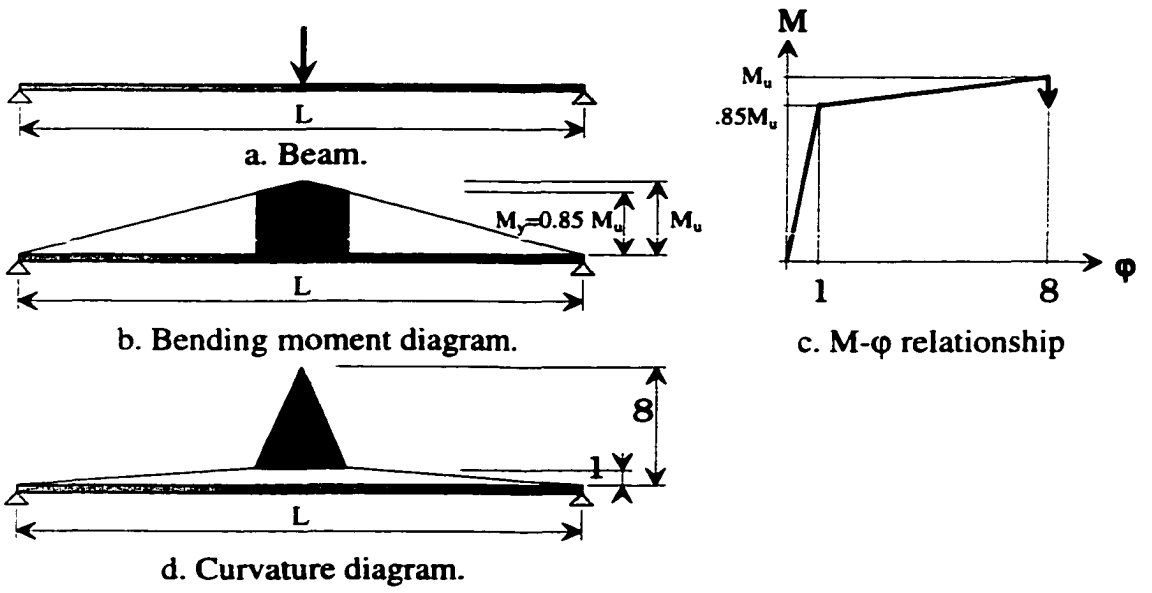

Figure 3.12. Description of L_p transfer model.

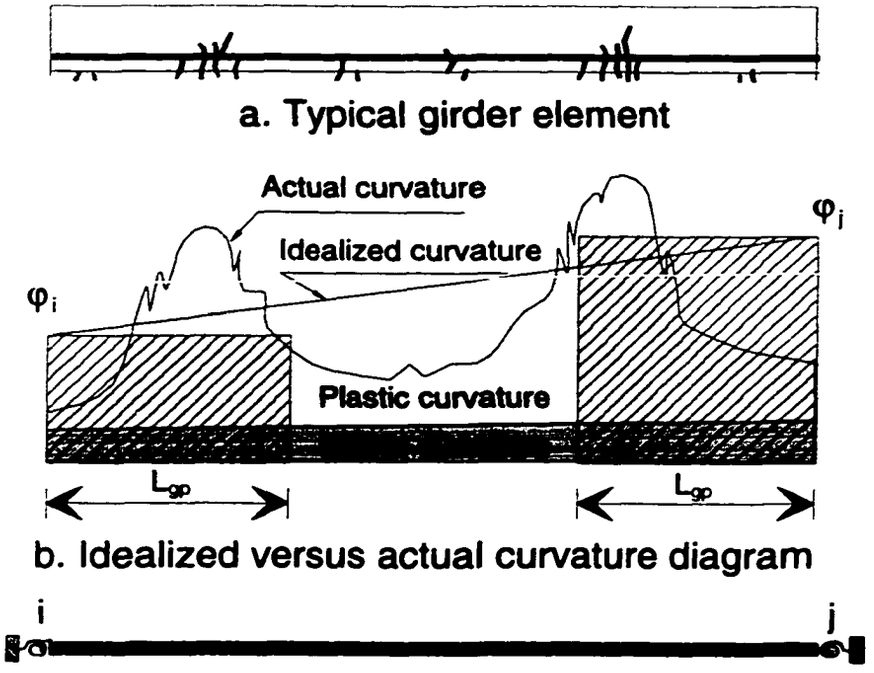

Figure 3.13. Plastification of girder element.

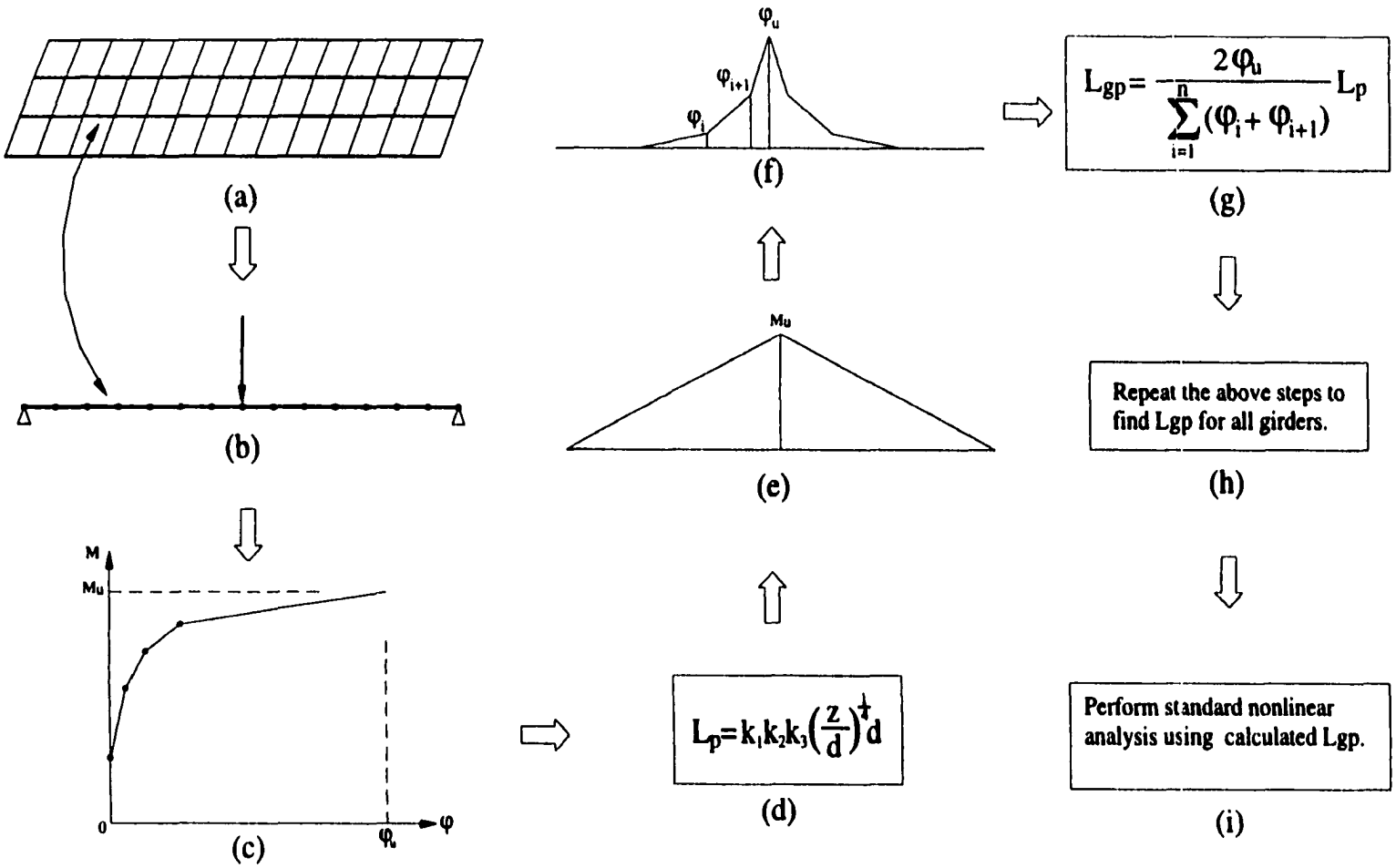

Figure 3.14. Flow chart for analysis procedure.

3.5 GENERALIZATION TO CONCRETE BRIDGE DECKS

The method described above can also be used to find the equivalent plastic hinge length of transverse beam elements that represent the concrete decks of bridges. Transverse elements in a bridge grid model represent the effects of transverse diaphragms or the load transfer capability of the deck slab. While creating the mesh for a complete bridge system, the nodes of the transverse elements are usually defined at the intersection of the slab with the main longitudinal girders. The discrete mesh in the transverse direction can be represented as shown in Figure 3.15.

According to AASHTO's design recommendations (1996), the ratio of the slab's span to the slab's height is between 25 to 35. When a slab's moment reaches its ultimate capacity, the distance, called z, between the critical section to the point of contraflexure is always greater than or equal to half the span length. This will produce an effective z over depth ratio, z/d, in the range of 13 to18. In most actual bridges the deck's concrete strength is on the order of 28 MPa (4 ksi). Given z/d= 18 and f'_c= 28 MPa (4 ksi), Baker's empirical formula (Eq. 3.3) gives a plastic hinge length $L_p \approx d$. Therefore, for simplification it would be reasonable to assume that L_p for transverse beams is always equal to the deck's effective depth, d. Using $L_p = d$, the L_p transfer model can be used to calculate L_{gp} for the transverse beams. If the transverse beam elements are chosen to have nodes at the cross points with the longitudinal members, then $L_{gp} = L_p = d$.

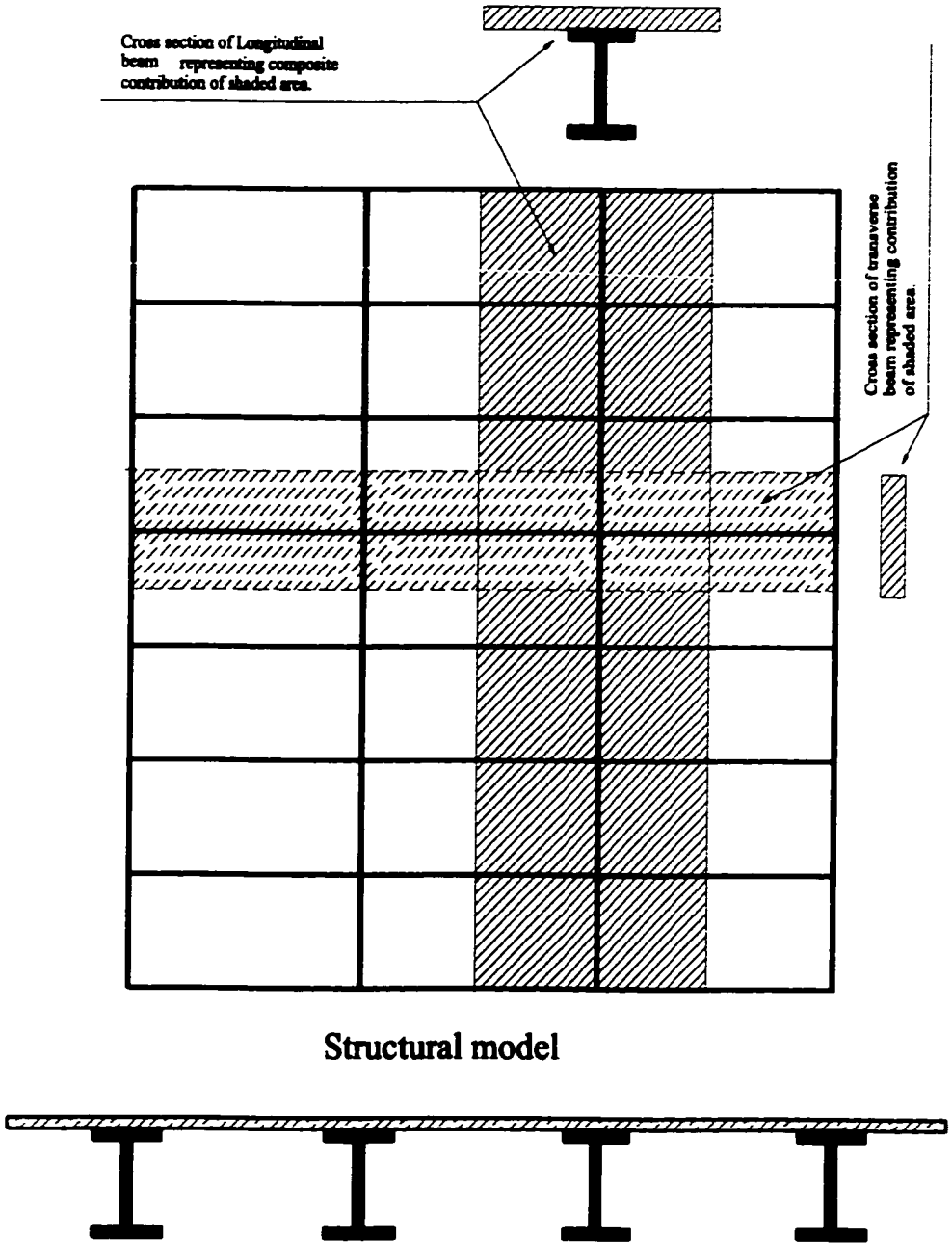

Figure 3.15. Discrete model for grillage analysis

3.6 MODEL VERIFICATION

The program NONBAN (NONlinear Bridge ANalysis) (Ghosn, Deng, Xu, Liu & Moses, 1997) was written to perform the nonlinear analysis of bridge systems using an incremental analysis technique which requires as input the linear and nonlinear properties of the bridge members including the moment-curvature relationship and the equivalent girder plastic hinge length, L_{gp}. To verify the validity of the method proposed in this chapter to calculated L_{gp}, the results of NONBAN are compared to those of three model-scale tests and two full-scale in-situ tests. The model-scale tests are for the two prestressed girders described above and a 1/3 scale bridge model. These tests were performed by Znidaric et. al. (1999) as part of the Slovene-US Research Project DOT 95-200. The two on-site tests were performed in Australia by Gossbell & Stevens (1968) and in Tennessee by Burdette and Goodpasture (1971).

3.6.1 Slovenia girders.

The two Slovenia girders produced the load-deflection curves shown in Figure 3.9. To perform the structural analysis using the approach proposed in this study, the girder is discretized into 40 identical beam elements. The values of L_{gp} are found to be equal to 0.0935 m for girder 1 and 0.122 m for girder 2 by using the L_p-transfer model described above. Figure 3.16 shows good agreement between the experimental results and the analytical results as calculated using NONBAN.

3.6.2 Slovenia bridge.

A model bridge (1/3 scale) with three girders was also designed and tested by Znidaric & Moses (1997, 1998). The bridge's span is 9.98 meter. The spacing between girders is 1100 mm. The bridge's cross section is shown in Figure 3.17.a. Two diaphragms are placed at both ends of the bridge. The girders properties are the same as those of girder 1 described above. The reinforcement steel in the slab is Φ6@200 in the transverse direction and Φ3.8@150mm in the longitudinal direction.

The load configuration used, as shown in Figure 3.17.b, simulates the rating loading scheme with a 5-axle 42-ton semi-trailer used for safety assessment of existing road bridges in Slovenia. The tendon in the edge girder broke at a load of 504 kN. Load redistribution allowed the continuation of the loading until a maximum value of 548 kN was reached that caused a displacement of 122 mm.

To perform the structural analysis using the approach proposed in this study, the girder is discretized into 20 identical beam elements as shown in Figure 3.18. The value of L_{gp} is calculated to be 0.175 m using the previously described L_{gp}-transfer model. Figure 3.19 compares the analysis results to those obtained during the testing.

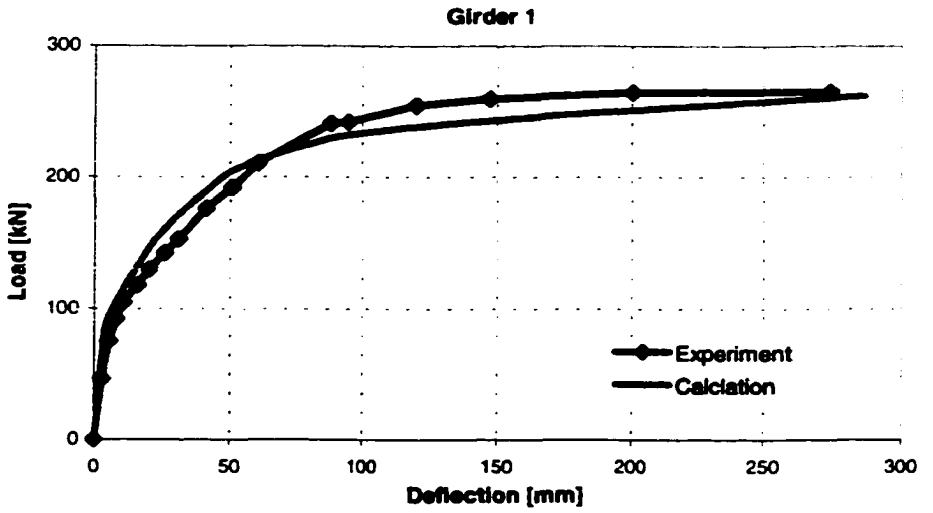

a. Load-deflection curve of girder 1

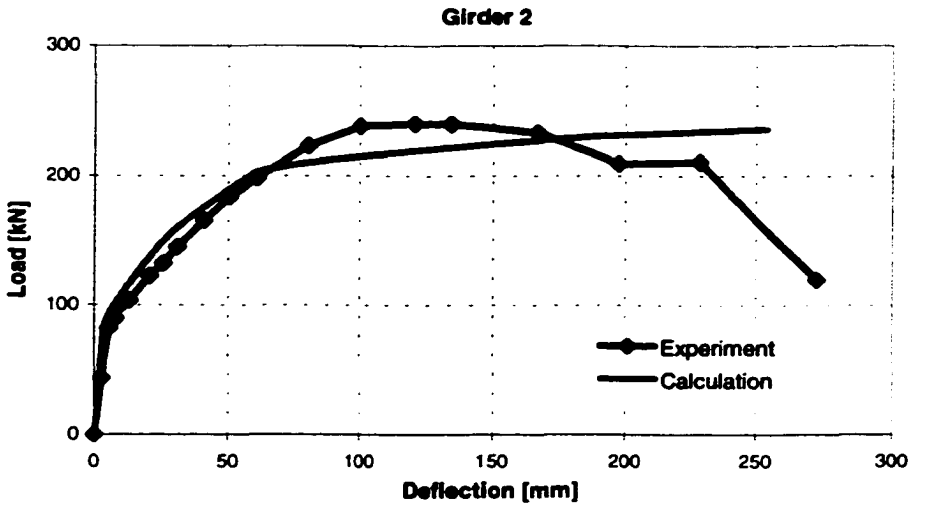

b. Load-deflection curve of girder 2

Figure 3.16. Comparison of NONBAN results to experimental results of Slovenia girders.

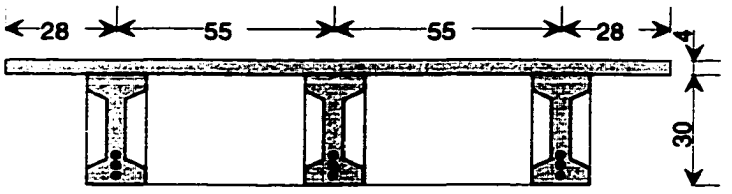

a) Bridge cross section

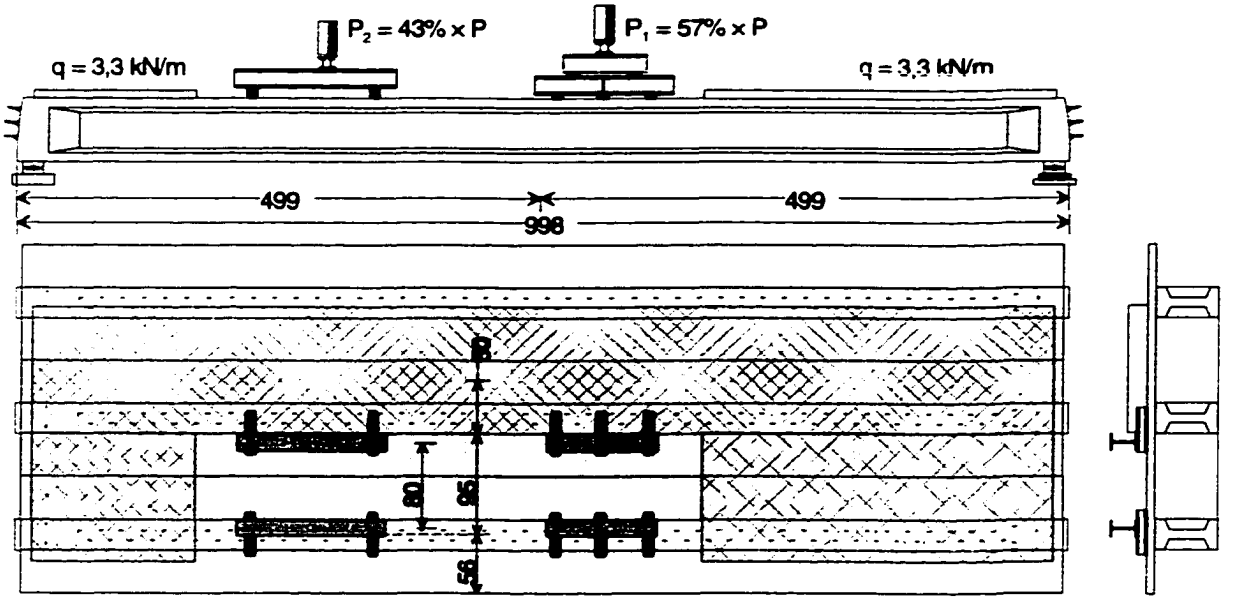

b) Loading configuration

Figure 3.17. Description of Slovenia bridge test set up.

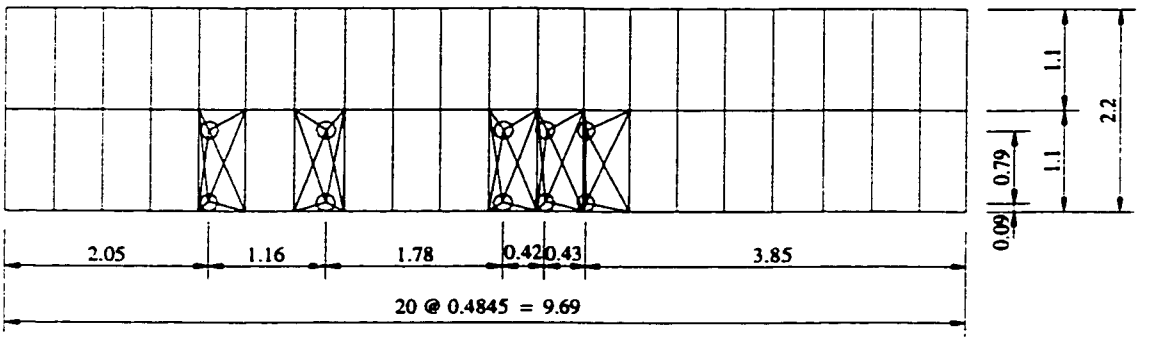

* Symbol O indicates the loading point.

Figure 3.18. Mesh discretization for Slovenia bridge.

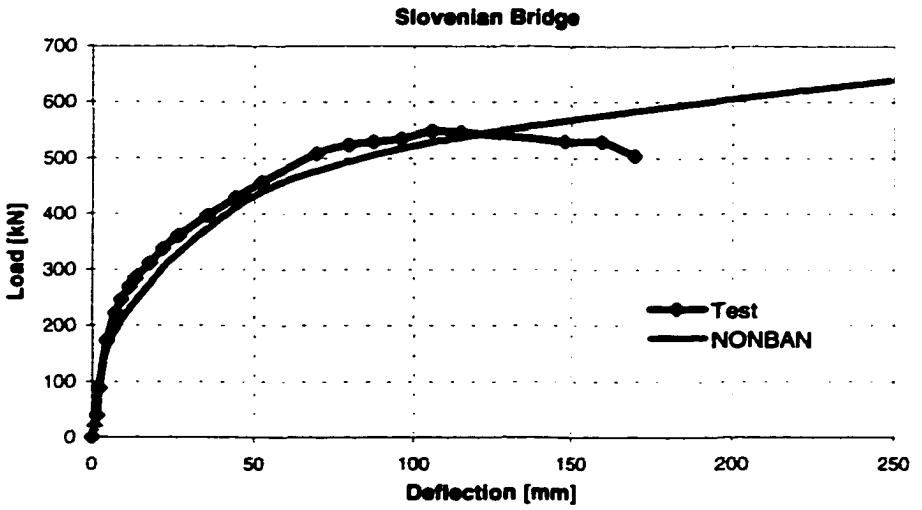

Figure 3.19. Comparison of NONBAN results to experimental results for Slovenia Bridge

3.6.3 Australia bridge.

The Australian field test was performed on a simply-supported bridge with a span length equal to 18.7 m (61.33 ft) Gossbell & Stevens (1968). The bridge consisted of seven prestressed I-beams at 1.45m (4.75) spacings supporting a 15 cm (6in) deck slab as described in Figure 3.20. Gossbell & Stevens (1968) give a complete description of the tested bridge. Core samples were used to estimate the properties of the concrete in the deck and the girders as well as the strength of the prestressing strands. The girders and the slab were built to act as composite sections. Similarly, the mid-span diaphragm was designed to act compositely with the slab in the transverse direction Gossbell & Stevens (1968).

Tests to determine the ultimate load capacity of the bridge were performed by placing two concentrated point loads at the bridge's midspan. The point loads were placed on one side of the deck to simulate unsymmetrical loading conditions. The first load was placed at 69 cm (2.25 ft) from the edge girder and the second load at 183 cm (6 ft) from the first load. The loads were then incremented in "an attempt to estimate the ultimate load capacity" (Gossbell & Stevens, 1968). Testing was stopped when the load reached 2090 kN (474 kips). At that point, the measured maximum deflection was about 12.7 cm (5in). The loading was stopped at that level because the field testing team observed that a "large separation had occurred between the diaphragm and the girder ... and because of fear of a catastrophic punching shear failure under the loads", although " ... no shear failures actually occurred ... and no separation between slab and longitudinal girders was detected". Gossbell & Stevens (1968) observed that the deflection profile across the

bridge's cross section remained essentially unchanged as the load was increased from the linear range until the test was discontinued. It was also noted that the curb and railings significantly increased the rigidity of the edge girders "vastly contributing to the ultimate capacity of the bridge". On the other hand, "the diaphragm did not contribute to the ultimate capacity nor to the distribution of the loads". The authors attributed this to the "weak steel reinforcement provided in the diaphragm" (Gossbell &Stevens, 1968).

The program NONBAN is run assuming that the curbs act compositely with the edge girders but ignoring the effects of the railings because the exact dimensions and material properties of the railings are not available. The inclusion of the curb's effect to the edge girder produced an increase in the ultimate capacity of the edge girder by about 20% relative to the interior girders. The moment of inertia of the edge girder was found to be about 70% higher than that of the interior girders. This 70% increase matches the estimate reported by Gossbell & Stevens (1968).

To prepare the mesh for the NONBAN analysis, each of the seven longitudinal members is divided into twenty equal segments. The longitudinal girders are connected by 21 equally spaced transverse beams representing the transverse capacity of the slab. Because the actual value of the prestressing force is not available, the moment-curvature curves of the longitudinal girders are derived assuming a prestressing force of 2174 kN (493 kips). This value is used herein because it matches the prestressing force that would have been used if the bridge were designed to meet the AASHTO requirements (1996).

Figure 3.21 shows a comparison between the field results published in reference (Gossbell & Stevens, 1968) and the results of NONBAN. Acceptable agreement is observed in the figure although NONBAN predicts that the bridge is capable of withstanding a load higher than that at which the test was actually stopped.

3.6.4 Tennessee bridge.

The Tennessee field test was performed on a simply-supported bridge with a span length equal to 19.8 m (65 ft) (Burdette & Goodpasture, 1971). The bridge consisted of four prestressed AASHTO Type III girders at 2.74 m(9.0 ft) spacings supporting a17.8 cm (7 in) deck slab. The bridge had a 75° skew and no information was provided concerning the diaphragms. Burdette & Goodpasture (1971) give a detailed description of the tested bridge. Core samples were used to estimate the properties of the concrete in the deck and the girders as well as the strength of the prestressing strands. The girder and the slab were built to act as composite sections.

Tests to determine the ultimate load capacity of the bridge were performed by placing eight concentrated point loads close to the bridge's midspan (Figure 3.22). Burdette & Goodpasture (1971) mention that visible cracking was observed at the center diaphragm at a load of 1926 kN (455 kips). The interior girders cracked at a load of 2317 kN (521 kips). At a load of 4226 kN (960 kips), the authors noticed considerable "dishing " as the interior girder's deflected more than the exterior. This caused the separation between the deck and the girders and the loss of composite action of the interior girders. At that point the concrete of the interior girders started crushing. Finally at 5070 kN (1140 kips) the

interior girders failed in shear. The authors developed a load versus average deflection curve based on an analytically derived moment curvature relationship. In their analysis, the authors assumed that the whole bridge behaves as one beam and the moment curvature relationship for the whole bridge cross section was obtained.

To prepare the mesh for the NONBAN analysis, each of the four longitudinal members is divided into twenty to twenty-one segments as shown in Figure 3.23. The difference in the number of elements is necessary to accommodate the skew. The longitudinal girders are connected by twenty to twenty-one equally spaced transverse beams perpendicular to the longitudinal girders to represent the transverse capacity of the slab. The moment-curvature relationships for the longitudinal girders were taken from the reference by Burdette and Goodpasture (1971).

Burdette & Goodpasture (1971) give an average measured load deflection curve from all the longitudinal girders. Figure 3.24 shows the average measured load deflection curve obtained by NONBAN to the curve provided by Burdette and Goodpasture (1971). Good agreement is observed in the figure. According to NONBAN, the ultimate capacity would be reached at a total load equal to 5360 kN (1205 kips). The test was actually stopped at 5070 kN (1140 kips) producing a difference on the order of 8%. Some of the difference may be due to the loss of composite action in the actual test when the bridge was close to failing.

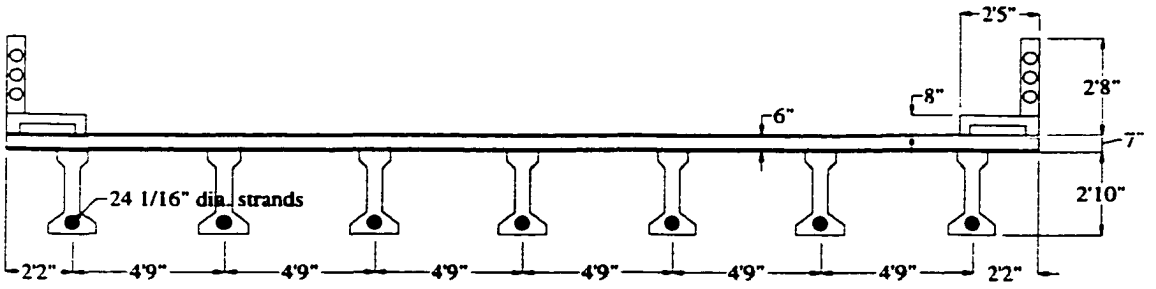

a) Cross section of Australia bridge

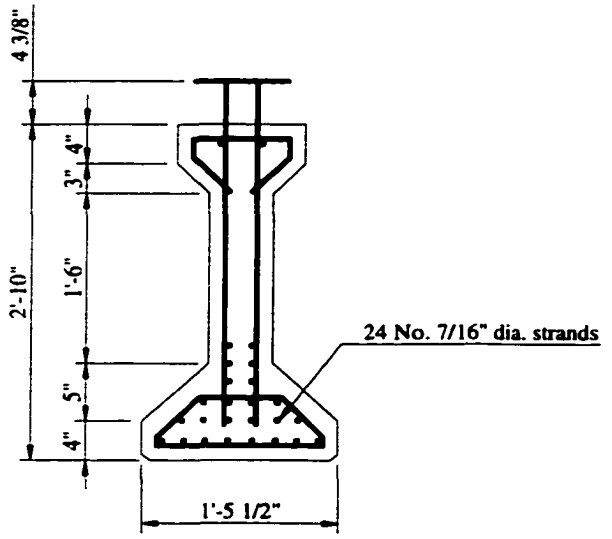

b) Cross section of typical girder

Figure 3.20. Description of Australia bridge.

c) Table of material properties

Material	Ultimate Strength f_u (ksi)	Young's Modulus E (ksi)
Strand Tendon	274.5	29,100
Deck Concrete	5.300	4,100
Beam Concrete	8.750	6,580

Figure 3.20 ct'd. Description of Australia bridge.

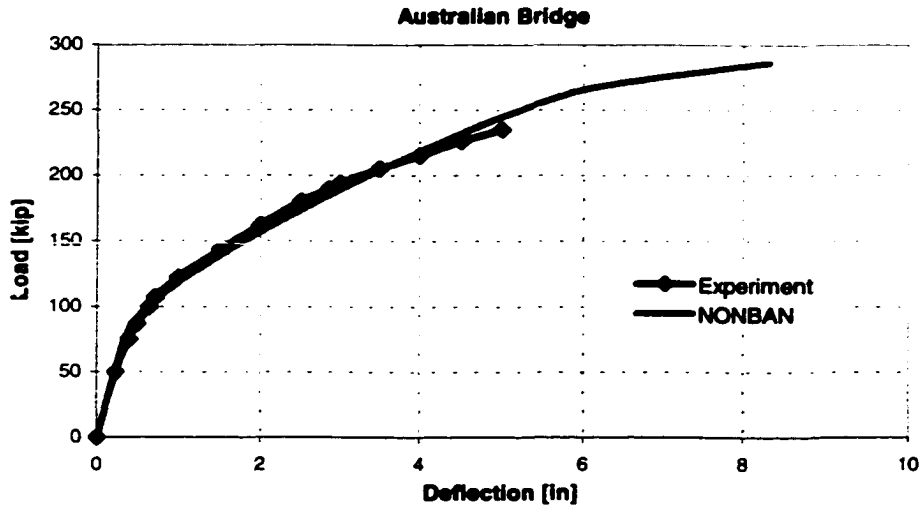

Figure 3.21. Comparison of NONBAN results to experimental results of Australia bridge.

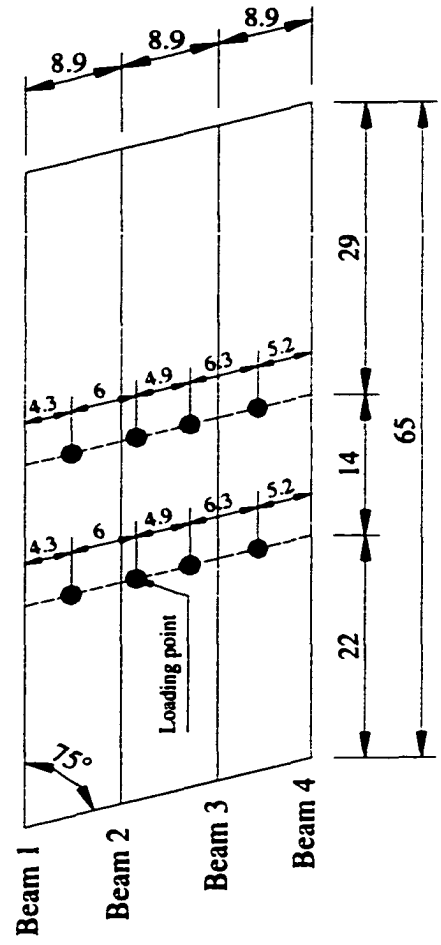

a). Tennessee bridge layout.

b). Table of material properties

Material	Yield Strength f_y (ksi)	Ultimate Strength f_u (ksi)
Tendon	245	275
Deck Concrete		5.500
Beam Concrete		8.700

Figure 3.22. Description of Tennessee bridge.

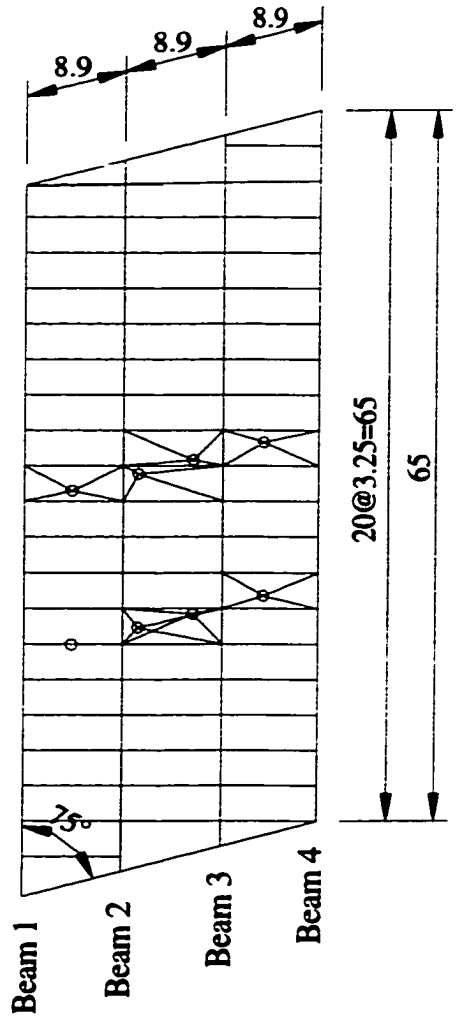

Figure 3.23. Mesh used in analysis of Tennessee bridge.

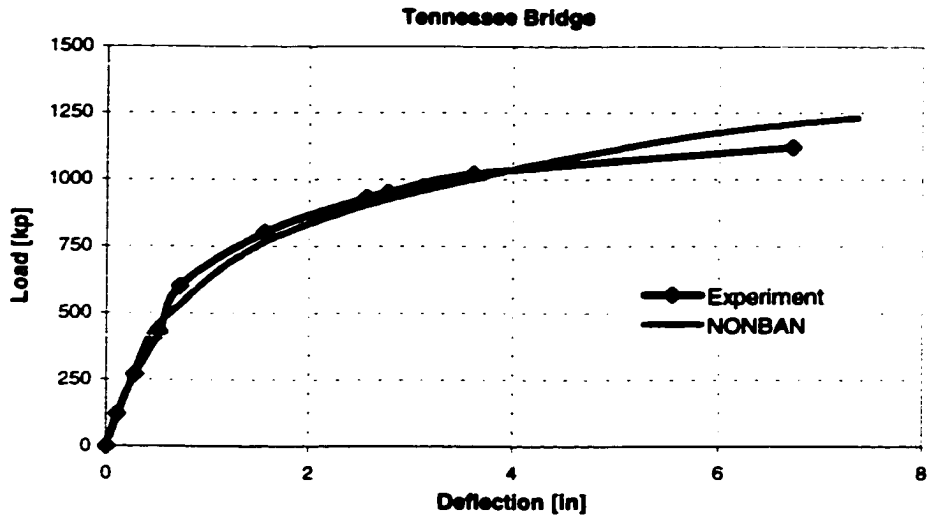

Figure 3.24. Comparison of NONBAN results and experimental results of Tennessee bridge.

3.6.5 Comments on Results

In the NONBAN analysis, the ultimate capacity is defined as the load level at which concrete crushing occurs in a main longitudinal member or when the prestressing steel ruptures. The results for the three bridges analyzed show the analytical load versus deflection curve is similar to that obtained experimentally up to deflection level up to span length/100. A span length/100 was previously used by Ghosn & Moses as a functionality limit state indicating that bridges exhibiting higher deflections can no longer function to safely carry the applied live loads.

The results of NONBAN for all three bridges slightly overestimate the ultimate system capacity as observed in the tests. The reasons for the overestimation may be due to the fact that NONBAN assumes uncoupling between the torsional properties and the bending properties of the girders and torsion is assumed to remain in the linear elastic range. This would overestimate the overall stiffness of the bridge at high loads as material nonlinearity spread. In addition, the tests have shown that a separation between the deck and the girder may occur at high loads which would soften the loading curve when this happens. On the other hand, the grillage method ignores many of the stiffening effects introduced from the two-dimensional (plate) behavior of the deck including membrane (or arching) actions.

Further analyses were performed to study the effect of the mesh size on the results. As an example, the Slovenia bridge described in the former section was analyzed for different mesh sizes varying between 10, 20, 30 and 40 elements for each longitudinal member. The procedure described above to develop the equivalent L_{gp} was used for each mesh size. Figure 3.25 shows how the results quickly converge as the mesh size is refined. The maximum difference in the estimate of the ultimate system capacity from different meshes is found to be 4.4%. The results for the finer mesh are slightly stiffer due to the changes in the L_{gp}. If the L_{gp} was not changed as a function of the mesh size, we notice that the results diverge as the mesh size is changed. This phenomenon is illustrated in Figure 3.26 where all the L_{gp}'s for all mesh sizes are taken equal to 80% of the value of L_p obtained from Baker's formula (Eq. 3.3). The errors observed when using a constant plastic hinge length demonstrate the importance of the proposed methodology where L_{gp} is a function of the mesh size. The results of Figure 3.25 demonstrate that the proposed approach is robust and insensitive to the chosen mesh size.

The similarity between the curve obtained by NONBAN and the load deflection curves from the test results illustrates the validity of the proposed method and the program NONBAN to perform the nonlinear analysis of prestressed concrete I-girder bridges. The simplicity of the method and its improved accuracy makes it quite attractive for use in engineering practice to determine the "actual" system capacity and study the nonlinear behavior of prestressed concrete I-girder bridges rather than relying on estimates based on linear elastic models.

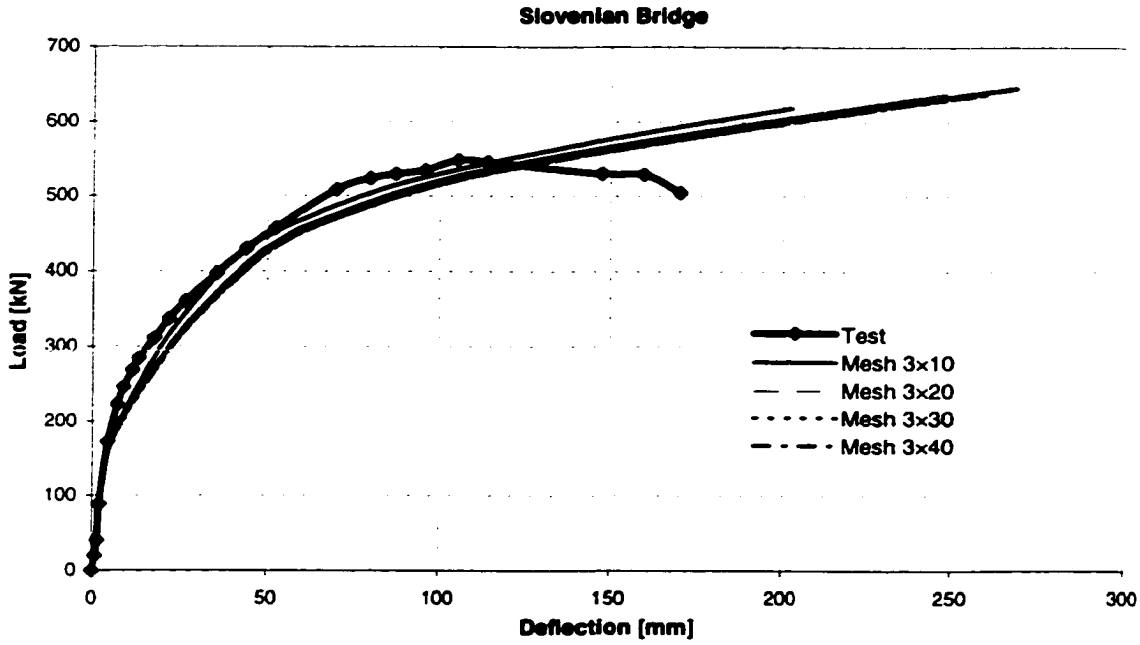

Figure 3.25. Results of Slovenia bridge for different meshes using L_p-transfer model.

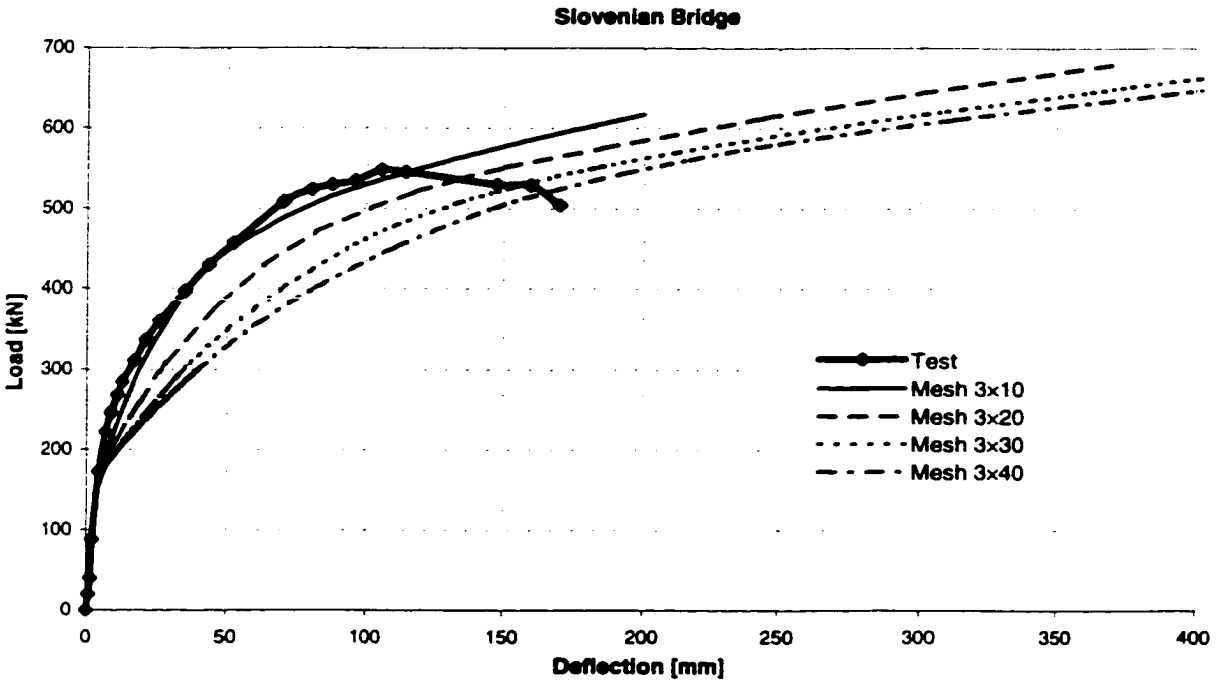

Figure 3.26. **Results of Slovenia bridge for different meshes using constant L_p value.**

3.7 SUMMARY

This chapter describes a method to analyze the nonlinear behavior of prestressed concrete girder bridges. The method has the following features:

- It provides a simple and reasonably accurate empirical tool to obtain detailed descriptions of the load-displacement behavior and ultimate capacities of prestressed concrete bridges.
- It is based on an L_p-transfer model that calculates an equivalent plastic element hinge length for each girder element.
- The input data is similar to that required for the linear analysis of bridges. This data consists of the bridge geometry (mesh) as well as the linear elastic properties of the members (moments of inertia, torsion constant, modulus of elasticity and shearing modulus). The only additional input data required is the ultimate moment capacity of each section M_u and shear capacity as well as the moment versus curvature, and shear versus shearing strain relationships.
- The validity of the analysis procedure was verified by comparing the analytical results to those from in-situ experimental tests and from full scale and model scale laboratory tests.
- Tracing the complete nonlinear behavior of the system provides information that may be useful for designing new bridges for ultimate limit states. In

addition, using this information during the rating process may result in a reduction in the retrofitting needs.

- Because the model produces a complete load versus deformation curve for each bridge structure, the bridge designer (or rater) would be able to check the deflection of a bridge at different load levels to ensure that the bridge remains functional at high live loads. Independent checks of the serviceability limit states may still be necessary depending on the applications.

CHAPTER 4

PSEUDOFORCE METHOD FOR NONLINEAR ANALYSIS AND REANALYSIS OF STRUCTURAL SYSTEMS

This chapter develops a robust solver to enhance the computational efficiency of finite element programs for the nonlinear analysis and the reanalysis of structural systems. The proposed solver does not require the re-assembly of the global stiffness matrix, and can be easily implemented in present-day finite element packages. It is particularly well suited to those situations where a limited number of members are changed at each step of an iterative optimization algorithm or reliability analysis. It is also applicable to a nonlinear analysis where the plastic zone spreads throughout the structure due to incremental loading. This solver is based on an extension of the Sherman-Morrison-Woodburg formula, and is applicable to a variety of structural systems including 2-D and 3-D trusses, frames, grids, plates and shells. The solver defines the response of the modified structure as the difference between the response of the original structure to a set of applied loads and the response of the original structure to a set of pseudoforces. The algorithm provides dramatic improvement of computational efficiency for structural redesign and optimization, and can perform a nonlinear incremental analysis no harder than the inversion of the global stiffness matrix. The proposed method's efficiency and accuracy are demonstrated through the nonlinear analysis of an example bridge and a frame redesign problem.

4.1 INTRODUCTION.

Structural design, reliability and optimization algorithms require repeated analyses as the structure under consideration is progressively modified. Nonlinear analysis procedures are also iterative in nature requiring high computational effort. Although computer power has increased substantially in recent years, the computational requirment is still excessive when the reliability analysis of nonlinear structures is under investigation. To reduce the computational effort in these situations, many methods have been recently developed (Gierlinski, Sears & Shetty 1993; Arora, 1976; McGuire and Gallagher, 1979; Abu-Kassim and Topping, 1987; Kirsh & Moses, 1995; Kirsh and Rubinstein, 1972). In particular, Makode, Corotis and Ramirez (1999) proposed a method called the Pseudodistortion method that seeks to reduce the computational effort during the reliability analysis of nonlinear systems and take advantage of modern computational tools. This method is an extension of the virtual distortion method (Holnichi, 1991) applicable for use in the analysis of frame structures. The basic concept in this "distortion" family is that the response of the modified structure is the sum of the response of the applied loads on the original structure and the response of the original structure to virtual distortions where the distortions are imposed on the members whose properties are being modified. In these methods, the types of virtual (or pseudo) distortions that must be applied vary according to the type of structure being analyzed. Thus, different distortion equations need to be developed for trusses, frames or continuous structures like plates and shells.

Another group of methods that also provide exact solutions for structural redesign problems are derived based on the Sherman-Morrison Identity (Sherman & Morrison, 1949 & 1950). These mathematically derived methods are usually robust and easy to program and implement in general purpose finite element packages and structural reliability programs. Abu-Kassim and Topping (1987) as well as Arora (1976) give a general review on the development of these methods. They report that Sack, Carpenter, and Hatch (1967) were the first to propose the use of Sherman-Morrison-Identity in structural reanalysis by using the reduced modified matrix derived by Argyris (1956). Kirsch and Rubinstein (1970, 1972) investigated various versions of the Sherman-Morrison identity, and investigated efficient methods to treat different redesign problems. Mohraz and Wright (1973) gave a dynamic version of Sherman-Morrison identity, where the size of the modified inverse matrix changes with changes in the nodes. They reported a 20 to 80% saving in computational effort compared to a complete inversion. To avoid the matrix inversion and related problems, Kirsh and Rubinstein (1970, 1972) presented a method where the generation of the modified inverse was avoided. Wang and Pilkey (1980, 1981, 1983) also developed a method from Sherman-Morrison identity by assuming that the modified response of a structure is expressed as a linear combination of the original response and a term depending on the pseudo-loads. Hirai, Wang and Pilkey (1984) presented a method with static condensation in finite element analysis by applying pseudo-loads.

By accounting for the change in structural properties during an incremental loading process that causes the spreading of plastic regions, reanalysis techniques, whether based

on pseudo-distrotion or Sherman-Morrison identity or other methods, have also been extended to nonlinear analysis applications (Makode, Corotis, and Ramirez, 1999; Abu-Kassim and Topping 1985; Holnicki-Szulc 1989, 1991). Several methods are currently used during the nonlinear analysis of structural systems including the traditional Newton-Raphson (NR) algorithm and its variations developed to improve its efficiency. These include the Initial Stress method, the Modified Newton-Raphson method (Bathe, 1996; Kohnke, 1997;). But, both the classical NR and its derivatives are known to have many convergence problems and can be very time-consuming when it comes to solving structural analysis equations.

Many engineering applications require the representation of the behavior of structural systems by following the whole range of structural response from the initiation of loading until total collapse. The Newton-Raphson algorithm cannot explicitly describe the spreading of the plastic zone, therefore, to model this complete behavior, the incremental loading technique is often used (Pail, and Buckle, 1970; Ghosn, Deng, Xu, Liu, and Moses, 1997). This approach requires the solution of a nonlinear system of equations at hundreds of load steps to describe the complete sequence of hinge formation. Thus, it is less efficient than Newton-Raphson method although it provides more information.

In this chapter, a robust solver, called the pseudoforce solver, is proposed to enhance the analysis efficiency by avoiding the need to re-assemble the global stiffness matrix. The proposed method is applicable to both Newton-Raphson and incremental loading algorithms. It is derived from the Sherman-Morrison-Woodburg formula (Golub & Van

Load, 1996), and defines the response of the modified structure as the difference between the response of the applied load on the original structure and the response of the same original structure subjected to a set of pseudoforces. The advantages of this method include optimization and reliability analysis of linear and nonlinear systems of any structural

optimization and reliability analysis of linear and nonlinear systems of any structural

type.

4.2 DESCRIPTION OF PSEUDOFORCE METHOD

To demonstrate the basic concept of the pseudoforce method, consider a truss whose original members' cross sectional areas are given as A_1, A_2, A_3, etc. Suppose that the cross section areas of members 1 and 2 are changed from A_1 and A_2 to $\overline{A}_1$ and $\overline{A}_2$ respectively. The steps of the reanalysis are illustrated in Fig. 4.1, where the response of the modified structure (Fig. 4.1.a) is the difference between the response of the original structure due to the original loads R (Fig. 4.1.b) and the response of the original structure due to a set of pseudoforces, F^c. The forces F^c are applied on the original structure at the joints connected to the modified members (Fig. 4.1.c).

The stiffness matrix of the modified structure, $\overline{K}$, is equal to the stiffness matrix of the original structure, K, plus a correction matrix, ΔK. The finite element stiffness equation can be expressed as:

$$[\overline{K}]\overline{\delta} = [K + \Delta K]\overline{\delta} = R \qquad \text{(Eq. 4.1)}$$

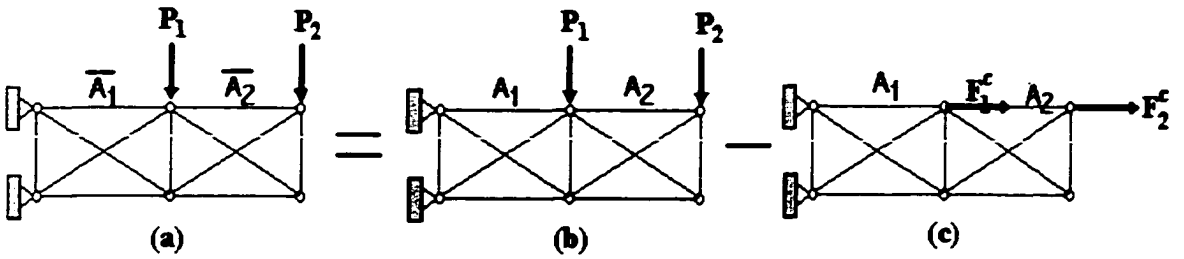

Figure 4.1. Illustration of reanalysis procedure by pseudoforce method.

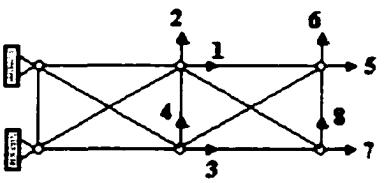

Figure 4.2. Description of example truss showing degrees of freedom.

Usually, only a few members change their properties during one reanalysis step. Thus, the correction matrix ΔK is highly sparse. For example, when the unknown displacements are numbered as shown in Figure 4.2, the stiffness matrix can be expressed as given in Equation 4.2:

$$\overline{K} = K + \Delta K$$

or (Eq. 4.2)

$$\begin{bmatrix} \overline{k_{11}} & \cdots & \cdots & \overline{k_{18}} \\ \cdots & & & \\ \cdots & & & \\ \overline{k_{81}} & \cdots & \cdots & \overline{k_{88}} \end{bmatrix} = \begin{bmatrix} k_{11} & \cdots & \cdots & k_{18} \\ \cdots & & & \\ \cdots & & & \\ k_{81} & \cdots & \cdots & k_{88} \end{bmatrix} + \begin{bmatrix} s_{11} & \cdots & s_{15} & \cdots & 0 \\ \cdots & 0 & 0 & 0 & \cdots \\ s_{51} & \cdots & s_{55} & \cdots & 0 \\ \cdots & 0 & 0 & 0 & \cdots \\ 0 & 0 & 0 & \cdots & 0 \end{bmatrix}$$

For illustration, and without losing generality, the matrix ΔK shown in Equation (4.2) has only two nonzero diagonal entries. For large scale systems, the number of nonzero diagonal entries in ΔK is much smaller than the dimension of matrix K. In structural analysis, this ΔK matrix has an important property: All the entries of a row and a column are equal to zero if the diagonal term is equal to zero. Therefore, the matrix ΔK can be expressed as the multiplication of two low rank matrices: U and V, as shown in Equation 4.3:

$$\Delta K = U\,V \qquad \text{(Eq. 4.3)}$$

Where U is an n×d pointer matrix, in which n is the dimension of matrix ΔK, and d is the number of nonzero diagonal entries in matrix ΔK. U is called a pointer matrix because it

points to the position of the pseudoforces or the Modified DOF (degrees of freedom) of the modified members. The coefficients of U are either 0 or 1. V is a d × n semi-compressed stiffness matrix. Matrices U and V can be easily assembled as follows:

V is composed of the rows of ΔK whose diagonal term is not equal to 0. The total number of rows in matrix V is d.

$U_{j,k}$ = 0; when $V_{k,j}$ ≠ diagonal term of ΔK for all k = 1, 2, ... d.

and $U_{j,k}$ = 1, when $V_{k,j}$ = diagonal term of ΔK for all k = 1, 2, ... d.

Matrix U's rank is equal to d, and matrix V's rank is less or equal to d. The matrix ΔK can be further decomposed as:

$$\Delta K = UWU^T \qquad \text{(Eq. 4.4)}$$

Where matrix U is the pointer matrix defined above, and matrix W is the compressed stiffness matrix which contains the nonzero entries of matrix ΔK. As an illustration, the ΔK corresponding to the structure shown in Figure 4.1 can be expressed as UV or UWU^T:

$$\Delta K = UV = UWU^T$$

or

$$\begin{bmatrix} s_{11} & 0 & 0 & 0 & s_{15} & 0 & 0 & 0 \\ 0 & 0 & 0 & 0 & 0 & 0 & 0 & 0 \\ 0 & 0 & 0 & 0 & 0 & 0 & 0 & 0 \\ 0 & 0 & 0 & 0 & 0 & 0 & 0 & 0 \\ s_{51} & 0 & 0 & 0 & s_{55} & 0 & 0 & 0 \\ 0 & 0 & 0 & 0 & 0 & 0 & 0 & 0 \\ 0 & 0 & 0 & 0 & 0 & 0 & 0 & 0 \\ 0 & 0 & 0 & 0 & 0 & 0 & 0 & 0 \end{bmatrix} = \begin{bmatrix} 1 & 0 \\ 0 & 0 \\ 0 & 0 \\ 0 & 0 \\ 0 & 1 \\ 0 & 0 \\ 0 & 0 \\ 0 & 0 \end{bmatrix} \begin{bmatrix} s_{11} & 0 & 0 & 0 & s_{15} & 0 & 0 & 0 \\ s_{51} & 0 & 0 & 0 & s_{55} & 0 & 0 & 0 \end{bmatrix}$$

$$= \begin{bmatrix} 1 & 0 \\ 0 & 0 \\ 0 & 0 \\ 0 & 0 \\ 0 & 1 \\ 0 & 0 \\ 0 & 0 \\ 0 & 0 \end{bmatrix} \begin{bmatrix} s_{11} & s_{15} \\ s_{51} & s_{55} \end{bmatrix} \begin{bmatrix} 1 & 0 & 0 & 0 & 0 & 0 & 0 & 0 \\ 0 & 0 & 0 & 0 & 1 & 0 & 0 & 0 \end{bmatrix}$$

(Eq4.5)

The Sherman-Morrison-Woodburg formula (Golub & Van Loan, 1996; Sherman & Morrison, 1949; 1950) gives a convenient expression for the inverse of (K+UV):

$$(K+UV)^{-1} = K^{-1}[I - U(I + VK^{-1}U)^{-1}VK^{-1}] \qquad \text{(Eq. 4.6)}$$

where $(I + VK^{-1}U)$ has the same rank as U (rank=d). Thus, a rank d correction to a matrix results in a rank d correction to its inverse. The stiffness equation as shown in Equation 4.1 can be solved as:

$$\overline{\delta} = K^{-1}[I - U(I + VK^{-1}U)^{-1}VK^{-1}]R \qquad \text{(Eq. 4.7)}$$

Equation 4.7 can be further expanded as:

$$\overline{\delta} = K^{-1}R - K^{-1}U(I + VK^{-1}U)^{-1}VK^{-1}R \qquad \text{(Eq. 4.8)}$$

where $(I + VK^{-1}U)^{-1}VK^{-1}R$ results in a vector of rank d. When this vector multiplies the matrix U, a force vector **F**, which is the global pseudoforce vector, is formed. This is a sparse vector with nonzero entries pointed out by matrix U, or in other words, with nonzero entries corresponding to the modified DOF attached to the modified members. Thus, Equation 4.8 can be expressed as:

$$\overline{\delta} = K^{-1}R - K^{-1}F = K^{-1}(R - F) \qquad \text{(Eq. 4.9)}$$

This equation shows that the response of a modified structure, $\overline{\delta}$, is equal to the difference between the response of the original structure due to the original applied loads, $K^{-1}R$, and the response of the original structure to the pseudoforce vector, $K^{-1}F$. In other words, the response of the modified structure is equal to the response of the original structure subjected to a set of forces equal to the difference between the original forces and the pseudoforces.

For simplicity and computational efficiency, let us define the following terms:

$$D = K^{-1}R$$
$$f = K^{-1}U \qquad \text{(Eq. 4.10)}$$
$$F^c = (I + Vf)^{-1}VD \quad \text{or} \quad F^c = (I + WU^T f)^{-1}WU^T D$$

where vector D is the response of the original structure to the originally applied loads, the influence matrix f with rank d gives the response of the original structure under the effect of virtual unit loads placed at the degrees of freedom (DOF) identified by matrix U. The vector F^c with rank d gives the local pseudoforces acting on the joints connected to the modified members (or the DOFs identified by U). It should be noted that although the matrix f is of rank d, most of the terms remain constant as the iterative process continues. When p new DOF are modified for the first time during an iteration step, then only p columns of f need to be updated. The other terms remain the same although the size d of matrix f may increase to reflect the total number of DOF that have been updated so far.

Thus, the modified structure's response can be simply calculated by:

$$\bar{\delta} = D - fF^c \qquad \text{(Eq. 4.11)}$$

By assuming that the stiffness matrix with dimension n and bandwidth m is decomposed as LDL^T. The execution of Equation 4.9 requires m*n multiplications plus n divisions and m*n additions/ subtractions. The execution of Equation 4.11 requires d*n multiplications and d*n additions/subtractions. Thus, Equation 4.11 is more efficient than Equation 4.9 because in most cases d<<n.

Knowing the response of the original (unmodified) structure, D, and the decomposed global stiffness with a bandwidth m (such as during LDL^T decomposition), the steps needed to calculate the response of the modified structure and the total number of operations related to these steps are listed in Table 4.1.

Thus, the total number of operations needed to calculate the response of the modified structure, N_1, is equal to:

$$N_1 = 2p*m*n+\frac{8}{3}d^3+\frac{5}{2}d^2+2d*n+2p*m-3p*n-\frac{5}{3}d \qquad \text{(Eq. 4.12)}$$

If the stiffness matrix of the modified structure with a constant bandwidth m is solved using the traditional LDL^T algorithm, the required number of operations including element address identification is shown in Table 4.2.

Or the total number of operations for LDL^T, N_2, is given as:

$$N_2 = m^2n+\frac{11}{2}mn-\frac{5}{2}n-\frac{8}{3}m^3+4m^2-\frac{2}{3}m \qquad \text{(Eq. 4.13)}$$

Depending on the number of new DOF that are modified during one iteration (represented by p), one of the most expensive computing operations is the updating of the influence matrix f. Once the coefficients of f are formed for particular DOF's, they can be reused for subsequent operations if these same DOF's are modified. Given f, the

remaining steps are "cheap" requiring little additional computation time for small values of d, although the number of computations increases with d. In practical applications, d remains much smaller than m. Thus, by comparing Equation (4.12) and Equation (4.13) it is observed that much computational effort is saved by using the proposed algorithm.

When equation (4.12) is equal to equation (4.13) the limit on the efficiency of the proposed algorithm is reached. Hence, it is herein proposed to restart the whole iterative process before they become equal. This efficiency threshold is primarily controlled by the sizes of d and p. If during an iteration step p is approximately equal to ½ the bandwidth m, the current step is inefficient but would not influence the total efficiency unless this situation is often repeated. On the other hand, if d is so large that Equation (4.12) becomes larger than Eq. (4.13) although p may be small, then the algorithm must be restarted because the size of d is continuously increasing with every iteration step. For large scale systems, the maximum value of d, d_{max}, that keeps the efficiency of the pseudoforce algorithm, can be calculated assuming that large values of p are not repeated often:

$$d_{max} = \frac{1}{2}\sqrt[3]{3m^2n} \qquad \text{(Eq. 4.14)}$$

Returning to the problem described in Figure 4.1, when only member 1 is modified, F^c can be easily calculated from:

$$F^c = \frac{S_{11} D_1}{1 + S_{11} f_{11}} \qquad \text{(Eq. 4.15)}$$

where f_{11} is the first term in the influence matrix f which is assembled from $K^{-1}U$ as shown in Equation (4.10). The solution of the modified truss is obtained by solving Equation (4.11). The total number of operations needed to analyze the modified truss is $O(m \times n)$[1].

In the second step, when members 1 and 2 are modified, F^c can be calculated as:

$$F^c = \left(\begin{bmatrix} 1 & 0 \\ 0 & 1 \end{bmatrix} + \begin{bmatrix} s_{11} & s_{15} \\ s_{51} & s_{55} \end{bmatrix} \begin{bmatrix} f_{11} & f_{15} \\ f_{51} & f_{55} \end{bmatrix} \right)^{-1} \begin{bmatrix} s_{11} & s_{15} \\ s_{51} & s_{55} \end{bmatrix} \begin{bmatrix} D_1 \\ D_5 \end{bmatrix} \qquad \text{(Eq. 4.16)}$$

The solution of the truss with two modified members (ie. members 1 and 5) requires the assembly of the second column of the influence matrix f (i.e. f_{15} through f_{85}), the first column (f_{11} through f_{81}) having been assembled from the previous step. Hence, only $O(m \times n)$ additional operations are needed for this second step.

The same procedure used for this truss example can be followed for the analysis of frames as will be demonstrated in the next section.

[1] O – notation gives an upper bound for a function to within a constant factor. It is herein used to give the order of magnitude for the number of computational operations needed.

Table 4.1. Computation steps and corresponding number of operations for pseudoforce method.

Step	Task	Operations needed in this step			
		Multiplication	Division	Addition/ Subtraction	Assignment
1	Updating the influence matrix $f = K^{-1}U$.	$p(m*n+m-n)$	n	$p(m*n+m-2n)$	
2	Calculating U^TD.				d
3	Calculating WU^TD after calculated U^TD.	$d*d$		$d*(d-1)$	
4	Calculating U^Tf.				$d*d$
5	Calculating WU^Tf after calculated U^Tf.	d^3		d^3-d^2	
6	Calculating $F^c = (I + WU^Tf)^{-1}WU^TD$ after calculating WU^Tf and WU^TD.	$d^3/3+d^2/2-5d/6$	$d^2/2+d/2$	$d^3/3+d^2/2-5d/6$	
7	Calculating $f F^c$ after calculating f and F^c.	$d*n$		$d*n$	
8	calculate $\delta = D - f F^c$ after calculating $f F^c$.			n	
Σ		The total number of multiplications is: $p*m*n+4d^3/3+3d^2/2+d*n+p*m-p*n-5d/6$ The total number of divisions is: $n+d^2/2+d/2$ The total number of additions/subtractions is: $p*m*n+4d^3/3+d^2/2+d*n+p*m-2p*n-n-11d/6$ The total number of assignments is: d^2+d			

Table 4.2. Number of operations for LDL^T

Method	Operations		
	Multiplication	Division	Addition (or subtraction)
LDL^T	$m^2n/4+3m*n/2-7n/4$ $-2m^3/3+m^2-m/6$	$m*n/2-n/2$	$3m^2n/4+7m*n/2-n/4$ $-2m^3+3m^2-m/2$

4.3 ILLUSTRATIVE EXAMPLE 1

To illustrate the efficiency of the proposed method, the solver is used for the reanalysis of a model forty-story frame building. The frame is subjected to a set of horizontal forces as shown in Figure 4.3. The side spans of the frame are 8m each, the middle span is 4m, while the height between floors is 3m. The magnitude of the horizontal force applied on each floor is 10 kN. The section and material properties for the beams and columns are shown in Table 4.3. To reduce the horizontal deformations, one possible building design procedure requires the use of braced floors at particular locations along the height of the frame. Suppose that the design of this building requires only one set of cross bracings. The bracings are to cross two floors in the middle span of the building. The objective of the design will be to find the optimum location of the cross bracing. Finding this optimum location requires an enormous computational effort if all possible locations are to be checked one by one and the analysis performed for each location independently. The proposed pseudoforce method can be used to solve this problem economically even if all possible locations where the bracing could be placed are checked. Figure 4.4 shows how the maximum deformation changes for different bracing locations.

From Figure 4.4, it is found that the most effective position for the bracing is along floors #2 & 3 if only one bracing is to be designed.

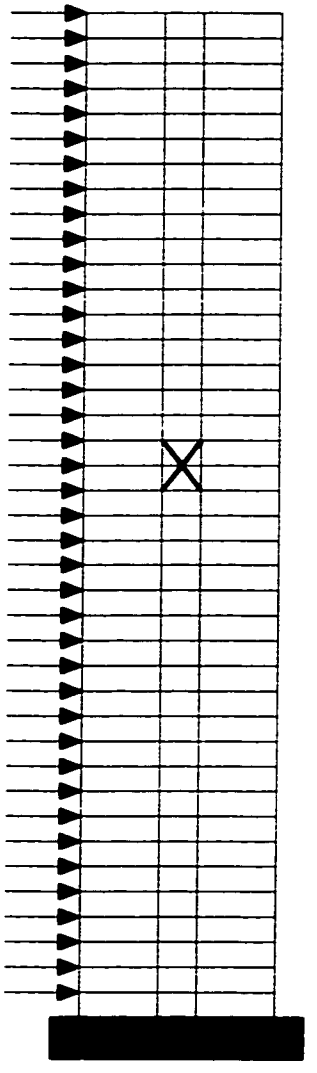

Figure 4.3. Elevation of a high-rise forty-story building.

Table 4.3. Building beam and column sections and material properties.

Member	Floors	Section (mm)	Elastic Modulus (KN/m^2)
Side column	1-20	400x500	4.2e7
Side column	21-40	300x400	4.2e7
Middle column	1-20	400x700	4.2e7
Middle column	21-40	300x500	4.2e7
Beam	1-40	300x550	4.2e7
Bracing		W40x328	2.0e8

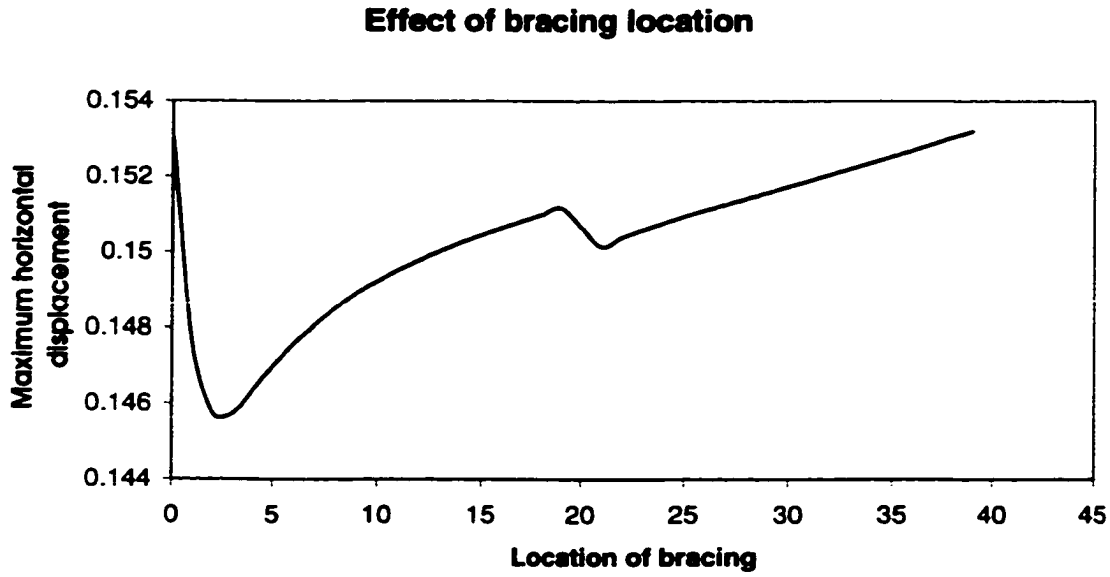

Figure 4.4. Effect of location of bracing on maximum deflection

If we analyze this problem using a traditional LDL^T solver, every analysis requires 2080 milliseconds to complete, resulting in a total of 83,000 milliseconds for the 40 steps. Out of these 83,000 seconds, 17,600 milliseconds are needed to solve the stiffness equation 40 times. The implementation of the proposed algorithm will reduce the time required for every step (beyond the first step) to 356 milliseconds, 110 milliseconds of which are needed to solve the stiffness equation. It is seen that the proposed solver reduces the computational effort in solving the global equation by a up to 400%. For larger scale problems, the savings in computational effort will even be more dramatic as demonstrated in Tables 4.1 & 4.2.

4.4 PROPOSED SOLVER FOR NONLINEAR STRUCTURAL ANALYSIS

During the nonlinear analysis of a structural system, the global stiffness matrix is assembled for a series of load increments. At each load increment, t, iterative methods may be used to solve the global equilibrium equation to obtain the nodal displacements. Let us define ${}^tK^i$ as the global stiffness matrix assembled at iteration i of load step t. A residual is the difference between the right side vector of the nonlinear equation and the vector calculated in the present iteration point through the corresponding linear equation (Bathe, 1996). ${}^tR^i$ is defined as the residual at iteration i for load step t. Using the Newton-Raphson's algorithm, we can calculate the incremental displacement ${}^t\delta^i$, at iteration i of load step t, through the equation:

$$ {}^tK^i \; {}^t\delta^i = {}^tR^i \qquad \text{(Eq.4.17)} $$

If the LDL^T matrix decomposition is used to solve the above equation given that the bandwidth of matrix ${}^tK^i$ is m and the dimension of matrix ${}^tK^i$ is n, $O(m^2n)$ operations are needed (Golub, and Van Loan, 1996). To save computational effort, the lower triangle, diagonal, and upper triangle matrices from the LDL^T defactorization of ${}^tK^i$ are stored for reuse in subsequent iterations.

In the subsequent iteration, i+1, for the same load step t, a few element stiffness matrices will change as the elements' tangent modulus changes. This will disturb the global stiffness matrix ${}^tK^i$ to form a new tangent matrix ${}^tK^{i+1}$ that can be expressed as:

$$ {}^tK^{i+1} = {}^tK^i + {}^t(\Delta K)^{i+1} \qquad \text{(Eq. 4.18)} $$

The global equilibrium equations at iteration i+1, can be expressed as:

$$ {}^tK^{i+1}\ {}^t\delta^{i+1} = {}^tR^{i+1}, \quad \text{or} \quad ({}^tK^i + {}^t(\Delta K)^{i+1})\ {}^t\delta^{i+1} = {}^tR^{i+1} \qquad \text{(Eq. 4.19)} $$

Where ${}^t(\Delta K)^{i+1}$ is a highly sparse matrix because only a small number of elements will go nonlinear at one iteration step. Its rank is much smaller than the dimension of matrix ${}^tK^i$. As described in the former section, the matrix ${}^t(\Delta K)^{i+1}$ can be expressed as:

$$ {}^t(\Delta K)^{i+1} = {}^tU^{i+1}\ {}^tV^{i+1} \qquad \text{(Eq. 4.20)} $$

Where ${}^tU^{i+1}$ is a $n \times {}^td^{i+1}$ pointer matrix, in which ${}^td^{i+1}$ is the number of nonzero diagonal terms in matrix ${}^t(\Delta K)^{i+1}$, and ${}^tV^{i+1}$ is a ${}^td^{i+1} \times n$ matrix. The rank of ${}^tU^{i+1}$ ${}^tV^{i+1}$ is the same as that of ${}^t(\Delta K)^{i+1}$, i.e. ${}^td^{i+1}$. As explained in the previous section, the matrices ${}^tU^{i+1}$ and ${}^tV^{i+1}$ can be easily assembled as follows:

${}^tV^{i+1}$ is composed of the rows of ${}^t(\Delta K)^{i+1}$ whose diagonal term is not equal to 0. The total rows in matrix ${}^tV^{i+1}$ are ${}^td^{i+1}$.

$({}^tU^{i+1})_{j,k} = 0$; when $({}^tV^{i+1})_{k,j} \neq$ diagonal term of ${}^t(\Delta K)^{i+1}$.

for all k = 1, 2, ... ${}^td^{i+1}$.

and $({}^tU^{i+1})_{j,k} = 1$, when $({}^tV^{i+1})_{k,j}$ = diagonal term of ${}^t(\Delta K)^{i+1}$.

for all k = 1, 2, ... ${}^td^{i+1}$.

In general, the global equation for iteration i+1 can be expressed as:

$$\left({}^tK^i + {}^tU^{i+1}\,{}^tV^{i+1}\right){}^t\delta^{i+1} = {}^tR^{i+1} \qquad \text{(Eq. 4.21)}$$

Using the same strategy described in the former section, this equation can be solved efficiently as:

$${}^t\delta^{i+1} = {}^t\delta^i - {}^tf^{i+1}\,{}^tF^{ci+1} \qquad \text{(Eq. 4.22)}$$

Where ${}^t\delta^i = [{}^tK^i]^{-1}\,{}^tR^{i+1}$ is the displacement vector in iteration i at load step t.

${}^tf^{i+1} = [{}^tK^i]^{-1}\,{}^tU^{i+1}$ is the influence matrix, and

${}^{t}F^{c\ i+1} = (I + {}^{t}V^{i+1}\ {}^{t}f^{i+1})^{-1}\ {}^{t}V^{i+1}\ {}^{t}\delta^{i}$ is the local pseudoforce vector.

As mentioned above, during iteration i, ${}^{t}K^{i}$ is decomposed as LDL^{T}. The above equation can be efficiently solved for iteration i+1 by utilizing the results from iteration i. The total number of operations needed for iteration i+1 are equal to $O({}^{t}d^{i+1}*m*n)$. The proposed solver becomes very efficient as long as ${}^{t}d^{i+1}$ is less than the bandwidth m of matrix ${}^{t}K^{i}$.

When the process is continued to the next iteration, i+2, a few additional structural members will have different tangent moduli than their moduli at steps i and i+1. This will further disturb the global stiffness matrix, and the new matrix will be identified as ${}^{t}K^{i+2}$. Hence, the new system of simultaneous equations can be expressed as:

$$ {}^{t}K^{i+2}\ {}^{t}\delta^{i+2} = {}^{t}R^{i+2} \qquad \text{(Eq. 4.23)} $$

In which, matrix ${}^{t}K^{i+2}$ can be decomposed into:

$$
\begin{aligned}
{}^{t}K^{i+2} &= {}^{t}K^{i+1} + {}^{t}(\Delta K)^{i+2} \\
&= {}^{t}K^{i} + {}^{t}(\Delta K)^{i+1} + {}^{t}(\Delta K)^{i+2} \\
&= {}^{t}K^{i} + {}^{t}(\overline{\Delta K})^{i+2} \\
&= {}^{t}K^{i} + {}^{t}U^{i+2}\ {}^{t}V^{i+2} \\
&= {}^{t}K^{i} + [{}^{t}U^{i+1}T_1 + {}^{t}(\Delta U)^{i+2}T_2]\ {}^{t}V^{i+2}
\end{aligned}
\qquad \text{(Eq. 4.24)}
$$

The matrices T_1 and T_2 in the above equation are transformation matrices that re-arrange the order of the columns in matrices ${}^{t}U^{i+1}$ and ${}^{t}(\Delta U)^{i+2}$ into matrix ${}^{t}(U)^{i+2}$. Assuming the

number of nonzero diagonal terms in $({}^{t}(\Delta K)^{i+1} + {}^{t}(\Delta K)^{i+2})$ is ${}^{t}d^{i+2}$ and if ${}^{t}(\Delta K)^{i+2}$ has rank d, the following inequality can be established:

$$ {}^{t}d^{i+2} \leq {}^{t}d^{i+1} + d \qquad \text{(Eq. 4.25)} $$

The inequality stems from the fact that some elements that change their tangent stiffness in iteration i+2 may have changed their tangent stiffness in the previous iteration. The matrix U does not change in this situation. In most nonlinear analysis procedures, this is true because ${}^{t}\delta^{i+2}$ is almost identical to ${}^{t}\delta^{i+1}$. In other words, the rank of ${}^{t}(\Delta U)^{i+2} << {}^{t}d^{i+2}$ in most cases. Using this fact will help reduce the computational effort as will be seen further below.

Following the same logic used in iteration i, ${}^{t}\delta^{i+2}$ can be calculated by:

$$ {}^{t}\delta^{i+2} = {}^{t}\delta^{i} - {}^{t}f^{i+2}\ {}^{t}F^{c\,i+2} \qquad \text{(Eq. 4.26)} $$

Where ${}^{t}f^{i+2} = [{}^{t}K^{i}]^{-1}\ ({}^{t}U^{i+1}\ T_1 + (\Delta U)^{i+1} T_2)$ is the influence matrix for step i+2.

${}^{t}F^{c\,i+2} = (I + {}^{t}V^{i+2}\ {}^{t}f^{i+2})^{-1}\ {}^{t}V^{i+2}\ {}^{t}\delta^{i}$ is the local pseudoforce vector.

As mentioned above, ${}^{t}K^{i}$ is decomposed by an LDL^{T} algorithm, the above equation for step i+2 can be solved very efficiently by taking advantage of the results of iterations i and i+1. The calculation effort, due to the fact that matrix ${}^{t}K^{i}$ is a n x n band matrix with bandwidth m, can be described as

$O((d^{i+2}-{}^{t}d^{i+1})*m*n)$. It is observed that the number of operations needed for iteration i+2 is not larger than the number needed during i+1. This is a major advantage of this algorithm.

The complete nonlinear structural analysis procedure up to iteration i of load step t as shown in Figure 4.5, can be expressed as:

$$\left({}^{0}K^{0}+\sum_{l=1}^{t-1}\sum_{k=1}^{Ts(l)}{}^{l}(\Delta K)^{k}+\sum_{k=1}^{i-1}{}^{t}(\Delta K)^{k}+{}^{t}(\Delta K)^{i}\right){}^{t}\delta^{i}={}^{t}R^{i} \qquad \text{(Eq. 4.27)}$$

Where ${}^{0}K^{0}$ is the stiffness matrix for the elastic system, at load increment t=0 and iteration i=0. Ts(l) is the total number of iterations needed to find the solution for load step l.

To solve for the displacements ${}^{t}\delta^{i}$, start by assembling and defactorizing the elastic matrix ${}^{0}K^{0}$. Then, the algorithm described above is followed to find the solution for iteration 1 of load step1. The process is continued for iteration 2 in load step1, ..., iteration 1 in load step 2, iteration 2 in load step 2, ... until the nonlinear analysis is completed or the total number of plastic nodes is so large that the proposed solver looses its efficiency because of the increase of d as shown in Equation 4.14. If this occurs, it is advisable to defactorize the stiffness matrix in this step, and restart the whole process. Otherwise, the proposed pseudoforce algorithm may cost more than the direct solver.

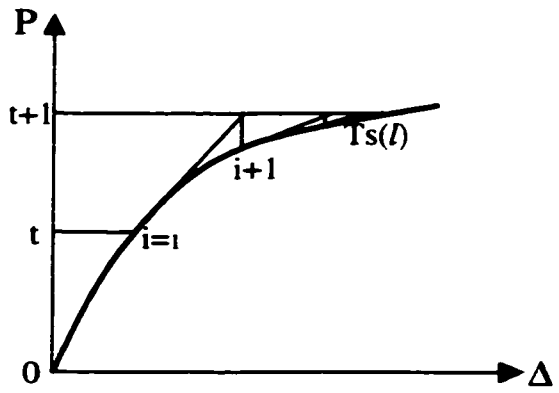

Figure 4.5. Illustration of Nonlinear Procedure

Perhaps a useful application of the proposed pseudoforce solver is to incoporate it into the Newton-Raphson's algorithm whereby a defactorization of the global matrix is performed at the beginning of every load step and the pseudoforce solver is used within each load steps independent of the number of iterations required for convergence. If the load steps are properly chosen, all the steps can be solved very efficiently. This process is illustrated in Figure 4.4, where the global stiffness matrix is defactorized at the load step t. The pseudoforce solver is used for iterations i=1 until i=Ts(*t*)

The Newton-Raphson algorithm becomes less efficient when the complete loading path of a structural system is required if each element's nonlinear stiffness is represented by a multilinear curve. In this case engineers often rely on the incremental loading technique. The nonlinear analysis procedure is thus reduced to a series of linear analyses and the final results are the summation of the results from these incremental load steps. The sizes of the load steps are chosen based on the load factors that produce a new change in any of the elements' stiffness matrices. The procedure is continued until structural failure.

The disadvantage of the incremental analysis is that it needs O(n) steps to reach the ultimate load which requires a huge computational effort. If the proposed pseudoforce algorithm is used in conjunction with the load increment technique, the efficiency of the analysis will be greatly improved. For every load step, the number of operations needed with the pseudoforce solver is only O(k*m*n), where m is the bandwidth of the global stiffness matrix, k is the number of nodes that go into a new nonlinear stage for the loading step, and n is the total number of DOF. The example presented in the next section

describes the applicability of the pseudoforce method for the incremental loading technique in more detail.

4.5 PROOF OF EFFICIENCY OF PSEUDOFORCE SOLVER FOR INCREMENTAL ANALYSIS

Suppose a structure with n Degrees of Freedom, DOF, is being analyzed. Each DOF's behavior may be described by an elasto-plastic curve. For convenience and simplicity, it is assumed that only one DOF reaches its plastic limit at each load step. Thus, to reach the ultimate state, these n DOF's will all reach their plastic limits after n loading steps at most. This is the worse case scenario for an incremental nonlinear analysis. If the problem is solved using a traditional LDL^T algorithm, the total number of operations needed is $n*O(m*m*n) = O(m^2*n^2)$. When using the proposed pseudoforce algorithm, and restarting the algorithm only when the number of plasticized DOF's reaches square root of n, there will be square root of n times "restarts". Between every "restart", there will be square root of n iterations to make the square root of n nodes go plastic. Therefore, the total number of operations, N_3, is:

$$N_3 = \sqrt{n}O(m*m*n) + \sqrt{n}\sqrt{n}O(k*m*n) = O(k*m*n^2) = O(m*n^2) \qquad \text{(Eq. 4.28)}$$

In the above equation, the average value of k is equal one based on the above mentioned assumption and by continually assuming $m \approx \sqrt{n}$.

If we invert the stiffness matrix by any traditional method, the operations needed for a banded matrix with dimension n and bandwidth m are $O(m*n^2)$ which is equal to the value shown in Equation 4.28. Thus, solving for the complete load path using the pseudoforce algorithm "is no harder" than inverting the stiffness matrix.

4.6 TREATMENT OF ILL-CONDITIONED STIFFNESS MATRICES

During the nonlinear analysis procedure, as the overall stiffness of the problem approaches 0 (near ultimate), the determinant of the global stiffness matrix approaches 0 rendering the solution of the simultaneous equations very difficult. When the size of the structural system is large, this situation becomes worse as the accumulated residual errors influences the global matrix's stability. On the other hand, for the pseudoforce algorithm, only the inner part of the Sherman-Morrison-Woodburg may become unstable. Hence, the ultimate solution will be easier to obtain because the size of the inner part of the Sherman-Morrison-Woodburg formula is much smaller than the global matrix. In fact, the singularity associated with a smaller matrix is easier to deal with allowing for the modeling of unloading systems. This topic will be the subject of a future research.

4.7 ILLUSTRATIVE EXAMPLE 2

The applicability and efficiency of the proposed solver for the incremental nonlinear analysis of structural systems is demonstrated through the analysis of a structural grid.

The grid represents the model of a 10m bridge (1/3 scale) with three girders, whose elevation and material properties are shown in Figure 4.6. The bridge that was tested by Znidaric & Moses (1997, 1998) as part of the US-Slovene project, has been used to investigate the ultimate capacity of highway girder bridges. The program NONBAN is used to perform the nonlinear analysis of the same bridge (Ghosn, Deng, Xu, Liu, and Moses, 1997). To perform the structural analysis using the program NONBAN, the girder is discretized into 20 identical beam elements as shown in Figure 4.7. The moment-curvature relationship for the girders are shown in Figure 4.8. The value of the element plastic hinge length, L_{gp}, associated with this mesh and the main girders' member properties is calculated to be 0.175 m (Deng, 2000). Figure 4.9 compares the analysis results to those obtained during the laboratory testing.

The program NONBAN has been modified so that it can perform the nonlinear analysis either, by assembling the global stiffness matrix and solving it at each loading step using the traditional LDL^T method, or the proposed solver based on the pseudoforce approach. For the pseudoforce method two options have been introduced: a) The first option performs the calculations at every increment of the loading process continuously using Equation 4.11. And b) The second option performs the calculations using Equation 4.11 for a number of steps after which the algorithm is restarted by reassembling the global stiffness matrix again.

As mentioned above, the restart option is very useful because the efficiency of the proposed algorithm is a function of the rank of the global stiffness matrix and the rank of

matrix W of Equation 4.4. The rank of the W matrix increases as the plastic zone spreads throughout the structural system. In this example, the restart option is triggered when the dimension of matrix W reaches half the bandwidth of the global matrix.

The analysis shows that the bridge reaches its ultimate capacity after 339 incremental steps. The times needed in every step for the three algorithms used in this study: 1) LDL^T algorithm; 2) Pseudo-force algorithm without a restart option; and 3) Pseudo-force algorithm with a restart option, are plotted in Figure 4.10. The curves give the total time required for each finite element analysis including the preprocessing time, solving time and postprocessing time. The plots show that the time required when using the LDL^T algorithm oscillates between 330 to 390 milliseconds except for the first step that prepares the calculation platform. The pseudoforce algorithm with the restart option shows peaks at the points of restarts followed by lower computing time where the average low value is around 130 millisecond and the average restart peak value is 310 millisecond. The time curve for the pseudo-force algorithm without the restart option is a cubic curve as described in Equation 4.12. The average time needed for each step with the LDL^T algorithm is 346 millisecond, the average time needed by the pseudo-force algorithm with restart option for each step is 157 millisecond, and the average time needed by the pseudo-force algorithm without the restart option for each step is 548 millisecond.

Figure 4.11 gives plots of the cumulative times for the three algorithms. The figure shows that the pseudo-force algorithm with the restart option is 220% faster than the

LDL^T solver. The pseudo-force algorithm without the restart option is not as efficient as the LDL^T solver when the total number of steps exceeds 202. From Figure 4.10 it is also observed that the non-start option compares less favorably than the LDL^T starting with step number 123. Thus, the pseudo-force algorithm should not be used without the restart option.

Clearly, the pseudo-force algorithm reduces the computational effort during the solution of the global stiffness equation. Figure 4.12 shows the time needed to only solve the global stiffness equation at every step using the LDL^T algorithm and the pseudo-force algorithm with the restart option. The average time needed by LDL^T algorithm for every step is 235 milliseconds with a range varying from 210 to 280. For the pseudoforce algorithm with restart option, the average solver time need at every step is 59 millisecond. The peaks average around 270 seconds at every restarting point. For the other steps the time varies between 110 to close to 0. Figure 4.13 shows how the cumulative solver times compare for the two algorithms. For the 339 steps need for the ultimate capacity to be reached, the total time required by the pseudoforce algorithm is ¼ the time required by the LDL^T solver. The efficiency of the proposed pseudoforce algorithm will increase even further for larger scale problems as proven in equation 4.28.

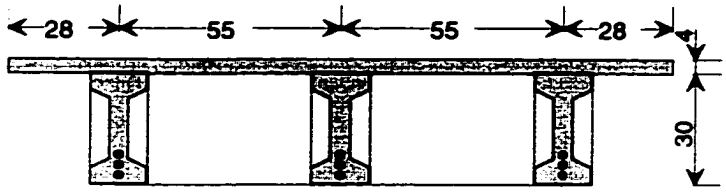

a) Bridge cross section. (units in cm)

b). Table of material properties

Material	Yield Strength f_y (MPa)	Ultimate Strength f_u (MPa)
Tendon	1600	1838
Deck Concrete		52.0
Beam Concrete		52.2

Figure 4.6. Description of Slovenia bridge.

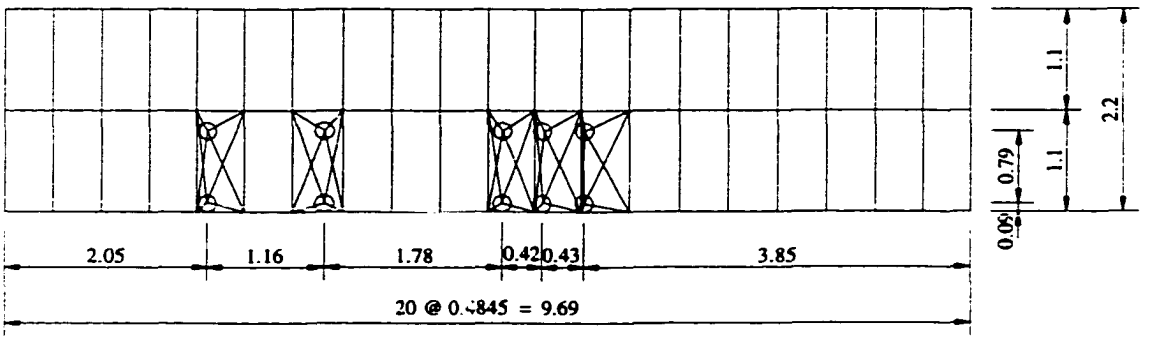

* Symbol O indicates the loading point.

Figure 4.7. Mesh discretization for Slovenia bridge (units in m).

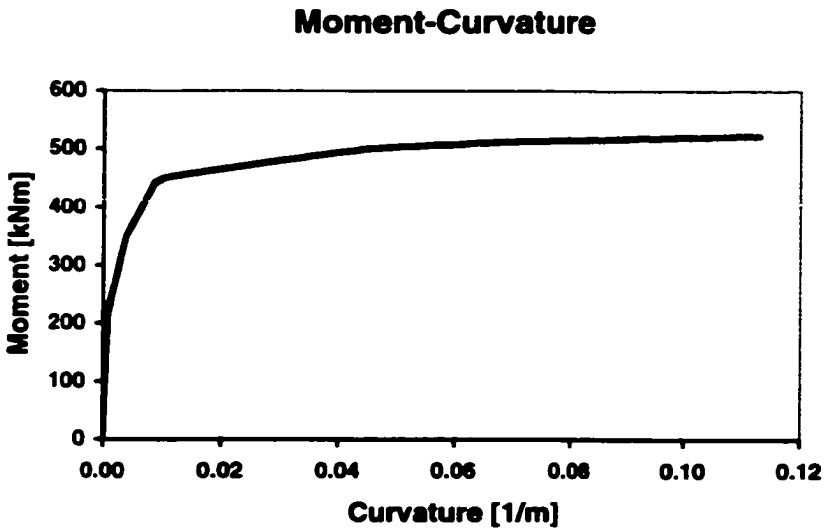

Figure 4.8. Moment-curvature relationship of girders

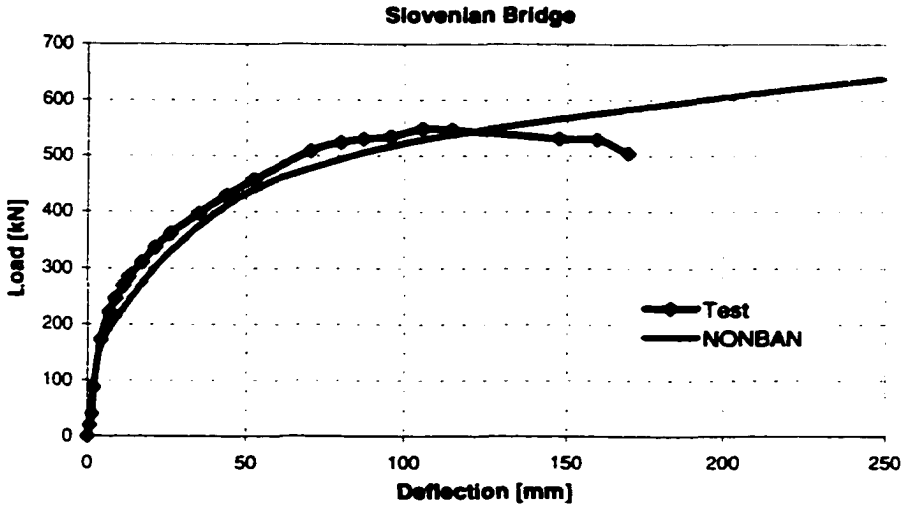

Figure 4.9. Comparison of NONBAN results to experimental results for Slovenia Bridge

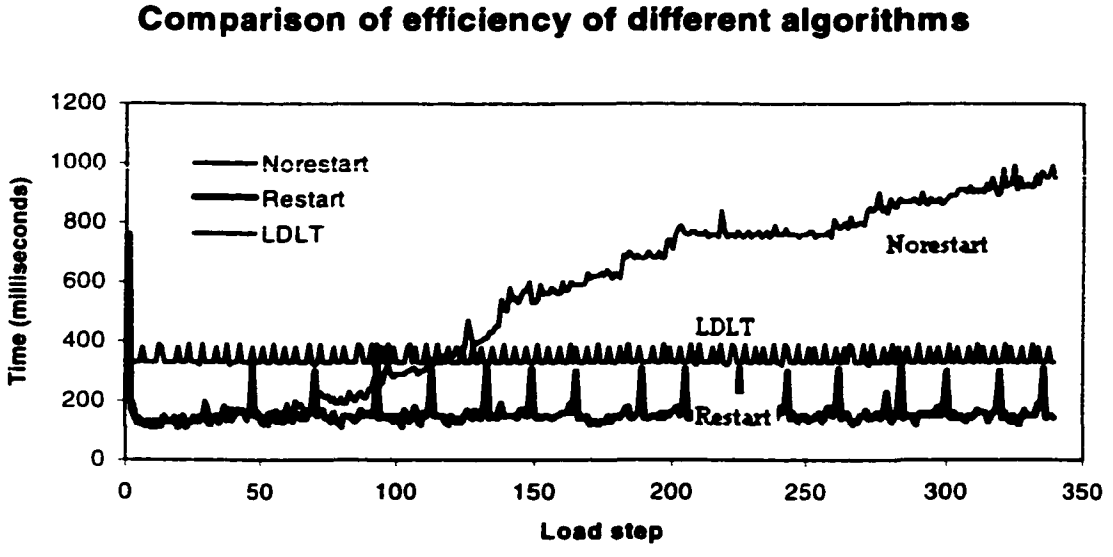

Figure 4.10. Comparison of computational time required at every load step.

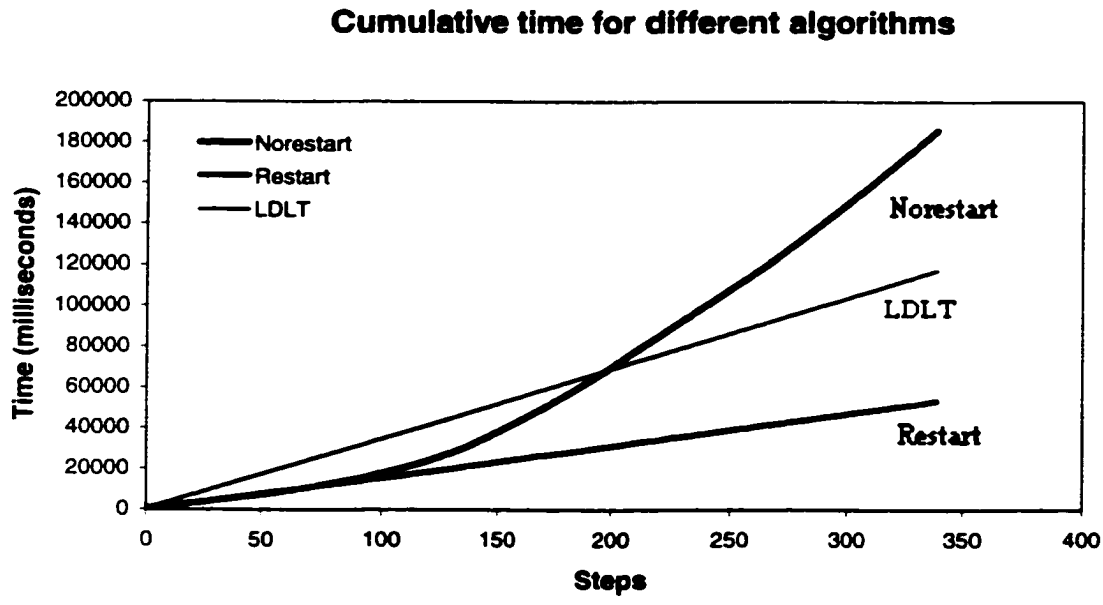

Figure 4.11. Cumulative time required by different methods.

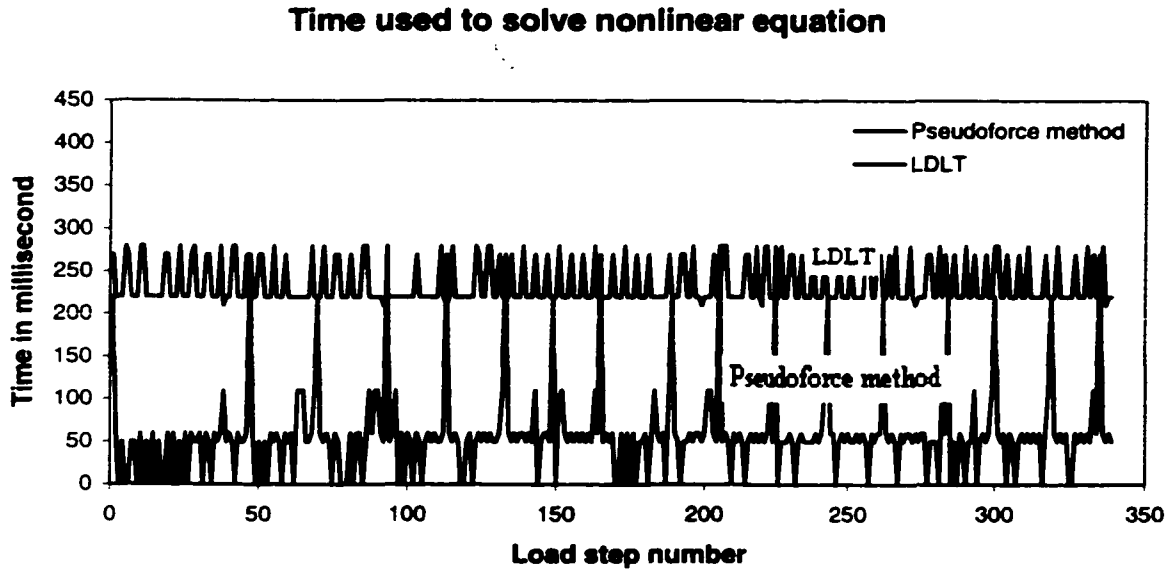

Figure 4.12. Comparison of solver time by LDL^T and the pseudoforce method.

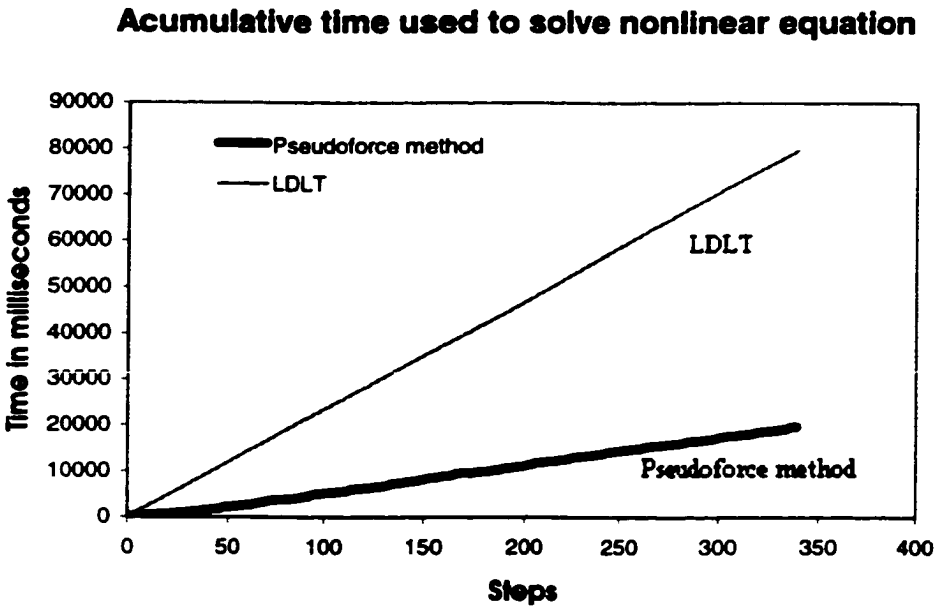

Figure 4.13. Cumulative solver time by LDL^T and the psudoforce method.

4.8 SUMMARY

A pseudoforce method is developed to solve finite element based structural analysis problems. The method has the following features:

- It is based on the Sherman-Morrison-Woodburg formula.
- It is applicable to a variety of problems including nonlinear structural analysis, structural redesign, reliability and optimization.
- It is shown to be more efficient than traditional solution methods.
- It is robust giving accurate solutions for a wide range of applications and matrix sizes.
- It is applicable to different types of structural systems including 2-D and 3-D truss, frame, plates and shells.
- It is easy to implement in existing finite element packages.
- It can be used in association with a variety of nonlinear solution schemes including the Newton Raphson algorithm and the incremental loading technique.
- It can be extended to predict and solve singularity problems associated with the global stiffness matrix for structural unloading.

CHAPTER 5

SHREDDING GENETIC ALGORITHM FOR RELIABILITY ANALYSIS OF STRUCTURAL SYSTEMS

This chapter proposes a modified genetic search algorithm referred to as the Shredding Genetic Algorithm (SGA) for the reliability analysis of structural systems. The classical genetic algorithm uses three operators namely: selection, crossover, and mutation, to reach a search's optimum goal based on a Darwinian survival-of-the-fittest principle. In modern breeding technology, scientists cultivate healthy and strong animals by interfering with the natural selection process and filtering out the weakest and unhealthy pubs using the principle of elitism. By simulating this filtering process, the proposed SGA improves the traditional genetic algorithm to focus the search around the most important genes and increase the convergence rate. To establish the filtration criteria, the first step of SGA shreds each chromosome into pairs of genes and calculates a fitness factor for each pair. The fitness factors are assembled into a fitness index matrix that is updated generation by generation. The chromosomes created during the crossover steps are filtered to meet a threshold value based on the fitness index matrix. The chromosomes with fitness below average are likely to be eliminated in this step following a probabilistic filtration standard. This makes the search procedure concentrate on the fittest gene pairs. This innovative step is defined as a filtration operator implemented between the crossover and mutation operators of the classic genetic algorithm. In this chapter the proposed algorithm is applied to the reliability analysis of structural systems. In comparison with classical reliability analysis techniques, SGA not only identifies

structural failure modes, but also gives detailed information about which random variables are primary contributors to the formation of these failure modes. Such useful information would eventually lead to better control of the safety of structural systems and improve the reliability of designs. Examples are provided in this chapter to demonstrate the application of the proposed SGA method and its efficiency.

5.1 INTRODUCTION

Current methods for the design and analysis of structural systems are based on a linear elastic structural analysis although structural members may be selected based on their ultimate capacity. During the design process, every member is considered separately. The interlocking of the members into one complete structural system is not properly considered particularly beyond the elastic limit. This may cause the design of systems of either inadequate or underestimated safety levels (Murotsu, Okada and Shao 1993). Current structural design codes account for the randomness in the design and analysis parameters by using safety (resistance and load factors) calibrated based on the level of uncertainty. Much work, however, is still needed to reconcile the differences between the simplifications used during the design process and the actual behavior of structural systems. Particularly that, the current calibration process still considers the reliability of individual members in isolation and ignores the system's effects. Recent work has proposed the use of system factors to account for the difference between the system reliability and the reliability of bridge members (Ghosn & Moses, 1998). This work however has concentrated on simple bridge configurations consisting of parallel members

by looking at a pre-selected single system failure mode. Thus, research is still needed to develop advanced structural reliability techniques applicable for large and complex structural systems with multiple failure modes.

Evaluating the reliability of a structural system is quite difficult because a closed-form representation of the resistance R of a system is often impossible to obtain. One way to simplify the system analysis is to assume that the system can be described by a series of sub-systems. Every sub-system describes one possible failure mode. If all the failure modes are known, the system reliability or at least bounds on the reliability can be obtained (Ditlevsen, 1979, Thoft-Christensen, P., Murotsu, Y. 1986). The system reliability is often dominated by a few critical modes. In order to identify the dominant failure modes, two analytical tools are required. The first is an accurate nonlinear structural analysis program capable of analyzing the behavior of structural systems for specific (deterministic) sets of loading conditions and material properties. Several programs are currently available for performing the nonlinear analysis of structural systems. For example, the authors and their colleagues were involved in the development of a specialized program for the analysis of bridge systems with parallel members. (Ghosn & Moses, 1998; Deng & Ghosn, 2000; Deng Ghosn, Znidaric & Casas, 2000). The second required tool is a systematic search algorithm capable of identifying the probabilistically dominant failure modes accounting for the randomness in applied loading and material properties.

Typical methods for identifying dominant failure modes can be broadly divided into three categories: a) Enumeration techniques, b) Plasticity-based procedures and c) Simulation-based methods. The enumeration approach is based on generating a failure tree to identify all possible structural failure paths. The approach consists of following the sequence of element failures step by step until system failure occurs. The incremental loading method (Moses 1982) and the branch and bound technique (Thoft-Christensen, Murotsu 1986; Karamchandani 1987) provide two typical applications of this approach. To speed up the search for dominant failure paths, various heuristic techniques have been introduced into the enumeration algorithms (Xiao and Mahadevan 1994; Shetty 1994). All these techniques simplify the enumeration process but provide no guarantee against missing important failure paths.

The plasticity-based approach is suitable only for elasto-plastic systems. It is based on plastic limit analysis using the lower and upper bound theorems. However, it is not capable of enumerating all the structural collapse mechanisms, nor identifying the dominant mechanisms directly. For example, the β-unzipping method (Thoft-Christensen & Murotsu 1986) starts from a set of basic plastic mechanisms, and generates new ones by combining the basic mechanisms. Another attractive method in this field is to apply mathematical programming algorithms, especially linear programming methods (LP), to systematically search for the dominant failure modes (Corotis and Nafday 1989).

Simulation-based methods are usually expensive tools for the reliability assessment of large structures. The Monte Carlo simulation is a classic example of simulation tools.

Variations on Monte Carlo simulations have long been available to improve efficiency. In particular, directional simulation discards the least important dimensions of a random vector (in polar coordinates) from the simulation process. Other approaches adopted by Ditlevsen & Bjerager (1989) and Corotis & Nafday (1989) consist of including the LP procedure mentioned above into the directional simulation to identify critical plastic mechanisms.

Current techniques have various limitations. For example, it has been observed that: (a) searching for dominant failure modes of a large structure on a probabilistic basis is inefficient and requires too much computational time; while (b) deterministic/heuristic search strategies may miss important failure paths. Hence, more efficient and accurate methods need to be developed if reliability theory is to be applied in practical safety evaluation of structural systems.

Recent developments in the field of artificial life provide several new computational techniques that can be applicable to solving structural reliability problems of large structural systems. For example, Genetic Algorithms (GAs) have been developed following the principles of genetics and natural selection to guide a search into the regions of a domain that have the highest potential (or fitness) for improving the objective of the search (Goldburg 1989). In other words, a genetic algorithm is a search/optimization technique based on a natural selection process. Successive generations evolve more fit individuals based on Darwinian survival of the fittest principle. The genetic algorithm is a computer simulation of such an evolution process

where the user provides the environment (domain) in which the population must evolve. Shao & Murotsu (1999) applied the GA algorithm to the reliability analysis of structural systems. The search strategy they followed is briefly outlined in the next section. The advantage of GA is that near-optimal results are obtained by evolution. Although more efficient than classical optimization techniques, GA algorithm still requires a large number of iterations. To help improve the GA's efficiency, this chapter proposes a modified genetic search strategy referred to as the shredding genetic algorithm (SGA). SGA increases the convergence rate by using a fitness index matrix to filter out the generated chromosomes and preserve those that are the most likely to survive.

The algorithm is based on the observation that modern breeding technology cultivates healthy and strong animals by interfering with the natural selection process and filtering out the weakest and unhealthy pubs using the principle of elitism. By simulating this filtering process, the proposed SGA improves the traditional genetic algorithm to obtain better results and simultaneously increase the convergence rate. This chapter describes in detail the proposed algorithm and its application to the reliability analysis of structural systems. This chapter demonstrates that the proposed SGA not only identifies structural failure modes, but also gives detailed information about which random variables are primary contributors to the formation of these failure modes. Such useful information would eventually lead to better control of the safety of structural systems and improve the reliability of structural designs. A Example in this chapter and three examples in the next chapter are provided to demonstrate the application of the proposed SGA method and its efficiency

5.2 RELIABILITY ANALYSIS BY GENETIC ALGORITHM

Consider an independent standard normal random variable space referred to as the U-space. The space is divided into a safe domain and a failure domain. The edge of the failure domain is identified by a failure surface formed by a number of failure modes g_1, g_2... g_i ... To find the failure modes, the space is searched in discrete directions identified as vectors I_i, I_j, etc. These vectors are tied to the origin as shown in Fig. 5.1. The failure modes, g_1, g_2, g_i... are reached by following the failure paths in the directions I_i. The angle θ between two adjacent directions is related to the correlation between the failure paths. In the method developed by Shao and Morutsu (1999), the number of search directions is preset as a function of the number of random variables. For examples, 3^n-1 discrete search directions are used in an n-dimensional space as shown in Fig. 5.2. Fig. 5.2 shows that the specified directions of the search vectors can be represented by their coordinate vectors, such as (1, 0, -1), (-1, 1, 1), (0, -1, 1).

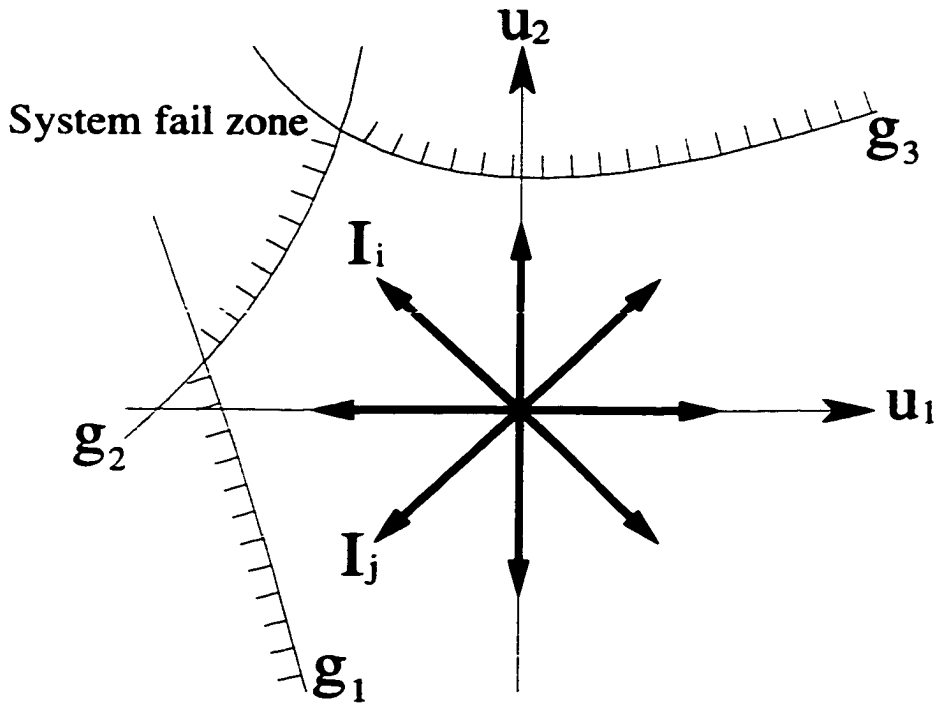

Figure 5.1. Discrete search directions.

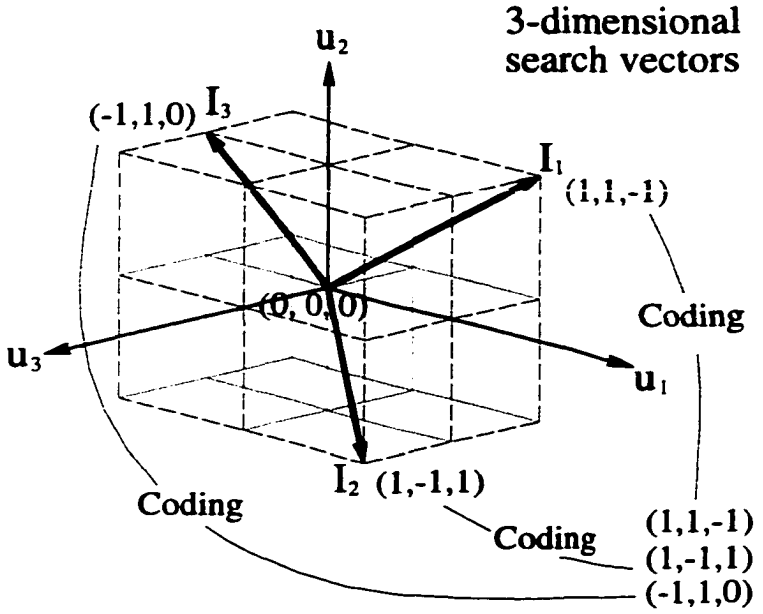

Figure 5.2. Coding of search direction vectors.

Since GAs work with a coding of variables, and not the variables themselves, the search direction vectors are expressed by a three-digit system where each of the digits belong to the set (-1, 0, 1). This "coding" originally proposed by Shao am Murotsu(1996) is described as shown in Fig. 5.2, where the rectangular coordinates of a direction vector constitute a string of digits known as chromosomes in GAs parlance. Hence, each chromosome in this problem corresponds to a search direction.

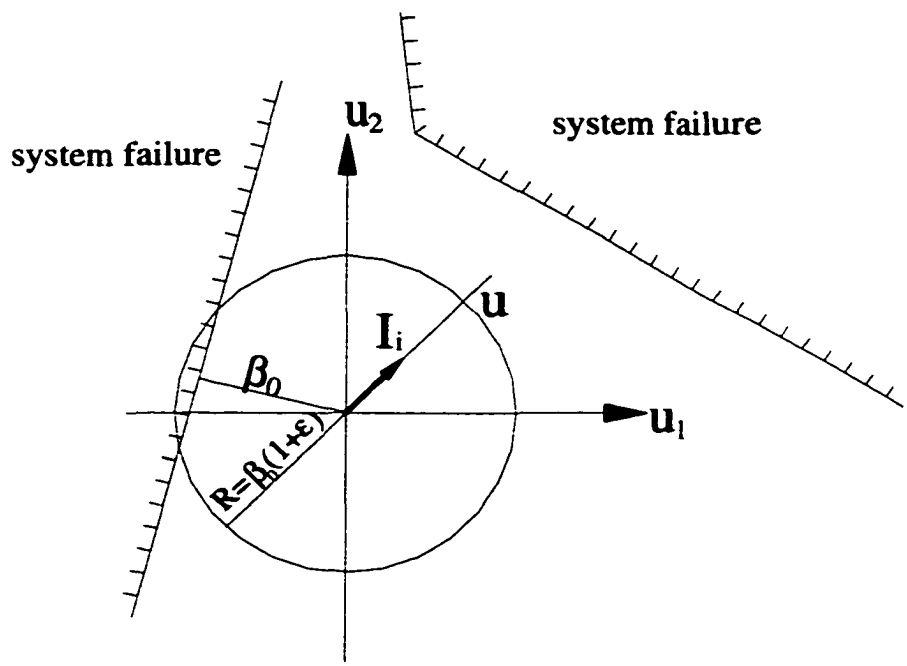

Figure 5.3. Illustration of GA search strategy.

In a natural selection process, the "most fit" genes are the ones that are most likely to survive from one generation to another. Hence, to simulate the natural selection process (in this case, which direction should survive and which direction should be killed off), GAs require the assignment of a level of fitness to each chromosome (direction). Fitness is herein determined based on the numerical value of the reliability index β, i.e. the distance from the origin of the U-space to the failure surface as shown in Fig. 5.3. A small β-value corresponds to a good fitness, which means a failure mode forms easily in that direction. In this sense, fitness is related to the probability of failure (i.e. the closer the failure surface is to the origin, the more fit is the search direction).

In order to save computational time, the search distance in each direction is limited to $\beta_{min}(1+\varepsilon)(\varepsilon>0)$. Where β_{min} is the minimum reliability index from previous search steps. If the structure is still safe at $\beta_{min}(1+\varepsilon)$, then, the search in that direction will be abandoned, because no significant failure mode has been found within a reasonable range. As shown in Fig. 5.3, the search in direction I_i is stopped at point u where no element has failed.

To initiate the search process, GA randomly generates a set of chromosomes to form a first generation of directions. Then, GA adjusts the search by modifying these chromosomes. The modification will produce a "new generation" of chromosomes that is created by using the following 3 operators: Selection, Crossover and mutation. The objective is to improve the "quality" of the chromosomes with each new generation.

Selection simulates the evolution process that allows the chromosomes with best "fitness" to survive and mate. "Fitness" is defined by fitness functions that may be chosen to be of the form $1/\beta$, $1/\beta^k$, $e^{(-\beta)}$, etc. The chromosomes in a new generation are the offsprings of the chromosomes selected from the previous generation. The selection is done randomly such that the strongest chromosomes (with high fitnesses) have higher probabilities to contribute offsprings to a new generation.

Crossover simulates the natural mating phenonenon whereby the chromosomes of the offsprings (directions) in a new generation are obtained by crossing the chromosomes of two "parent" directions. In the Genetic Algorithm, each randomly selected chromosome mates with another to form a "pair". During the crossover a chromosome swaps a part of its character with its mate to produce a pair of offsprings that have the combined characters of the parents. In this way, some important "schemata" (strong characters) may be composed and kept in the new strings. The corssover process is illustrated in Figure 5.4.

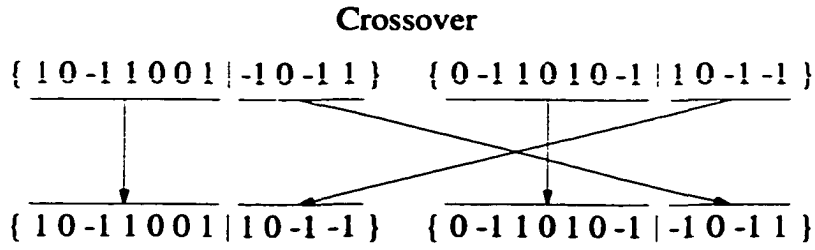

Figure 5.4: Illustration of crossover operator

Mutation is a secondary operator that simulates an inheritence that goes astray. It is an explorative operation that allows the search to wander into regions of the solution space which may never have been reached from the crossover operator. The purpose of the mutation operator is to reduce "in-breeding" that may misdirect the search process. Some new "genetic material" is occasionally introduced into the new generation by randomly changing digits in each string. For example, a 1 is randomly changed to 0 or to −1, or vice-versa. This is done only with a very low probablity to generate new genetic material without loosing track of the important directions that the search has produced so far.

In general, the above search strategy, proposed by Shao and Murotsu (1996, 1999), is a flexible and fairly efficient method to search the complex structural domains for optimum solution during structural optimization and reliability analysis. As mentioned by Goldberg & Samtani (1986) the GA has the following main characteristics:

- Robustness. It efficiently gives good solutions for any optimization problem.
- Flexiblility. The same procedure, operators and modeling scheme are applicable to different physical variables.
- Bunching. The search is initiated from a population of points, rather than a single point.
- Probabilistic. It uses probabilistic transition rules, whereas traditional methods use deterministic gradient information (Goldberg 1989).

Despite its general efficiency and adaptability, classical GA requires a fairly large number of iterations to converge. The reliability analysis of structural systems requires a nonlinear analysis to find the reliability index for each point along each possible failure path. This requires a huge computational effort. Hence, any improvement in the search efficiency will help reduce the compuational effort tremendously. Such improvements are possible by interfering in the natural selection process and filtering out the chromosomes that follow unlikely search directions. The next section describes the Shredding Genetic Algorithm that introduces a proposed filtration operator that is shown to improve the classical GA's efficiency.

5.3 SHREDDING GENETIC ALGORITHM

The genetic search algorithm generates search directions in the random variable space of the parameters related to structural loading and material. A structural analysis program then performs a nonlinear structural analysis to follow the failure path in each search direction and to find the corresponding system capacity. The safety level associated with this system capacity is measured by the reliability index β. Through evolution, GAs find the most critical combinations of loads and material properties. Simultaneously, the most critical structural failure paths (and modes) are identified. The reliability index β for each chromosome is obtained using common Level II reliability algorithms. A huge computational effort is required when analyzing a large complex nonlinear structural system. To improve the efficiency, the Shredding Genetic Algorithm (SGA) is

introduced. The proposed method shreds a chromosome into small strings (in this case the strings are formed by pairs of genes) and uses information on the fitness of these pairs to filter out the chromosomes that have lower chances of survival.

The concept of SGA's shredding a chromosome into pairs is borrowed from the ideas used during the human genome project (US Dept. of Energy, 1997). The decoding project realized that identifying genes in a genome is an agonizingly slow process, as scientists typically spent years locating and decoding a single one (Lemonick & Thompson1999; Thompson 1999). By using a technique called shot-gunning, Dr. Venter and his team (Lemonick & Thompson 1999) were able to find genes in an manner much easier and more efficient than traditional techniques. The process has been so successful that the 1000 scientists who had spent 10 years decoding a yeast genome could complete their work in one day (Thompson 1999). In essence, shot-gunning amounts to putting DNA into a chemical "Cuisinart" where high-frequency sound waves shred the long stringy molecule into tiny fragments. The fragments are cloned in bacteria, and identified through a gene-sequencing machine. The code of the whole chromosome is reassembled back from the identified shredded strings.

Ideally in GA, crossover allows important string fragments of a chromosome with high fitness to cross over into the next generation. These fragments form a base from which strong chromosomes could more successfully evolve. As a fragment with good fitness meets with other fragments with good fitness, they most likely produce a new fragment with better fitness. Hence, identifying the fragments with high fitness can be an important

improvement for GA methods in general and the use of GA in structural reliability analysis. The object of the SGA is to identify strings formed by a pair of genes with high fitness index and allow the chromosomes with such pairs to survive and mate.

Consider a typical chromosome that is formed by a total of n genes. For example (1, 0, 1, 1, 0, 0, 1, 1, 1, 0, ...) is one representation of such a chromosome. The m genes (or variables) associated with 1 in the sequence are called active variables. In this example, the active variables are located in positions 1, 3, 4, 7, 8, 9... The other genes are not active. The reliability index associated with the failure mode described by the chromosome is β. An approximation to the probability of failure P_f can be obtained by assuming that the safety margin M (or failure function) is linear in the space defined by the n variables (x_1, x_2, ... x_n). This linear equation can be expressed as:

$$M = \frac{1}{\sqrt{m}}(x_1 + x_3 + x_4 + x_7 + x_8 + x_9 + ...) + \beta = 0$$
$$or: \quad (x_1 + x_3 + x_4 + x_7 + x_8 + x_9 + ...) + \sqrt{m}\beta = 0 \qquad \text{(Eq. 5.1)}$$

Notice that only the active variables appear in Equation 5.1. The non-active variables are known constant (deterministic) parameters that don't affect the safety index, β, in the direction associated with this chromosome.

In order to identify the most fit strings of the chromosome, the chromosome is shredded into several fragments. To simplify the analysis procedure without losing generality, we

shred each chromosome into fragments formed by 2 genes each. The above safety margin function can then be shredded in several ways. For example, as:

$$(x_1 + x_3) + (x_4 + x_7) + (x_8 + x_9) + \ldots + \sqrt{m}\beta = 0$$
$$or: \quad (x_1 + x_4) + (x_7 + x_8) + (x_9 + x_3) + \ldots + \sqrt{m}\beta = 0 \qquad \text{(Eq. 5.2)}$$
$$or: \quad \ldots$$

According to the theory of combinations, we can have C_m^2 different fragmented pairs. Suppose that a fragment is composed of two variables x_i, x_j and that the fragment has a fitness index equal to the safety index, β_{ij}. A chromosome fails when all its fragmented pairs (m/2 pairs) fail. Therefore, we can model this failure mode as a parallel system with m/2 pairs as shown in Figure 5.5.

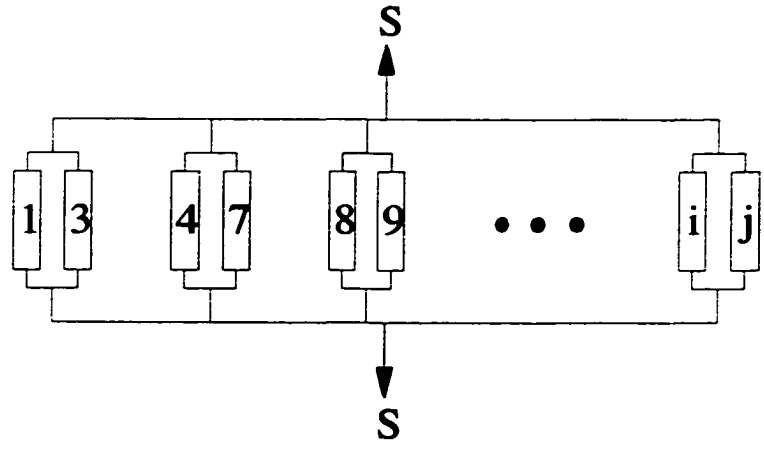

Figure 5.5. Modeling of a chromosome as a parallel system of gene pairs.

Grigoriu & Turkstra (1979) investigated the reliability of parallel systems under the following assumptions:

- The loading S is deterministic and constant in time.
- The strengths of members are identical normally distributed random variables.
- All elements are designed to have a common reliability index β_e.
- There is a common correlation coefficient ρ between any pair of elements.

Based on the above assumption, they proved that the reliability of a parallel system is:

$$\beta = \beta_e \sqrt{\frac{n}{1+\rho(n-1)}} \qquad \text{(Eq. 5.3)}$$

In equation (5.3), n is the number of members in parallel (=m/2 in this case). In SGAs, parallel elements are the fragmented pairs with the reliability index β_{ij}. Because SGA searches in a pre-determined set of discrete directions of the U-space, the coefficient ρ is equal to 1. If we assume that β_{ij} of all pairs of one chromosome are equal to each other, then applying Equation 5.3 for the parallel system shown in Figure 5.5, where β_e is equal to the safety index β_{ij} of one pair, n is the number of pairs, the reliability index of each pair can be approximated by:

$$\beta_{13} = \beta_{47} = \beta_{89} = \beta_{ij} = \beta \qquad \text{(Eq. 5.4)}$$

In a similar way, a fitness index can be calculated for all the other possible pairings that give the direction for one safety margin equation M. Although β_{ij} of all pairs of one chromosome are originally assumed equal for any one pairing scheme, updating the β_{ij} calculated from different pairing schemes and chromosomes will eventually produce β_{ij} values that vary depending on the safety index of the modes that contain the ij pair.

The fragment fitness index β_{ij} gives a measure of the importance of a particular fragment. These fragments play the same role as human genes where every chromosome is composed of genes with various fitness indexes. During the process of crossover, a chromosome is split at a given point, and some of the alleles are replaced by the alleles of the mate. Thus, if a fragment with a high fitness index is inherited by an offspring, it is highly likely that it would proliferate in a gene pool and it is likely to be found in the winning percentage of organisms chosen to reproduce in the next generation. It is reasonable to assume that after several generations a fragment with high fitness would find itself proliferating in the gene pool. Chromosomes' fitnesses are dependent on the fitnesses of the pairs that form them. The filtering operator introduced in this chapter serves to preserve the chromosomes with highly fit pairs. Offsprings that end up with weak pairs are filtered out. Similarly, if one offspring was created during the cross-over in such a way that the integrity of a "fit" fragment is lost, by splitting it, the whole chromosome's fitness is reduced and this weak offspring is not likely to be selected for reproduction.

The fragment's fitness changes for each chromosome and generation. To manage these changes, we establish a Fitness Index matrix, F, with dimension 2n*2n where n is the number of variables. Every item of this matrix gives a measure of a pair's fitness. For example, F[2, 5] gives the fitness index of the pair composed by random variables x_2 and x_5.

Within a given generation, the final β_{ij} of one pair is taken as the average value of all β_{ij} for that pair. To model the evolutionary process, the Fitness Index matrix is updated from generation to generation using a weighting factor. The weighting factor is used so that the Fitness Index matrix, F, preserves some of the information from all the chromosomes of one generation and from previous generations. This weighting factor can be chosen as 0.5 or 0.25 or as a combination of the existing fitness index. This is achieved as follows, if two pairs i and j were found to have a fitness index equal to $\beta_{ij,k}$, obtained from generation k, then if $\beta_{ij,k+1}$ for the same i and j genes of generation k+1 is found to be different than the previously calculated value, the final β_{ij} placed in matrix F will be $0.5*\beta_{ij,k}+0.5\beta_{ij,k+1}$ or $0.25*\beta_{ij,k}+0.75\beta_{ij,k+1}$.

As the fitness index matrix is established and updated, a filtering threshold can be defined. This threshold can be the average value of all the fitness indexes of all the paired fragments. It can also be chosen as the 80, 90-percentile or another percentile of the fitness indexes depending on the convergence requirements. The information in fitness index matrix can then be used to filter the chromosome obtained after the crossover operation. When a new chromosome is born, its estimated fitness can be calculated by

taking the average of the fitness index of C_m^2 pairs that are shredded from this new chromosome. By comparing the estimated fitness value and the threshold value, this new chromosome may be filtered out if it does not satisfy preset selection criteria. Two selection criteria are used in this chapter: a) If the estimated fitness value is higher than the threshold, the new chromosome is unconditionally accepted. b) If the estimated fitness value is smaller than the threshold value, the new chromosome may be accepted using a probabilistic acceptance criterion. In this study, the selection criteria are summarized as shown in Eq (5.5).

$$P = \begin{cases} 1 & \text{when } E \geq T \\ \left(\frac{E}{T}\right)^2 & \text{when } E < T. \end{cases} \qquad \text{(Eq. 5.5)}$$

where P is the probability of acceptance, E is the estimate fitness, and T is the threshhold value.

As will be shown in the examples presented in this chapter and mext chapter, the filtration operator plays an important role in improving the convergence of SGA. This operator is essentially an expert system that helps eliminate new chromosomes with low fitness and replace them with reasonbly strong ones. This operator simulates the interfence into the natural selection process encountered in breeding farms.

In summary, the proposed SGA can be represented using the following steps:

1. Define the space of random variables that affect the reliability of a bridge system. This must include the variables' probability distribution types and statistics including means, variances, etc.
2. Transfer the random variables into the normalized U-space as done in Level II reliability methods.
3. Determine an optimum population size that corresponds to the expected number of "important failure modes".
4. Create randomly and/or use experience to define a first generation of chromosomes in the U space. The chromosomes establish the direction of a search for a mode of failure.
5. Assume a value for the safety index corresponding to each chromosome in the population.
6. Convert each chromosome into realizations of random variables using the assumed safety index, β.
7. Use a structural analysis program to check whether the chosen β is correct for the chosen chromosome (direction).
8. Repeat steps 5 through 7 until convergence to get the β for each chromosome.
9. Establish the fitness index matrix.
10. Calculate the threshold fitness value.
11. Select two "good" "parents" randomly according to their fitness.
12. "Mate" the two "Parents" using the cross over operator to create two new children.
13. Calculate an estimated fitness for each chromosome from the fitness index matrix.

14. Repeat steps 12 and 13 if a child's chromosome does not satisfy the criteria of Equation (5.5).
15. Expose the "children" to a low mutation rate, flopping or switching a few bits.
16. Calculate the true reliability index for the new children using the structural analysis program.
17. Upgrade the fitness index matrix.
18. Repeat steps 11 through 17 until there are as many "children" as parents.
19. Discard one of the "children" at random, and replace him with the best "parent". This is called "Elitism".
20. Transfer the "children" array to the "parents" array to form a new generation.
21. Repeat steps 10) through 20) until the "population" converges. i.e. every new generation looks the "same" as the previous one.

The process is illustrated in the examples solved in the next section. Note that the search is executed in discrete directions. Thus, the final results produced are approximations to the actual dominant failure mode equation and safety indexes. The more refined the search directions are, the more "exact" are the final results. It is possible to combine SGA method with other techniques such as the response surface method to improve the accuracy of the final results.

5.4 ILLUSTRATIVE EXAMPLE

In this section, a simple example is presented to illustrate the proposed method. The example consists of the three-bar truss loaded by three forces L_1, L_2 and L_3 as shown in Figure 5.6.

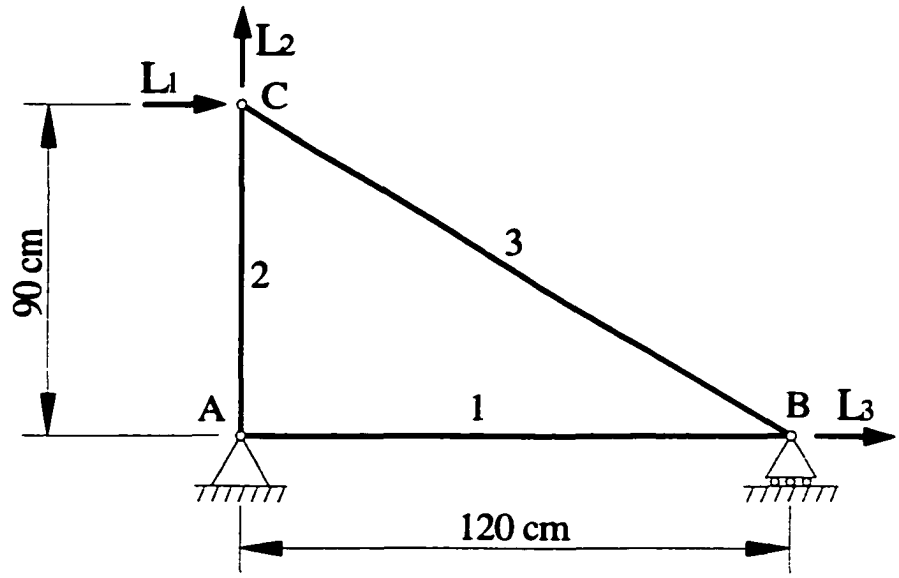

Figure 5.6. Three member truss example.

The input data for the loads and member strengths are listed in Table 5.1 where all the random variables are assumed to follow independent normal probability distributions. All truss members have the same cross sectional area A=2.3 cm^2.

Table 5.1. Load and material data for three-member truss example.

Random Variables	Mean	COV
L_1	35 kN	10%
L_2	20 kN	10%
L_3	15 kN	10%
σ_{y1}	27.6 kN/cm^2	5%
σ_{y2}	27.6 kN/cm^2	5%
σ_{y3}	27.6 kN/cm^2	5%

Table 5.1 gives the mean and the COV of the random variables identified as the loads L_1, L_2 and L_3 and the yielding stresses for members 1, 2, and 3 respectively identified as σ_{y1}, σ_{y2}, σ_{y3}. Each member may fail in tension or compression. The potential member failure modes are labeled: 1+, 1-, 2+, 2-, 3+ and 3-, where the number indicates which member fails, the "+" sign denotes failure in tension, while the "-" sign denotes failure in compression. It is assumed that the yielding stresses for tension and compression are independent random variables with the same mean and standard deviations.

Equilibrium gives the following member forces:

$$N_1 = L_1 + L_3$$

$$N_2 = L_2 + 0.75\, L_1 \qquad \text{(Eq. 5.6)}$$

$$N_3 = -1.25\, L_1$$

Where N_i gives the axial force in member i, and L_j gives the applied load j.

The reliability index, β_{1+}, for the failure of member 1 in tension is calculated as:

$$f = R - S = A\sigma_{y1} - (L_1 + L_3)$$

So, we have

$$\overline{f_{1+}} = 2.3 * 27.6 - (3.5 + 15.0) = 13.48 \qquad \text{(Eq. 5.7)}$$

$$\sigma_{f_{1+}} = \sqrt{2.3^2 * 1.36^2 + 3.5^2 + 1.5^2} = 4.93$$

$$\beta_{1+} = \frac{\overline{f_{1+}}}{\sigma_{f_{1+}}} = 2.735.$$

where f is the failure function, R is the member resistance, S is the applied load, $\overline{f_{1+}}$ is the mean value of the failure function, f, for member 1 in tension. σ_{f1+} is the standard deviation of f_{1+}. The reliability indexes for all other failure modes can be calculated in the same way and the results are listed in Table 5.2.

Table 5.2. Reliability indexes for the six possible failure modes.

Mode	β
1+	2.735
3-	3.67
2+	3.79
3+	19.94
1-	23.03
2-	24.12

Table 5.2 clearly shows that the dominant modes of failure are for member 1 in tension, member 3 in compression and member 2 in tension.

The objective of this example is to verify the ability of SGA to identify the dominant modes of this three-member truss. The analysis follows the same steps outlined in the previous section.

Since SGAs work with a coding of the variables, not the variable themselves, the random variables are converted into "binary" strings. For a given search direction in the U-space, the failure point (design point) is designated by A in Figure 5.7. The failure point coordinates are expressed as OA in Equation 5.8:

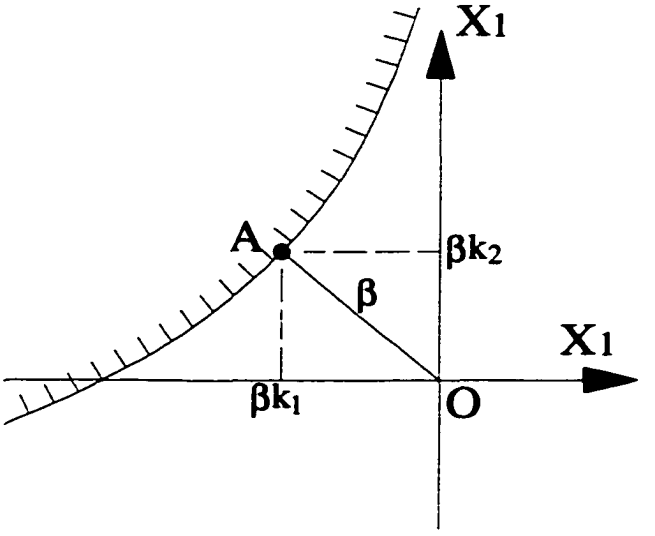

Figure 5.7. Illustration of a search direction.

$$OA = \beta\ (k_1 x_1, k_2 x_2, ..., k_n x_n) \qquad \text{(Eq. 5.8)}$$

Where $k_1, k_2, \ldots, k_n$ are the vector OA's coordinates in directions $x_1, x_2, \ldots x_n$, and $(k_1^{\,2} + k_2^{\,2} + \ldots + k_n^{\,2})^{1/2} = 1$.

Finding the reliability of one mode as described in Figure 5.7 reduces to finding the shortest possible distance between the mean point O (or the origin) and point A located on the failure surface. The SGA algorithm searches along pre-set directions with a known set of coordinates $k_1, k_2, \ldots, k_n$ of the unit direction vector of OA. The direction is represented as:

$$(k_1, k_2, ..., k_n) = (I_1, I_2, ..., I_n)\frac{1}{\sqrt{m}} \qquad \text{(Eq. 5.9)}$$

Where $I_i = 1, 0$, or -1 where 1 indicates an increase in the direction of variable x_i, 0 indicates that x_i remains at its mean value (origin), and -1 indicates a decrease in the direction of variable x_i. The index $i=1, 2, \ldots n$ identifies the variable. m, gives the total number of non zero terms in the set $(k_1, k_2, \ldots, k_n)$.

Plugging Equation 5.9 into equation 5.8, OA is calculated as:

$$OA = \frac{\beta}{\sqrt{m}}(I_1 x_1, I_2 x_2, ..., I_n x_n) \qquad \text{(Eq. 5.10)}$$

In SGAs, the search for the failure modes is executed by following the failure paths in the directions having the form of Equation 5.9. The I_i 's are identified as the chromosomes that represent the directions of x_1 ... x_6 which in turn represent the sequence of random variables L_1, L_2, L_3 and σ_{y1}, σ_{y2}, σ_{y3} in that order. In the normalized U-space these random variables are denoted by l_1, l_2, l_3, s_{y1}, s_{y2}, s_{y3}. This correspondence is symbolized as shown in Equation 5.11:

$$(I_1, I_2, I_3, I_4, I_5, I_6) \Leftrightarrow (l_1, l_2, l_3, s_{y1}, s_{y2}, s_{y3}) \qquad \text{(Eq. 5.11)}$$

An appropriate number of chromosomes define the population at some point in time. If there are too few chromosomes in any generation, GA has only few possibilities to perform the crossover operator and only a small part of the search space is explored. On the other hand, if there are too many chromosomes, GA slows down. Research shows that after some limit (which depends mainly on encoding and the problem) it is not useful to increase the population size, because it does not help solve the problem faster. Several search studies have investigated this problem. For example, Prof. Caroll D.C. gave a crude population scaling law:

$$npopsize = order(\frac{l}{k}2^k) \qquad \text{for binary coding.} \qquad \text{(Eq. 5.12)}$$

Where npopsize= optimum population size, l = length of chromosome and k is the average size of the schema of interest (effectively the average number of bits per

parameter). Caroll also suggested that this scaling law is usually overkill, i.e. you can most likely get by with population at least twice as small.

Because SGA uses a three-number representation rather than a binary system, the optimum population size in SGA is projected to be on the order of:

$$\text{npopsize} = \text{order}\left(\frac{l}{k}3^k\right) \qquad \text{(Eq. 5.13)}$$

Thus, the population size for this example reduces to: $(6/1)*3^1 = 18$. Following the recommendation of Caroll, the optimum population size in this example is chosen as 10. The first generation is created randomly. Its chromosomes are listed in Table 5.3.

The reliability index for each chromosome can be calculated by standard level II methods. For example, the reliability index of chromosome No. 2 (1-1 0 0-1 0) can be calculated by the following steps :

$$l_1 = \beta\frac{1}{\sqrt{3}} = \frac{L_1 - \overline{L_1}}{\sigma_{L1}} = \frac{L_1 - 35}{3.5} \longrightarrow L_1 = 2.021\beta + 35$$

$$l_2 = \beta\frac{-1}{\sqrt{3}} = \frac{L_2 - \overline{L_2}}{\sigma_{L2}} = \frac{L_2 - 20}{2.0} \longrightarrow L_2 = -1.155\beta + 20$$

$$s_2 = \beta\frac{-1}{\sqrt{3}} = \frac{\sigma_{y2} - \overline{\sigma_{y2}}}{\sigma_{\sigma_{y2}}} = \frac{\sigma_{y2} - 27.6}{1.38} \longrightarrow \sigma_{y2} = -0.797\beta + 27.6$$

Table 5.3. Generation 1's chromosomes and their results.

Index	Chromosomes						β	Fitness
1	1	0	0	0	0	0	3.851	0.260
2	1	-1	0	0	-1	0	6.671	0.150
3	0	-1	-1	0	0	-1	10.767	0.093
4	0	1	1	0	1	-1	12.432	0.080
5	1	0	-1	0	1	1	13.480	0.074
6	0	1	-1	0	0	1	14.922	0.067
7	-1	0	-1	-1	0	-1	27.766	0.036
8	-1	-1	-1	-1	0	1	31.043	0.032
9	-1	0	-1	1	-1	-1	31.762	0.031
10	0	0	-1	1	1	1	1000	0.001

From Equation (5.6), the member forces can be expressed as:

$$N_1 = L_1 + L_3 = 2.021\beta + 35 + 15 = 2.021\beta + 50$$
$$N_2 = L_2 + 0.75L_1 = -\beta + 20 + 0.75(2.021\beta + 35) = 0.515\beta + 46.2$$
$$N_3 = -1.25L_1 = -1.25(2.021\beta + 35) = -(2.526\beta + 43.75)$$

Chromosome 2 shows that member 1's yielding stress remains at its mean value (because the 4th digit is 0). Then, assuming that member 1 fails, the reliability index is obtained as:

$$R - N = 0$$

Or: $2.3*27.6-(2.021\beta+50) = 0$

Giving: $\beta = 6.671$.

In a similar way, $\beta = 7.359$ is found for the failure of member 2, $\beta = 7.811$ for the failure of member 3. By comparing the three failure modes associated with chromosome No. 2, it is observed that in the direction of chromosome No. 2 the failure mode corresponding to member 1 occurs first. Thus, the reliability index β for the chromosome (1-1 0 0-1 0) is chosen as the lowest reliability index β=6.671.

Following the same procedure, the reliability indices for all the other chromosomes in the population are calculated and listed in Table 5.3. In this example, the fitness index is defined as $1/\beta$. The fitness indices for all chromosomes of the first generation are also listed in Table 5.3.

After the reliability indices for the chromosomes of generation 1 are established, the fitness index matrix is assembled by shredding each chromosome into pairs and calculating each pair's fitness index as explained above. The fitness matrix after the first generation is provided in Table 5.4. For example, in Table 5.4 the fitness index of a pair corresponding to random variables L_1+ and σ_{y2}+ is equal to 0.15. The 0.15 value was obtained by taking the average fitness index from all the chromosomes that contain this particular pair.

Table 5.4. Fitness index matrix for generation 1.

	L_1^+	L_1^-	L_2^+	L_2^-	L_3^+	L_3^-	σ_{y1}^+	σ_{y1}^-	σ_{y2}^+	σ_{y2}^-	σ_{y3}^+	σ_{y3}^-
L_1^+	.161	0	0	.150	0	.074	0	0	.074	.150	.074	0
L_1^-	0	.033	0	.032	0	.033	.031	.034	0	.031	.032	.034
L_2^+	0	0	.074	0	.080	.067	0	0	.080	0	.067	.080
L_2^-	.150	.032	0	.092	0	.063	0	.032	0	.150	.032	.093
L_3^+	0	0	.080	0	.080	0	0	0	.080	0	0	.080
L_3^-	.074	.033	.067	.063	0	.048	.016	.034	.038	.031	.043	.053
σ_{y1}^+	0	.031	0	0	0	.016	.016	0	.001	.031	.001	.031
σ_{y1}^-	0	.034	0	.032	0	.034	0	.034	0	0	.032	.036
σ_{y2}^+	.074	0	.080	0	.080	.038	.001	0	.052	0	.038	.080
σ_{y2}^-	.150	.031	0	.150	0	.031	.031	0	0	.091	0	.031
σ_{y3}^+	.074	.032	.067	.032	0	.064	.001	.032	.038	0	.044	0
σ_{y3}^-	0	.034	.080	.093	.080	.053	.031	.036	.080	.031	0	.060

From Table 5.4, it is observed that even after one generation, some good pairs of genes are detected. A few bad genes have also been identified. For example, the pairs including L_1^- have much lower fitness index than the corresponding pairs including L_1^+, the pairs including σ_{y1}^+ have much lower fitness index than the corresponding pairs including σ_{y1}^-. This information will be used to determine the new chromosome's fitness index and filter out the new chromosome with low fitness index.

The birth of new chromosomes for a new generation is achieved through the crossover operation. The fitness index matrix is updated from one generation to another using a bias toward the values obtained in the most recent generation. This bias is achieved by putting more weight on the values of the latest generation. The weights chosen in this example are such that the indexes evaluated during the latest generation have a weight factor of 0.50 and the values combined from previous generations have a weight of 0.50. In this way, the fitness index of a pair has 50% influence to the next generation, has 25% percent to generation after next generation... The influence of a pair with fitness predicted wrong would be eliminated soon in this weight strategy. The fitness index matrix will becomes more and more accurate to describe the fitness index for each pair.

Table 5.3 shows that the maximum fitness for the 10 chromosomes of generation 1, is 0.260, the minimum fitness is 0.001, the average fitness is 0.0825. The sum of all the fitness indices of all chromosomes in this generation is 0.825. The average fitness of all pairs in the fitness index matrix of Table 5.4 is 0.0553. These numbers will serve to decide on the filtration threshold.

In this example, the threshold value for the filtration operator is chosen as the average of the maximum fitness from the former generation and the average fitness of the former generation (average (max, average)). Thus, the threshold for generation 2 of this example is equal to (0.260 + 0.0825)/2) which leads to 0.1712.

Following the standard selection and crossover operators, the first new chromosome produced in generation 2 is (0-1-1 0 0-1). Using the fitness index matrix, the chromosome's estimated fitness can be calculated as 0.0696. This chromosome is rejected during the filtration operator because its acceptance probability is $(0.0696/0.1711)^2$ which is low. A newborn chromosome created by another crossover operation replaces the rejected chromosome. The replacement chromosome is itself filtered out and the process is repeated until a chromosome passes the filtration process.

The accuracy of the fitness index matrix is very rough in the first generation. At this point it only gives a rough evaluation of the strength of each pair. However, SGA quickly updates the matrix by self -education. After only few generations, the matrix is able to provide remarkable precision on the estimate fitness of a new chromosome and the most important pairs of genes that control the failure modes. For example, using the fitness index matrix in generation 4, the chromosome (1-1 10-1 0-1) has an estimated fitness equal to 0.207 which compares well to the actual fitness of 0.271; the chromosome (1-1 0-1 0-1) has an estimated fitness equal to 0.201 which compares well to the actual fitness of 0.247; the chromosome (1 1 0 0 0-1) has an estimated fitness equal to 0.165 which compares well to the actual fitness of 0.221; the chromosome (1-1 0 0 0 1) has an estimated fitness equal to 0.206 which compares well to the actual fitness of 0.150. Although these results have some errors, they are good enough to make the filtering operation. The estimated fitness indexes of chromosomes for generation 20 are much better described. For example, the chromosome (1 1 0-1 0-1) has an estimated fitness equal to 0.228 which compares well to the actual fitness of 0.248; the chromosome (1 1

0-1 0 0) has an estimated fitness equal to 0.259 which compares well to the actual fitness of 0.286.

The total possible number of chromosomes for the three-member truss with 6 random variables is $3^6 - 1 = 728$. The two dominant chromosomes are known to be (1, 0, 1, -1, 0, 0) with $\beta = 2.85638$, and (1, 0, 0, -1, 0, 0) with $\beta = 2.8564$. These can be easily identified for the three-member truss using hand calculations. After only 15 generations, SGA found the second most dominant mode (1, 0, 0, -1, 0, 0) with $\beta = 2.8564$ and within 17 generations both dominant modes were identified. This is found to be twice faster than the classical GAs. The results for generations 10, 20, 40 are listed in Table 5.5. Table 5.6 lists the most important failure modes identified within 50 generations.

Table 5.5. Results of SGA search for example 1.

Generation 10	β	Generation 20	β	Generation 40	β
1 0 1-1 0-1	3.29826	1 0 1-1 0 0	2.85638	1 0 1-1 0 0	2.85638
1 1 0-1 0 0	3.49836	1 0 0-1 0 0	2.8564	1 0 0-1 0 0	2.8564
1-1 1-1 0-1	3.68757	1 1 1-1 0 0	3.29826	1 0 1-1 0-1	3.29826
1 0 0 0 0-1	3.69618	1 0 1-1 0-1	3.29826	1 1 1-1 0 0	3.29826
1 0 0 0 0 0	3.85143	1 0 1-1 0 1	3.29826	1 0 1-1 0 1	3.29826
1 1 0-1 0-1	4.03956	1 1 0-1 0 0	3.49836	1 0 1-1-1 0	3.29826
1-1 0-1 0-1	4.03956	1 0 0-1-1 0	3.49836	1-1 1-1 0-1	3.68757
1-1 0-1-1-1	4.51636	1 1 1-1 0-1	3.68757	0 0 1-1 0 0	4.07865
1 0-1 0 0-1	4.52687	1 1 0-1 0-1	4.03956	1 0 1 1 0-1	5.22718
1 1 1 1 0-1	5.84417	1 0 1 1 0 1	13.1276	1-1 1 1-1 1	11.1094

Table 5.6. Final results for example 1.

Chromosome	β
1 0 1-1 0 0	2.85638
1 0 0-1 0 0	2.8564
1 0 1-1 0-1	3.29826
1 1 1-1 0 0	3.29826
1 0 1-1 0 1	3.29826
1 0 1-1-1 0	3.29826
1-1 1-1 0 0	3.29826
1 0 1-1 1 0	3.29826
1 1 0-1 0 0	3.49836
1 0 0-1-1 0	3.49836
1-1 0-1 0 0	3.49836
1 0 0-1 0-1	3.49836
1 0 0-1 0 1	3.49836
1-1 1-1 0-1	3.68757
1 1 1-1 0-1	3.68757
1 0 1-1-1 1	3.68757
1 1 1-1 0 1	3.68757
1 0 1-1 1 1	3.68757
1 1 1-1-1 0	3.68757
1-1 1-1-1 0	3.68757
1-1 1-1 0 1	3.68757
1 0 0 0 0-1	3.69618
1 0 1 0 0 0	3.81272
1 0 0 0 0 0	3.85143

1-1 1-1 1 1	4.03953
1 1 1-1-1 1	4.03953
1-1 0-1 0-1	4.03956
1 1 0-1 0-1	4.03956
1 0 0-1-1-1	4.03956
1 1 0-1 0 1	4.03956
1 0 0-1 1 1	4.03956
1-1 0-1-1 0	4.03956
1 0 0-1-1 1	4.06956

From this list it is observed that the failure modes where member 1 fails (e.g. chromosome (1 0 1-1 0 0)) and where member 3 fails (e.g. chromosome (1 0 0 0 0-1)), are detected. But the failure mode that correspond to the failure of member 2 is not detected.

When the classical GA without the shredding and filtration operators is used to solve the same problem, starting with the same chromosome of Generation 1 given in Table 5.3, the dominant chromosome (1, 0, 1, -1, 0, 0) is not found until generation 31. The summarized results for generations 10, 20, 40 obtained with the classical GA are listed in Table 5.7.

Table 5.7 Results of GA search for example 1.

Generation 10	Generation 20	Generation 40
1 0 0 0 0-1 3.69618	1 0 0-1 0 0 2.8564	1 0 1-1 0 0 2.85638
1 0 1 0 0 0 3.81272	1 0 0-1-1 0 3.49836	1 0 0-1 0 0 2.8564
1 0 0 0 0 0 3.85143	1 0 0 0 0-1 3.69618	1 0 1-1-1 0 3.29826
1 0 0 0-1 0 4.20191	1 0 1 0 0 0 3.81272	1-1 1-1 0 0 3.29826
1 0 0 0 1-1 4.52687	1 0 0 0 0 0 3.85143	1 0 1-1 0-1 3.29826
1 1 0 0 0-1 4.52687	1 0 0 0-1 0 4.20191	1 0 0-1-1 0 3.49836
1-1 0 0 0-1 4.52687	1 0 0 0 1-1 4.52687	1 0 0-1 0-1 3.49836
1-1 0 0 1-1 5.22718	1 1 0 0 0-1 4.52687	1-1 0-1 0 0 3.49836
1-1 0 1 1-1 5.84417	1 0 1 0-1 0 4.66961	1 0 0-1 0 1 3.49836
-1 0 0 0 1-1 24.603	1 0 0 0 0 1 5.44674	1 0 0-1-1-1 4.03956

Table 5.8 compares the speed of convergence of the classical GA and the proposed SGA. It gives the number of generations needed in each case to identify the dominant chromosome (1, 0, 1, -1, 0, 0) starting from different initial populations. In each case, both SGA and GA start from the same initial population.

Table 5.8. Number of generations to reach the dominant and the second dominant chromosome.

Case	The best (1 0 1-1 0 0)		The second best (1 0 0-1 0 0)	
	SGA	GA	SGA	GA
Case 1	10	14	3	11
Case 2	14	12	15	22
Case 3	2	13	4	3
Case 4	8	8	11	4
Case 5	4	15	2	1
Case 6	7	10	3	8
Case 7	4	3	14	9
Case 8	4	22	12	16
Case 9	5	8	16	7
Case 10	18	32	16	17
Average	7.6	13.7	9.6	9.8

From this simple example, it is observed that the proposed SGA converges much faster than the classical GA. On the average SGA finds the dominant mode in 7.6 generations while GA finds it after an average of 13.7 generations. SGA nearly improves the search efficiency by a factor of two. The second most important mode is found by SGA at almost the same speed as classical GA.

The chromosomes identify the corresponding failure mode. For example, the dominant chromosome (1 0 1-1 0 0) with reliability index β = 2.85638 represents in the real random variable space the following realizations:

$$
\begin{aligned}
&L_1 = 2.021\beta + 35 = 40.772;\\
&L_2 = 20;\\
&L_3 = 0.866\beta + 15 = 17.531;\\
&\sigma_{y1} = -0.797\beta + 27.6 = 25.324;\\
&\sigma_{y2} = 27.6;\\
&\sigma_{y3} = 27.6;
\end{aligned}
\qquad \text{(Eq. 5.14)}
$$

Every member force can be calculated as:

$$
\begin{aligned}
&N_1 = L_1 + L_3 = 58.303 \approx A\,\sigma_{y1} = 2.3*25.324 = 58.245\\
&N_2 = L_2 + 0.75\,L_1 = 50.579 < A\,\sigma_{y2} = 2.3*27.6 = 63.48.\\
&N_3 = -1.25\,L_1 = -50.965 > -A\,\sigma_{y3} = -2.3*27.6 = -63.48
\end{aligned}
\qquad \text{(Eq. 5.15)}
$$

Equation 5.15 shows that the dominant chromosome indicates the failure of member 1 in tension while the other two members are still in the elastic range. The other chromosomes will identify other failure modes.

Chromosome (1 0 1-1 0 0) with reliability index 2.85638 which is the dominant mode gives a reliability index very close to the value of 2.735 found by hand calculations.

In addition to finding the reliability index, each chromosome releases detailed information about which variables control the particular failure mode. For example, chromosome (1 0 1-1 0 0) indicates that structural failure occurs as forces L_1 and L_3

increase from their means at the same time as member 1's yielding stress decreases from its mean, while all the other random variables remain at their means. Similarly, chromosome (1 0 0-1 0 0) with reliability index 2.8564 indicates that structural failure occurs as force L_1 increases from its mean and member 1's yielding stress decreases from its mean. By noticing that the two chromosomes (1 0 1-1 0 0) and (1 0 0-1 0 0) have similar reliability indices describing closely correlated failure equations, the engineer can improve the system reliability by concentrating on the two common factors of these chromosomes: namely, force L_1 and member 1's yielding stress.

From the six chromosomes with the same reliability index 3.29826: (1 1 1-1 0 1), (1-1 1-1 0 0), (1 0 1-1 1-1), (1 0 1-1-1 0), (1 0 1-1 0 1) and (1 0 1-1 0-1), the factors that affect the system failure the most are forces L_1 and L_3 and member 1's yielding stress. It is noticed that the other random variables have little effect on the reliability index at this level. The lack of importance of the three other variables is observed through their changing from -1 to 1 and vice versa. This conclusion coincides with the conclusion obtained from member 1's failure function: $f = R - S = A\sigma_{y1} - (L_1 + L_3)$ where only L_1, L_3 and σ_{y1} are active. This proves the accuracy and the ability of SGA. The capability of SGA to give such detailed information on the contributions of some variables to particular failure modes is very important for the analysis of large and complex problems where the closed forms of the failure functions are hard to express.

5.5 SUMMARY

In this chapter, a shredding genetic algorithm (SGA) is proposed. Its application to the reliability analysis of structural systems is also discussed. The method has the following features:

- It introduces a new operator, called filtration, which can filter out the unhealthy chromosomes through a fitness index matrix.
- It converges faster than standard GA without losing its effectiveness.
- It gives out the physical meanings of failure modes by providing information on the factors that control a particular failure mode.
- It is suitable for reliability analysis of any structural system and bridge systems in particular.
- It is applicable for use in any structural or nonstructural optimization problems.

CHAPTER 6

APPLICATION: RELIABILITY ANALYSIS OF GIRDER BRIDGE SYSTEMS

The previous chapters of this dissertation developed nonlinear analysis procedures and a probabilistic shredding genetic search algorithm applicable for the reliability analysis and the safety assessment of steel and concrete girder bridges. The improvements in analysis efficiency and accuracy produced by the methods developed are necessary to encourage the use of reliability based simulation techniques in everyday engineering practice. This Chapter presents examples to illustrate the use of the proposed models and techniques to find the dominant failure modes of steel and concrete girder bridges. The important factors that influence the system reliability are also identified. The results obtained are consistent with the experience of bridge engineers with such simple structures. The method can in the future be used to also account for the random positioning of the vehicular loads on the bridge deck and for the reliability analysis of more complex bridge structural systems with multiple, equally important failure paths.

6.1 INTRODUCTION

Reliability concepts have been recently implemented in the design and analysis specifications of all types of structural systems including bridges, buildings, offshore platforms, etc. (AASHTO LRFD, 1994; AISC LRFD, 1994; ACI, 1995). Traditional methods for evaluating the reliability of bridges, like traditional methods for the design and deterministic analysis of bridge systems, are based on a linear elastic structural analysis although member resistances are evaluated based on their ultimate capacity (AASHTO, 1994). During the design process, the safety of each member is considered separately and load and resistance factors are used to account for the uncertainties encountered during the analysis of the structure and when estimating the capacity of each member. Although this traditional approach has been successfully used for generations, it does not accurately model the true behavior of the bridge, and consequently does not give a true representation of the actual safety of the complete structural system (Thoft-Christensen, Murotsu, 1986). For this reason, changes have been recently introduced in the AASHTO LRFD specifications to improve the bridge design and analysis process. This is achieved by including system factors during the member design process (Ghosn & Moses, 1998). To account for the large level of uncertainty encountered while predicting bridge system performance, the calibration of the system factors has been based on structural reliability concepts. These factors were calibrated by checking the single most likely failure mode of the system. But, in reality bridge structures have high levels of redundancy and multiple load paths that produce numerous possible failure modes that depend on the possible combination and points of application of the applied loads, and

are related to the geometric configuration of the structure, its material properties, and member ductility. Thus, it is often difficult to enumerate all possible failure modes or even to predetermine the dominant ones. For this reason, failure mode analysis forms one of the most important tasks in the system reliability evaluation of structures in general and bridges in particular. From a system point of view, only some of the failure modes have high probability of occurring. These "important" failure modes affect the probability of system failure significantly. On the other hand, most modes are not so important and have low probability of occurrence.

In order to identify the dominant failure modes of bridge systems, two tools are generally required: The first tool is an accurate and efficient nonlinear structural analysis program capable of analyzing the behavior of the bridge system for a specific (deterministic) set of loading conditions and material properties. The second tool is a systematic search algorithm that determines the probabilistically dominant failure modes accounting for the randomness in the applied loading and material properties. The purpose of this study is to develop the two tools necessary to evaluate the safety of bridge structural systems. The first tool, as described in Chapters 2 and 3 consists of new analysis models for steel and prestressed concrete highway bridges that are implemented in a modified and more efficient version of the program NONBAN. The new models accurately represent the nonlinear behavior of bridge members using empirically derived information from moment-rotation curves and plastic hinge length equations. The second tool consists of a new Shredding Genetic Algorithm (SGA) that is designed to efficiently identify dominant

failure modes of bridge structural systems. SGA improves the traditional genetic algorithm by interfering with the natural selection process and filtering out the weakest and unhealthy offsprings using the principle of elitism. This chapter illustrates the application of these two tools to the reliability analysis of steel and concrete girder bridges.

6.2 DATA MODELING

The value that a random variable can take is described by its probability law, which is characterized by a probability distribution function. In other words, a random variable may take a specific value with a certain probability and the ensemble of these values and their probabilities are described by a Probability Density Function (PDF). In many cases, the most important characteristics of a random variable, that can also be used to determine its PDF, are its mean value or average, its standard deviation and its probability distribution type. The standard deviation gives a measure of dispersion or a measure of the uncertainty in determining the variable. The standard deviation of a random variable R with a mean $\overline{R}$ is often symbolized by σ_R. A dimensionless measure of the uncertainty is the coefficient of variation (COV) which is the ratio of the standard deviation divided by the mean value. As recommended by Nowak (1993) and Ellingwood, Galambos, MacGregor & Cornell (1980), typical COV's for bridge applications range from 5 to 15 percent for material strength, 5 to 10 percent for dead load, and 15 to 30 percent for live load and even higher for wind and seismic effects.

During the design or the safety evaluation of a bridge, the engineer checks every structural component to verify that the effect of the applied load does not exceed the component's capacity. However, since the applied load and its predicted effect as well as the component capacity are random, the engineer's conclusions regarding the component's safety are associated with a high level of uncertainty. To reduce the level of risk, bridge design and evaluation codes often specify safe or nominal values for the variables used in the design equations. For example, the values of the resistances used to verify the adequacy of a bridge component are often lower than the actual values observed. In addition, bridge specifications often require the use of safety (load and resistance) factors to account for the levels of uncertainty associated with determining the values of the design variables, and the structural modeling and analysis procedures used.

The nominal values of loads and resistances specified in the codes are related to the means through bias values. The bias is defined as the ratio of the mean to the nominal value used in design. For example, if R is the member resistance, the mean of R, $\overline{R}$, can be obtained from the nominal or design value R_n using a bias factor, b_r, as shown in Equation 6.1:

$$\overline{R} = b_r R_n \qquad \text{(Eq. 6.1)}$$

where: b_r is the resistance bias and R_n is the nominal value as specified by the design code. For example, A36 steel has a nominal design yield stress of 36 ksi but coupon tests show an actual average value close to 40 ksi. Hence the bias of the yield stress is 40/36 or 1.1. The bias values vary between from 1.0 to 1.3 for resistance random variables and

dead load random variables. Nowak (1993) also shows the actual moment effect for live loads has a bias of about1.8 to 2.0 relative to the Standard AASHTO HS-20 design truck.

In structural reliability, safety may be described as the situation where capacity (strength, resistance, fatigue life, etc.) exceeds demand (load, moment, stress ranges, etc.). Probability of failure, i.e., probability that capacity is less than demand, may be formally calculated; however, its accuracy depends upon detailed data on the probability distributions of the loads and resistances. Since such data are often not available, approximate models are used in practice. For example, resistance models are usually described as lognormal distributions. The load models are usually described as lognormal or Gumbel distributions.

For the purpose of illustrating the proposed reliability analysis procedures for typical bridge systems, the random variables that influence the safety assessment of bridge structures have been assembled from the available literature (Nowak, 1993; Ellingwood, Galambos, MacGregor & Cornell 1980; Kennedy 1982). For example, Table 6.1 and Table 6.2 show the random variables, distribution types, COV's and biases for prestressed concrete girder bridges and steel girder bridges respectively. This data is assembled for the two bridges analyzed in this Chapter. The prestressed concrete bridge is the same Slovenia bridge analyzed in Chapter 3. The steel bridge is a "hypothetical" two-span continuous bridge that has been designed to satisfy the current criteria of the AASHTO LRFD Specifications. The definition of the input data has been described in Chapters 2 and 3.

Table 6.1, Random variable definitions for Slovenia prestressed concrete girder and bridge.

Member type	No.	Variable	Distribution	COV	Bias	Girder's Nominal values (kN & meters)	Bridge's Nominal values (kN & meters)
Longitudinal Girders	1	Section rigidity, EI_z	Lognormal	0.1	1.1	373800	373800
	2	Torsion coefficient, GJ	Lognormal	0.1	1.1	2450	2450
	3	Maximum allowable rotation, θ_{max}	Lognormal	0.4	1.15[1]	0.00822	0.00822
	4	M-ϕ curve[2]	Lognormal	0.08	1.05	482.0	482.0
Transverse Beams	5	Section rigidity, EI_z	Lognormal	0.1	1.0	N/A	487
	6	Torque coefficient, GJ	Lognormal	0.25	1.0		722
	7	Maximum allowable rotation, θ_{max}	Lognormal	0.4	1.15[1]		1000[5]
	8	M-ϕ curve[2]	Lognormal	0.13	1.14		3.81
Loads	9	Permanent dead load, L_{dead1}	Lognormal	0.1	1.03	4.5	4.5
	10	Surface dead load, L_{dead2}	Lognormal	0.1	1.05	3.3[3]	3.3[3]
	11	Live load, L_{live}	Gumbell	0.19	1.75	94[4]	168[4]

[1] The value shown here is for positive maximum allowable rotation.

[2] The moment versus curvature relationship is modified by assuming a change in the slopes of the multi-linear curve as well as changes in the points of intersection. The value given under "Mean" is for the member ultimate moment capacity.

[3] Surface dead load is applied only on segments of the beam where there is no live load

[4] Total live load = sum of all axle loads.

[5] A high value is used to indicate that the transverse beam may go into the inelastic range but would not break.

Table 6.2, Random variable definitions for steel girder bridge.

Member type	No.	Variable	Distribution	COV	Bias	Nominal values (kips & inches)
Longitudinal Girders	1	Section rigidity, EI_z	Lognormal	0.1	1.03	1.09×10^9
	2	Torsion coefficient, GJ	Lognormal	0.1	1.03	8.02×10^6
	3	Maximum allowable rotation, θ_{max}	Lognormal	0.4	1.15[1]	0.0418
	4	M-ϕ curve[2]	Lognormal	0.1	1.12	44420.6
Transverse Beams	5	Section rigidity, EI_z	Lognormal	0.1	1.0	8.17×10^6
	6	Torque coefficient, GJ	Lognormal	0.25	1.0	9.34×10^6
	7	Maximum allowable rotation, θ_{max}	Lognormal	0.4	1.15[1]	0.0214
	8	M-ϕ curve[2]	Lognormal	0.13	1.14	1808.8
Loads	9	Permanent dead load, L_{dead1}	Lognormal	0.1	1.03	0.077
	10	Surface dead load, L_{dead2}	Lognormal	0.1	1.05	0.015
	11	Live load[3], L_{live}	Gumbell	0.19	1.85	AASHTO

[1] The value shown here is for positive maximum allowable rotation. The bias for negative maximum allowable rotation is 1.0.
[2] The moment versus curvature relationship is modified by assuming a change in the slopes of the multi-linear curve as well as changes in the points of intersection. The value given under "Nominal value" is for the member ultimate moment capacity.
[3] Total live load = sum of all axle loads.

6.3 RELIABILITY ANALYSIS OF BRIDGE SYSTEMS

A bridge structure usually has high levels of redundancy and multiple load paths that produce numerous possible failure modes. It is often difficult to enumerate all possible failure modes or even to predetermine the dominant ones. Hence, failure mode analysis forms one of the most important tasks in the system reliability evaluation of bridge structures. Bridge system failure modes depend on the possible combinations of loads, section properties, material properties, and member ductility. All these properties are defined as random variables in structural reliability applications. In this study, it is assumed that the reliability of a bridge system is controlled by the 11 independent random variables listed in Tables 6.1 & 6.2. The values given in the Tables are based on the values provided by Ellingwood, Galambos, MacGregor & Cornell (1980) and Nowak (1993).

The Shredding Genetic Algorithm, SGA, described in Chapter 5 can be used to perform the reliability analysis of bridge systems using as input the random variables described in Tables 6.1 & 6.2. The advantage of SGA over traditional gradient-based optimization techniques was described in the previous Chapter. In this Chapter three examples illustrating the application of SGA to the reliability analysis of bridge systems are presented. These examples demonstrate the advantages of SGA when combined with a nonlinear analysis program such as the program NONBAN (NONlinear Bridge Analysis) for identifying the typical failure modes of bridge systems.

The program NONBAN evaluates the ultimate capacity and the nonlinear behavior of a bridge system and accounts for the interaction of its members into a complete structural system by considering the transverse and longitudinal redistribution of the load. It uses a grillage (grid) model where the superstructure of a bridge is discretized into longitudinal and transverse beam elements. The longitudinal elements model the behavior of the longitudinal members such as main girders while the transverse elements represent the behavior of slab, bracings and diaphragms.

In the NONBAN program, the linear elastic stiffness matrices of the beam element are modified to account for possible flexural and shear nonlinearities. This is achieved by assuming that nonlinearity due to bending is concentrated at the ends of a beam element and that its effect can be represented by rotational springs attached to the ends of the elements. Shear nonlinearity is also considered by updating the shear stiffness. Deng & Ghosn (2000) and Deng, Ghosn, Znidaric & Casas (2000) give more detailed descriptions of NONBAN.

6.4 ILLUSTRATIVE EXAMPLE 1:

Reliability Analysis of Slovenia Girder and Slovenia Bridge

To illustrate the reliability analysis procedure, the calculations are executed for a single prestressed concrete girder and a three-girder prestressed concrete bridge having the configurations of the 1/3 scale composite prestressed concrete girder and the 1/3 scale

three-girder prestressed concrete bridge that were previously designed and tested through the US-Slovene research project DOT 95-200 "Redundancy of prestressed parallel beam superstructures." (Znidaric & Moses, 1998). The prestressed concrete I girder is constructed to act compositely with a 1100 mm × 80 mm concrete slab section. The girder is 9.98 m long, spanning 9.68 m between the centers of supports as described in Chapter 3 and shown in Figures 3.5 and 3.8.

The 1/3 scale three-girder bridge model also spans 9.98 meter. The spacing between girders is 1100 mm. The bridge's cross section is shown in Figure 3.17. The girders' properties are the same as those of the Slovenia girder described above. The load configuration used, as shown in Figure 3.17, simulates the European rating loading scheme with a 5-axle 42-ton semi-trailer used for safety assessment of existing road bridges in Slovenia.

During the structural analysis, each main girder is discretized into 20 identical beam elements. Figures 3.16 and 3.19 show the comparison between the experimental results and the analytical results for the Slovenia girder and bridge as calculated using NONBAN where the input data for material properties and ultimate capacities is based on the results of coupon tests collected during the construction of the models. Because of the good agreement between the experimental results and those of NONBAN, it is concluded that NONBAN is a suitable program for modeling the nonlinear behavior of girder bridge systems and can be combined with SGA to evaluate the reliability of highway bridges. The SGA calculations are executed for the single girder and the three-

girder bridge using as input the data provided in Table 6.1. The results of the reliability analysis using SGA are provided in Tables 6.3 and 6.4 for different points of the search process namely for the first, tenth, twentieth and fortieth generations.

Table 6.3. SGA results for Slovenia girder.

Generation	Chromosomes	β
1	0 0 0 0 0 0 1	2.6491
	0 0 0-1 0 1 1	2.99935
	-1 0 0 0 0 0 1	3.73821
	-1 0 0-1 1-1 1	4.20165
	-1 0 0 0 0 1 1	4.33711
	-1 0 1-1 1 0 1	6.02676
	-1-1 1-1 1 0 1	6.26909
	1 0-1-1 0 1 0	6.68775
	-1 0 1 0 0 0 1	9.89516
	-1-1 1 0 1 0 1	9.98586
	-1-1 1 1 0 1 1	13.7452
	-1 1 0 1-1 1 1	13.7452
	1 1 0-1 1-1 0	15.5752
	-1 1 0-1 1-1 0	15.5752
	0 0-1 0 1-1 0	36.8824
	-1-1-1-1 0-1-1	37.0969
	-1 1-1 1-1 1 0	47.1805
	-1 0-1 0-1 0-1	190.369
	1-1-1 0 0-1-1	204.729
	-1-1-1 1 0-1-1	306.193
	0 0 0 1 0-1-1	437.437
10	0 0 0-1 0 0 1	2.56596
	0 0 0 0 0 0 1	2.6491
	0 0-1-1 0 1 1	2.99697
	0 0 0-1 0 1 1	2.99935
	0 0-1 0 0 0 1	3.13032
	1 0-1-1 0 0 1	3.13101
	0 0-1-1 1 0 1	3.13101
	-1 0 0-1 0 0 1	3.14142
	0-1 0-1 0 0 1	3.14164
	0 0 0-1 1 1 1	3.46173
	-1 0 0-1 0 1 1	3.46173
	1 0-1-1 1 0 1	3.50037
	0 0 0 0 0 1 1	3.54778
	0 0-1 0 0 1 1	3.63551
	1 0-1-1 1 1 1	3.66871
	0 1 0 0 0 0 1	3.7366
	-1-1 0 0 0 0 1	4.57065
	-1 0 0 0-1 1 1	5.02606
	0 0 0-1 0 1 0	5.81049
	-1 1 0 0 1-1 1	5.88009

20	0 0 0-1 0 0 1	2.56596
	0 0 0 0 0 0 1	2.6491
	0 0-1-1 0 0 1	2.71141
	0 0-1-1 0 1 1	2.99697
	0 0 0-1 0 1 1	2.99935
	0 0-1 0 0 0 1	3.13032
	0 0-1-1-1 0 1	3.13101
	1 0-1-1 0 0 1	3.13101
	0 0-1-1 1 0 1	3.13101
	-1 0-1-1 0 0 1	3.13101
	-1 0 0-1 0 0 1	3.14142
	1 0 0-1 0 0 1	3.14164
	0-1 0-1 0 0 1	3.14164
	0 0 0-1 1 0 1	3.14164
	0 0 0-1-1 0 1	3.14164
	0 1 0-1 0 0 1	3.14164
	0 0 0-1 1 0 1	3.14164
	0 0-1-1 0-1 1	3.24961
	0 0 0-1 0-1 1	3.25991
	0 0 0-1 0 0 0	4.97968
	1-1-1 1 0 0 1	8.60406
40	0 0 0-1 0 0 1	2.56596
	0 0 0 0 0 0 1	2.6491
	0 0-1-1 0 0 1	2.71141
	0 0-1-1 0 1 1	2.99697
	0 0 0-1 0 1 1	2.99935
	0 0-1 0 0 0 1	3.13032
	1 0-1-1 0 0 1	3.13101
	0 0-1-1 1 0 1	3.13101
	-1 0-1-1 0 0 1	3.13101
	-1 0 0-1 0 0 1	3.14142
	1 0 0-1 0 0 1	3.14164
	0-1 0-1 0 0 1	3.14164
	0 0 0-1 1 0 1	3.14164
	0 0 0-1-1 0 1	3.14164
	0 1 0-1 0 0 1	3.14164
	0 0-1-1 0-1 1	3.24961
	0 0 0-1 0-1 1	3.25991
	1 0-1-1 0 1 1	3.3502
	1 0 0-1 0 1 1	3.46173
	0 0 0-1 1 1 1	3.46173
	-1 0 0-1 0 1 1	3.46173

Table 6.4. SGA results for Slovenia bridge.

Generation	Chromosome	β
1	0 0 0 0 0 0 0 0 0 0 1	3.56906
	0 0-1-1 0 0-1 0 0 0 1	4.10531
	0 0 0 0 0 0 0 0 0 1 1	4.78108
	0 0 0 0 0 0-1 0 0 0 1	5.06321
	-1 0 0 0 0 0 0 0 0 0 1	5.07984
	-1 0 0-1-1 0 0 0 0 0 1	5.24589
	1 0 0-1-1 0 0 0 0 0 1	5.24861
	-1 0 0-1 0 0-1 0 0 1 1	5.55975
	-1 0 0 0 0 0 0 0 0 1 1	5.8721
	-1 0-1-1 1 1 0 1 0 1 1	5.88317
	0 0 0-1-1-1-1 1 0 0 1	6.23437
	0 0 0-1-1-1-1 1 0 1 1	6.48685
	-1-1 0-1-1-1-1 1 0 1 1	7.19481
	-1 0 0-1-1 0 1 0 1-1 1	7.20626
	-1 1 0-1-1 0 1 0 1-1 1	7.7536
	-1 0 0 0 0 1 0 0 1 0 1	8.20168
	1 0-1-1 1 0 0 0 0 1 0	8.78588
	1 0-1-1 1-1 0 0 0 1 0	9.21042
	-1-1 1-1 0 0 0 1 0 0 1	12.289
	-1 0 1-1-1 1-1 0 1 0 1	16.4147
	-1 1 0 1 1 0 0 0-1 1 1	21.7389
10	0 0-1-1 0 0 0 0 0 0 1	3.55156
	0 0 0 0 0 0 0 0 0 0 1	3.56906
	0 0 0-1 0 0 0 0 0 0 1	3.70855
	0 0-1 0 0 0 0 0 0 0 1	3.85097
	0 0-1-1 0 0 0 0 0 1 1	3.91062
	1 0-1-1 0 0 0 0 0 0 1	4.09847
	0 0-1-1-1 0 0 0 0 0 1	4.10295
	0 0-1-1 0 0-1 0 0 0 1	4.10531
	1 0-1-1 0 0 0 0 0 1 1	4.37111
	0 0-1-1-1-1 0 0 0 0 1	4.44791
	0-1-1-1-1 0 0 0 0 0 1	4.52796
	-1 0 0-1 0 0 0 0 0 0 1	4.55815
	1 0 0-1 0 0 0 0 0 0 1	4.55957
	0 0-1-1-1-1 0 0 0 1 1	4.61846
	0-1-1-1-1-1 0 0 0 0 1	4.82532
	0 0-1-1-1 1 0 0 0 1 1	5.01509
	0 0 0 0-1 0 0 0 0 0 1	5.08955
	0 0 0 0 0 0 0-1 0 1 1	5.68231
	1 0 0-1-1-1 0 0 0 1 1	5.79565
	0 0-1 1-1-1 0 0 0 0 1	8.92454
	0 0-1-1 0 0 0 0 0 0-1	60.1276
20	0 0-1-1 0 0 0 0 0 0 1	3.55156
	0 0 0 0 0 0 0 0 0 0 1	3.56906
	0 0 0-1 0 0 0 0 0 0 1	3.70855
	0 0-1 0 0 0 0 0 0 0 1	3.85097
	0 0-1-1 0-1 0 0 0 0 1	3.9233
	0 0-1-1 0 0 0-1 0 0 1	4.02217
	0 0 0-1 0-1 0 0 0 0 1	4.2601
	0 0-1-1 0 0 0-1 0 1 1	4.29955

	0 0 0-1 0 0 0 0 0 1 1	4.3066
	1 0-1-1 0 0 0-1 0 1 1	4.68204
	0 0-1-1-1 0 1 0 0 1 1	4.77159
	0 0 0-1 0-1 0-1 0 0 1	4.77416
	0 0-1-1 0 1 0 0 1 0 1	4.81509
	0 0-1-1 0 1-1 0 0 0 1	4.81509
	0 0-1 0 0 0 0 0 0-1 1	4.91959
	0 0 0-1-1 0 0-1 0 1 1	5.42041
	0 0 0-1 0 0 0-1-1 1 1	5.47421
	1 0-1-1 0 1-1 0 1 0 1	5.66792
	0 0-1 1 0 0-1-1 0 0 1	8.99276
	0 0-1-1 0 1 0 0 0 0-1	57.7342
	0 0-1-1 0 0 0 0 0 0-1	60.1276
40	0 0-1-1 0 0 0 0 0 0 1	3.55156
	0 0 0 0 0 0 0 0 0 0 1	3.56906
	0 0 0-1 0 0 0 0 0 0 1	3.70855
	0 0-1 0 0 0 0 0 0 0 1	3.85097
	0 0-1-1 0 0 0 0 0 1 1	3.91062
	0 0-1-1 0-1 0 0 0 0 1	3.9233
	0 0-1-1 0 0 0-1 0 0 1	4.02217
	0-1-1-1 0 0 0 0 0 0 1	4.04095
	0 0-1-1 1 0 0 0 0 0 1	4.0944
	0 1-1-1 0 0 0 0 0 0 1	4.13176
	0-1-1-1 0 0 0 0 0 1 1	4.32336
	0 0 0-1 0 0 0-1 0 0 1	4.41407
	0 0-1 0 0 0 0 0 0 1 1	4.45176
	0 0-1-1 1 0 0 0 0-1 1	4.48981
	0-1-1-1 0 0 1 0 0 0 1	4.53336
	0 0-1-1 1 0-1 0 0 0 1	4.56359
	0 0-1-1 1-1 0 1 0 0 1	4.93674
	0 0-1 0 0 0 1 0 0 1 1	5.14044
	0 1 0-1 0 0-1 0 0 1 1	5.58647
	0 0 0-1-1-1 0-1 1 0 1	5.81828
	0 0 0 1 0-1 0 1 0 0 1	11.7628

The results of tables 6.3 and 6.4 show that for both examples convergence to the most dominant mode is achieved before the 20th generation. The analysis is continued beyond the 20th to search for other possible important modes.

The discrete search directions strategy for the Slovenia girder and the Slovenia bridge are set up in the independent normalized random variable space defined earlier as the U-space. These directions are represented by chromosomes as shown in Tables 6.3 and 6.4. The seven digits in each chromosome of Table 6.3 represent random variables of girder's

section rigidity, girder's torsion coefficient, girder's maximum allowable rotation, girder's M-φ curve, permanent dead load, surface dead load, and live load. The eleven digits in each chromosome in Table 6.4 represent random variables of girder's section rigidity, girder's torsion coefficient, girder's maximum allowable rotation, girder's M-ϕ curve, transverse beam's section rigidity, transverse beam's torsion coefficient, transverse beam's maximum allowable rotation, transverse beam's M-φ curve, permanent dead load, surface dead load and live load. "0" means that the random variable remains at its mean value in this particular search direction. "-1" denotes a negative deviation from the mean, and "1" denotes a positive deviation from the mean. For instance, in the first generation, chromosome (0 0 0 0 0 0 0 0 0 0 1) is included to consider a large positive change in the last random variable which represents the live load L_{live} when the other random variables are set at their means. This chromosome is purposely included in the first generation based on past experience that shows that the live load has a large effect on the system reliability of bridges.

As another example, a chromosome (0, 0, -1, -1, 0, 0, -1, 0, 0, 0, 1) in generation 1 of Slovenia bridge indicates that system failure is influenced by a reduction in the main girders' maximum plastic rotation capacity (3^{rd} variable), a reduction in the main girders' ultimate moment capacity and softening of the M-φ curve (4^{th} variable), a reduction in the slab's maximum plastic rotation capacity (7^{rd} variable), and an increase in the applied live load (11^{th} variable). The reductions and increases are from the mean values of each variable.

Based on previous experience with the analysis of bridge systems, the most important factors in the safety assessment of reliability analysis of bridge system are known to be the section rigidity, surface dead load and live load. Three chromosomes in the first generation of Slovenia girder, (0 0 0 0 0 0 1), (-1 0 0 0 0 0 1) and (-1 0 0 0 0 1 1), and three chromosomes in the first generation of Slovenia bridge, (0 0 0 0 0 0 0 0 0 0 1), (-1 0 0 0 0 0 0 0 0 0 1) and (-1 0 0 0 0 0 0 0 0 1 1), are purposely chosen based on these observations to guide the search into the most important directions. Such input serves as a sort of "expert system" that helps improve the convergence of SGA. The other chromosomes in the first generation are all randomly selected using a random number generator. As described in former sections, the coordinates of the search directions are transformed from the U-space to real loads and material properties before the program NONBAN is run. NONBAN follows the direction set by the chromosomes to generate a structural failure path and calculate the reliability index or β-value for each search direction.

In this example, the total number of possible search directions for the Slovenia bridge is (3^{11}-1 = 177146). A total of 357 directions are searched during the analysis. These constitute only 0.2% of all possible discrete directions in the 11 dimensional space. Thus, SGA proves to be an efficient method to minimize the number of iterations and search directions needed to find the most important failure modes of bridge systems.

As seen in Tables 6.3 and 6.4, most of the randomly generated search directions in the first generation have low probability of failure (i.e. high β) and the search in these

directions is abandoned early. After an evolution through 40 generations, the chromosomes in the 40^{th} generation as shown in Tables 6.3 and 6.4 give much smaller β-values than those from the first generation. It is also observed that at the 40^{th} generation, the schemata in the surviving chromosomes have similar characteristics. These schemata represent special combinations of loads and material properties that highly control bridge system safety.

After 40 generations, the results of the Slovenia girder converged to produce the most dominant failure mode which is associated with the lowest reliability index, $\beta = 2.566$. This 2.566 reliability index corresponds to the chromosome (0 0 0 −1 0 0 1) indicating that the dominant failure mode is formed by a combination of low member ultimate capacities (and soft M-ϕ curves) for the longitudinal girders and a large live load L_{live} value. Chromosome (0 0 0 0 0 0 1) with $\beta = 2.649$ that has been purposely included in the first generation, becomes the second most important failure mode. Chromosomes, (0 0 −1 −1 0 0 1) with $\beta = 2.711$, (0 0 −1 −1 0 0 1 1) with $\beta = 2.997$ are also quite interesting to study. From these chromosomes with low β values, one concludes that the most important variables influencing the reliability of Slovenia girder are associated with the magnitudes of the live load, M-φ curve, maximum allowable rotation and surface dead load. The importance of the variable that describes the section rigidity, EI does not show in this chromosome because the capacity of the girder is controlled by its nonlinear properties represented by the M-φ curve while the section rigidity only affects the elastic response.

The relative influence of the important random variables on the structural failure probability can be quantitatively evaluated by looking at the partial derivatives of the probability of failure with respect to each of the random variables. This is accomplished as follows:

$$\frac{\partial P_{f_i}}{\partial u_{ij}} = \frac{dP_{f_i}}{d\beta_i} \cdot \frac{\partial \beta_i}{\partial u_{ij}} = \frac{d\Phi(-\beta_i)}{d\beta_i} \cdot \frac{u_{ij}}{\beta_i} = -\phi(-\beta_i) \cdot \sin g(u_{ij}) \frac{1}{\sqrt{n}} \qquad \text{(Eq. 6.2)}$$

Where P_f denotes the probability of failure, the subscript *i* gives the search direction in the U-space (chromosome), the subscript j identifies the random variable, u_{ij} gives the coordinate of the failure point in U-space, β_i gives the distance between the origin of the U-space and the failure surface in direction i, it is calculated as $\beta_i = \sqrt{\sum_{j=1}^{j=n} u_{ij}^2}$, where n is the total number of nonzero digits (i.e. number of −1 and 1 digits) in chromosome *i*, Φ and ϕ are respectively the cumulative probability and the density functions of the standard normal distribution.

Using Equation 6.2, for the most important random variables, the sensitivity of the probability of failure for the most dominant mode can be described as shown in Table 6.5.

Table 6.5. Influence of dominant random variables on the probability of failure of Slovenia girder.

Random variable	$\left\lvert \frac{\partial P_{f_i}}{\partial u_{ij}} \right\rvert$	Weight*
Live Load, L_{live}	0.0119	100%
M- φ Curve, M –φ	0.0105	88%
Maximum allowable rotation, θ_{max}	0.0058	49%
Surface dead load, L_{dead2}	0.0022	19%

* The weight defines the relative influence of each variable on sytem reliability. The dominant variable is assigned the weight 100%. The other weights are determined by linear interpolation.

The relative influence of each pair of variables, that are formed by shredding the dominant chromosomes into pairs of "genes", on the structural failure probability can also be quantitatively evaluated in a similar way. Assuming that x_{ij} denotes a pair j in the search direction i, or x_{ij} represents a pair j which is shredded from chromosome i, its influence can be expressed as follows:

$$\frac{\partial P_{f_i}}{\partial x_{ij}} = \frac{dP_{f_i}}{d\beta_i} \cdot \frac{\partial \beta_i}{\partial x_{ij}} = \frac{d\Phi(-\beta_i)}{d\beta_i} \cdot \frac{\sqrt{2}}{\beta_i} = -\phi(-\beta_i) \cdot \frac{\sqrt{2}}{\sqrt{n}} \qquad \text{(Eq. 6.3)}$$

Where P_f denotes the probability of failure, the subscript i gives the search direction in U-space (chromosome), the subscript j identifies the random pair, such that $\beta_i = \sqrt{\sum_{j=1}^{j=n/2} x_{ij}^2} = \sqrt{\sum_{j=1}^{j=n} u_{ij}^2}$, where n is the total number of nonzero digits in chromosome i, Φ and ϕ are the cumulative probability and density functions of the standard normal distribution. Some of the important pairs can be identified as shown in Table 6.6

Table 6.6. Influence of dominant pairs on probability of failure of Slovenia girder.

Random variable	$\left\|\frac{\partial P_{f_i}}{\partial x_{ij}}\right\|$	Weight*
(L_{live}, M- φ)	0.0148	100%
($\theta_{max.}$ M- φ)	0.00836	55%
($\theta_{max.}$ L_{live})	0.00836	55%
($\theta_{max.}$ L_{dead2})	0.00316	21%
(M- φ, L_{dead2})	0.00316	21%
(L_{dead2}, L_{live})	0.00316	21%

* The weight defines the relative influence of each pair of variables on sytem reliability. The dominant pair is assigned the weight 100%. The other weights are determined by linear interpolation.

Tables 6.5 and 6.6 show that the random variable L_{live} and M-φ and the random pairs ($\theta_{max.}$ M- φ), ($\theta_{max.}$ L_{live}) and (M-φ, L_{live}) have dominant influence on this girder's

reliability. This information can be used to help engineers improve the reliability of their designs by focusing their attention on these variables. It is noted that this information coincides with the information already contained in the fitness index matrix.

In engineering practice, engineers can use this information to design a system with adequate reliability and minimum cost, or to choose the optimum method to modify the reliability of existing structures. For example, Murotsu, Okada and Shao (1993) successfully analyzed transmission line structures that suffered from extensive damage caused by violent typhoons and severe snow storms in Japan. They found the dominant failure mode, and developed a methodology to reduce its failure probability by modifying the properties of the identified dominant random variable which in their case was the pipe thickness.

For the Slovenia bridge, the lowest reliability index $\beta = 3.552$ is associated with chromosome (0 0 -1 −1 0 0 0 0 0 0 1), indicating that the dominant failure mode is formed by a combination of a low value of the maximum allowable rotation, low member ultimate capacities (and soft M- φ curves) for the longitudinal girders and a large live load L_{live}. Chromosome (0 0 0 0 0 0 0 0 0 0 1) with $\beta = 3.569$ that has been purposely included in the first generation, becomes the second most important failure mode. Chromosomes, (0 0 0 −1 0 0 0 0 0 0 1) with $\beta = 3.709$, (0 0 −1 0 0 0 0 0 0 0 1) with $\beta = 3.851$, (0 0 −1 −1 0 0 0 0 0 0 1) with $\beta = 3.911$ and (0 0 −1 −1 0 −1 0 0 0 0 1) $\beta = 3.923$ are also quite interesting to study because the β values are close to the minimum value of 3.552. It is observed that the most important variables influencing the

reliability of Slovenia bridge are the live load, M- φ curve, maximum allowable rotation, surface dead load and the torsional constant of the transverse beams (representing the effect of the slab). The importance of the section rigidity does not show in these chromosomes because the capacity of this simply-supported bridge is controlled by its nonlinear properties as represented by the M- φ curve.

Following the same procedure outlined above for the Slovenia girder, the relative influence of the important random variables on the structural failure probability and the relative influence of each shredding pair on the dominant chromosomes of the Slovenia bridge can be calculated as shown in Tables 6.7, and 6.8.

Table 6.7. Influence of dominant random variables on probability of failure of Slovenia bridge.

Random variable	$\left\|\frac{\partial P_{f_i}}{\partial u_{ij}}\right\|$	weight
Live Load, L_{live}	0.000684	100%
M- φ Curve, M- φ	0.000419	61%
Maximum allowable rotation, θ_{max}	0.000419	61%
Surface dead load, L_{dead2}	0.000095	14%
Slab's torque coefficient GJ	0.000091	13%

Table 6.8. Influence of dominant pairs on probability of failure of Slovenia bridge.

Random variable	$\left\lvert\frac{\partial P_{f_i}}{\partial x_{ij}}\right\rvert$	weight
(L_{live}, M- φ)	0.000592	100%
(θ_{max}, M- φ)	0.000592	100%
(θ_{max}, L_{live})	0.000592	100%
(θ_{max}, L_{dead2})	0.000134	23%
(M- φ, L_{dead2})	0.000134	23%
(L_{dead2}, L_{live})	0.000134	23%
(θ_{max}, GJ)	0.000129	22%
(M- φ, GJ)	0.000129	22%
(L_{live}, GJ)	0.000129	22%

From the results given in Tables 6.7 and 6.8, the random variable L_{live}, girder's maximum allowable rotation θ_{max} and M- φ and the random pairs (θ_{max}, M- φ), (θ_{max}, L_{live}) and (M- φ, L_{live}) have dominant influence on the reliability of the bridge system. As explained above, this information can be used to improve the reliability of structures in practice.

Also from this example, the random variables associated with the transverse members are found not to be important in comparison with the properties of the main longitudinal members except for the slab's torsion coefficient, GJ. The combination of GJ with the

other dominant random variables consisting of the live load L_{live}, the girders' maximum allowable rotation θ_{max} and M- φ forms a chromosome (0 0 –1 –1 0 –1 0 0 0 0 1) with safety index equal to 3.923. The corresponding pairs (θ_{max}, GJ), (M- φ, GJ) and (L_{live}, GJ) also influence are associated with 22% weight in comparison to the dominant pair (L_{live}, M- φ) with 100% weight.

6.5 ILLUSTRATIVE EXAMPLE 2:

Reliability Analysis of a typical continuous steel girder bridge

The second example illustrating the applicability of SGA for finding the reliability of bridge systems considers a 4 girder continuous bridge with 2 spans designed to satisfy the criteria of the AASHTO LRFD Specifications. The length of each span is 200 feet. The spacing between the four parallel I-girders is 8 feet 4 inch. The originally applied live load consists of 4 AASHTO trucks with 2 trucks in each span. The expected maximum live load is assumed to be 1.85 times the AASHTO trucks based on the data provided by Nowak (1993). For the reliability analysis, the loads and the material properties are considered to be random variables with the distribution types, biases and COV listed in Table 6.2. The nominal values of these tandom variables are also included in Table 6.2. The nominal live load, L_{live}, is simulated by AASHTO trucks where the front tires are 4 kips each and all other tires are 16 kips each. Program NONBAN was used to perform the deterministic analysis while this bridge's reliability is obtained using SGA. The mesh used in NONBAN analysis is shown in Figure 6.1. The results are summarized in Table 6.9.

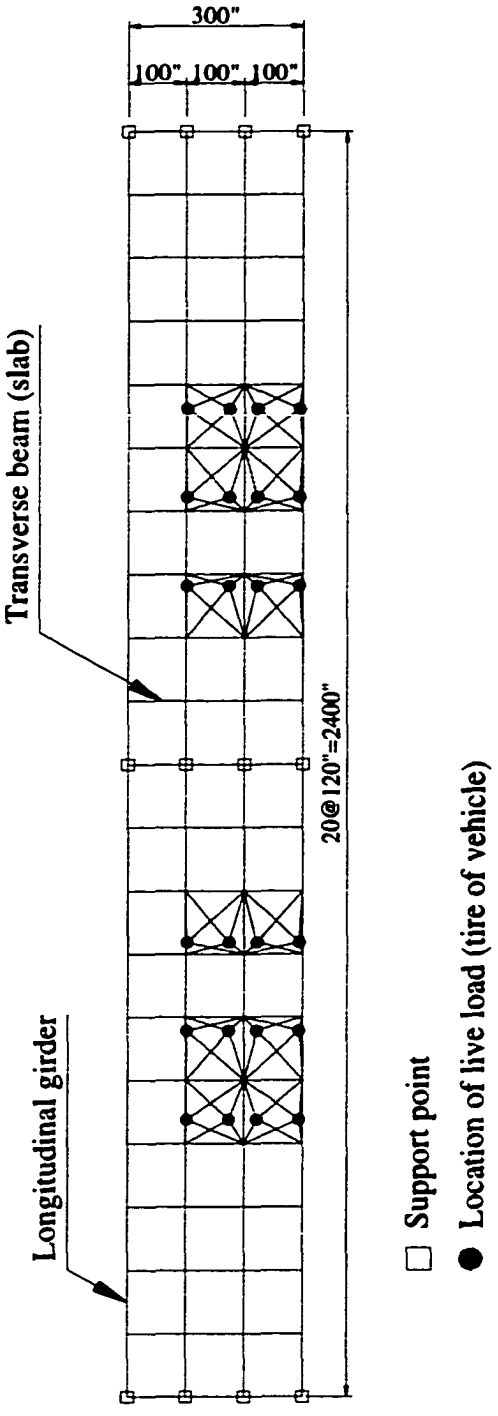

Figure 6.1 Model of superstructure of Example 2

Table 6.9. SGA results for continuous bridge.

Generation	Chromosome	β
1	0 0 0 0 0 0 0 0 0 0 1	4.01584
	-1 0 0 0 0 0 0 0 0 0 1	6.25551
	-1 0 0-1-1 0 0 0 0 0 1	6.33348
	0 0 0-1-1-1-1 1 0 1 1	6.35711
	-1 0 0 0 1 0 0 0 0 1 1	6.85681
	-1 0 0 0 0 0 0 0 0 1 1	6.94525
	-1 0 1-1-1 1-1 0 1 0 1	7.30467
	1 0-1-1 1-1 0 0 0 1 0	7.47095
	-1-1 1-1 0 0 0-1 1 0 1	8.17372
	1 0 0-1-1 0 1 0 1-1 1	8.19619
	-1 0 0-1-1 0 1 0 1-1 1	8.22149
	-1 0 1 0 0 0 0 1 0 0 1	8.28794
	-1 1-1 1 1 1-1 0-1 1 0	13.2805
	-1 0-1 0 0-1 0-1-1 0-1	14.5457
	-1 1-1 1 1 1-1 0-1 1 1	15.0013
	0 0-1 0 0 0 0 0 1-1 0	15.24
	0 0 1 1 0 0 0 1 0 0 1	15.4516
	-1 0-1-1 0-1 1-1 0-1-1	16.2871
	0 0 0 0 0 0 1 0 1-1 0	18.3397
	-1 0 1 0 1 1 1 0-1 1 0	20.7961
	-1-1-1 1 1 1 1-1 0-1-1	30.5975
10	0 0 0 0 0 0 0 0 0 0 1	4.01584
	0 0 0-1 0 0 0 0 0 0 1	4.04507
	-1 0 0-1 0 0 0 0 0 0 1	4.69219
	0 0 0 0 0 0 0 0 0 1 1	4.79483
	0 0 0-1-1 0 0 0 0 0 1	4.94058
	1 0 0-1 0 0 0 0 0 0 1	4.97543
	-1 0-1-1 0 0 0 0 0 0 1	5.24993
	1 0 0-1-1 0 0 0 0 0 1	5.25296
	0 0 0-1 1 0 0 0 0 1 1	5.28898
	0 0 0-1 1 0 0 0 0 0 1	5.53111
	-1 0-1-1 0 0-1 0 0 0 1	5.86967
	1 0-1-1 1 1 0 0 0 0 1	6.19032
	0 0 1-1 0-1 0 0 0 0 1	6.25008
	0 0 0-1 1 0-1-1 0 0 1	6.43939
	1 1 0-1 1 0 1 0 0 0 1	6.52441
	1 0-1 0 0 0 0 0 0 1 1	6.78928
	0 0 1-1 0-1 1 0 0 0 1	7.02058
	0 0 0-1 1-1 1-1 0 0 1	7.10963
	-1 0 1-1 0 1 0 0 0 0 1	7.29356
	1 0 0 0-1 0 1 0 0 0 1	9.65963
	0 0 0 1 0 0 0 0 0 1 1	12.6158
20	0 0 0 0 0 0 0 0 0 0 1	4.01584
	0-1 0-1 0 0 0 0 0 1 1	4.03928
	0 0 0-1 0 0 0 0 0 0 1	4.04507
	0 0 0-1 0 0-1 0 0 0 1	4.32872
	0 0 0-1 0 0 0 0 1 0 1	4.32872
	0 0 0-1 0 0 0 0 0 1 1	4.41143
	0 0 0-1 0-1 0 0 0 0 1	4.51183
	0 0 0-1 0 0 0 0-1 1 1	4.57066

	-1 0 0-1 0 0 0 0 0 0 1	4.69219
	1 0 0-1 0 0 0 0 0 1 1	4.75271
	0 0 0 0 0 0 0 0 0 1 1	4.79483
	0 0-1-1 0 0-1 0 0 0 1	4.8811
	0 0 0-1-1 0 0 0 0 0 1	4.94058
	1 0 0-1 0 0 0 0 0 0 1	4.97543
	0 0 0-1 0-1 0 0 0 1 1	5.00039
	0-1 0-1 0 0 0 0 1 0 1	5.34875
	0 0 0-1 0 0 1 0-1 1 1	5.5141
	0 0 0-1 0-1 0 0 1 0 1	5.67068
	0 0 0-1-1 0 0 0 1 0 1	5.72068
	0-1 0-1-1 0 0 0 0 1 0	6.10262
	-1-1 0 0 0 0 0 0 1 0 1	9.7965
40	0 0 0 0 0 0 0 0 0 0 1	4.01584
	0-1 0-1 0 0 0 0 0 1 1	4.03928
	0 0 0-1 0 0 0 0 0 0 1	4.04507
	0 0 0-1 0 0 0 0 1 0 1	4.32872
	0 0 0-1 0 0-1 0 0 0 1	4.32872
	0 0 0-1 0 0 0 0 0 1 1	4.41143
	0 0 0-1-1 0 0 0 0 0 1	4.94058
	0 1 0-1 0 0 0 0 0 0 1	5.05617
	0-1 0-1 0 0 0 0 1 0 1	5.34875
	-1-1 0-1 0 0 0 0 0 1 1	5.4476
	0 0 0-1 0 0 0 0 0-1 1	5.54017
	0 0-1-1 0-1 0 0 1 0 1	5.6584
	0 1 0-1 0 0 0-1 0 1 1	5.78822
	0-1-1-1 0-1 0 0 1 0 1	5.83009
	0-1 0-1 0-1 0 0 1 0 1	5.89544
	0 0 0-1 0 0 1 0 1 0 1	6.05587
	0 0 0-1 0-1 0 1 1 0 1	6.11905
	0 1-1-1 0-1-1 0 0 0 1	6.5599
	0 1-1-1 0-1 1 0 0 0 1	6.5599
	-1-1 0-1 0 0 0 0 1 0 1	6.68225
	0 1 0-1 0 0-1 0 0-1 1	7.30725

Table 6.9 shows the results of the reliability analysis of the complete bridge system obtained by the SGA search strategy. The SGA coding is the same as that described with the example for Slovenia bridge. As seen in Table 6.9, most of the randomly generated search directions of the first generation don't reach critical regions. Their β-value values are quite high, i.e., they don't have good fitnesses. After an evolution through 40 generations with SGA, the chromosomes of Table 6.9 show much smaller β-values. It is

also observed that there exist some similarities in the schemata in the chromosomes after evolution. These schemata represent strong characteristics of this bridge system that are identified in the evolution process. These schemata represent the special combinations of loads and material properties which affect bridge system safety. At the 40^{th} generation, chromosome (0 0 0 0 0 0 0 0 0 0 1) with safety index β = 4.016, which has been purposely included in the first generation to simulate the effect of the most important random variable of live load, becomes the most important. The next four most important chromosomes are: (0-1 0-1 0 0 0 0 0 0 1 1) with β = 4.039, (0 0 0-1 0 0 0 0 0 0 1) with β = 4.045, (0 0 0-1 0 0 0 0 1 0 1) with β = 4.329 and (0 0 0-1 0 0-1 0 0 0 1)with β = 4.329.

These dominant chromosomes have their corresponding physical meanings. For example, chromosome (0-1 0-1 0 0 0 0 0 0 1 1) indicates a reduction in the main girders' torsion coefficient (2^{nd} variable), a reduction in the main girders' ultimate moment capacity and softening of the M- φ curve (4^{th} variable), an increase in the surface dead load (10^{th} variable) and an increase in the applied live load (11^{th} variable); Chromosome (0 0 0-1 0 0 0 0 0 0 0 1) indicates a reduction in the main girders' ultimate moment capacity and softening of the M- φ curve (4^{th} variable) and an increase in the applied live load (11^{th} variable); Chromosome (0 0 0-1 0 0 0 0 1 0 1) indicates a reduction in the main girders' ultimate moment capacity and softening of the M- φ curve (4^{th} variable), an increase in the permanent dead load (9^{th} variable). and an increase in the applied live load (11^{th} variable); Chromosome (0 0 0-1 0 0-1 0 0 0 1) indicates a reduction in the main girders' ultimate moment capacity and softening of the M- φ curve (4^{th} variable), a reduction in

the transverse beams' maximum plastic rotation capacity (3rd variable) and an increase in the applied live load (11th variable).

Following the same procedure described above for the Slovenia girder and Slovenia bridge, the relative influence of the important random variables on the probability of failure of the continuos steel bridge and the relative influence of each pair of variables can be calculated as shown in Tables 6.10, and 6.11.

Table 6.10. Influence of dominant random variables on probability of failure of continuous steel bridge

Random variable	$\left\|\frac{\partial P_f}{\partial u_i}\right\|$	Weight
Live Load, L_{live}	0.000126	100%
M- φ Curve, M- φ	0.000079	63%
Girder's torsion coefficient, GJ	0.000057	45%
Surface dead load, L_{dead2}	0.000057	45%
Slab's Maximum allowable rotation, θ_{max}	0.000019	16%
Surface dead load, L_{dead1}	0.000019	16%

Table 6.11. Influence of dominant pairs on probability of failure of continuous steel bridge.

Random variable	$\left\lvert \frac{\partial P_f}{\partial x_{ij}} \right\rvert$	Weight
(L_{live}, M-ϕ)	0.000112	100%
(GJ, M- φ)	0.000081	72%
(GJ, L_{dead2})	0.000081	72%
(GJ, L_{live})	0.000081	72%
(M- φ, L_{dead2})	0.000081	72%
(L_{dead2}, L_{live})	0.000081	72%
(M- φ, L_{dead1})	0.000027	25%
(L_{dead1}, L_{live})	0.000027	25%
(M- φ, θ_{max})	0.000027	25%
(L_{live}, θ_{max})	0.000027	25%

Tables 6.10 and Table 6.11 show that the random variable L_{live}, girder's section rigidity GJ and M- φ and the random pairs (M- φ, L_{live}), (GJ, M- φ), (GJ, L_{dead2}), (GJ, L_{live}), (M- φ, L_{dead2}), (L_{dead2}, L_{live}) have dominant influence on the system reliability of the continuous steel bridge. Such information provides very useful output that would help engineers improve the reliability of structures in practical design applications by focusing their attention on these parameters.

Also from this example, it is observed that the random variables associated with the transverse member properties are not important in comparison with those of the main longitudinal members except for the random variable that controls the slab's maximum allowable rotation θ_{max}. The combination of θ_{max} of the transverse members (slab) along with the dominant random variable L_{live}, and the girder's M- φ produces a chromosome (0 0 0 −1 0 0 −1 0 0 0 1) with a safety index equal to 4.328. The corresponding pairs (M- φ, θ_{max}) and (L_{live}, θ_{max}) have 25% influence weight by comparison to the dominant pair (L_{live}, M- φ) with 100% weight.

In this example, a total of 352 directions are searched, which constitute only 0.2% of all the possible discretiezed directions in the 11 dimensional space (3^{11}-1 = 177146). This shows that SGA is a very efficient tool for the reliability analysis of large structural systems.

6.6 SUMMARY

In this chapter, the application of the shredding genetic algorithm (SGA) to the reliability analysis of bridge systems is demonstrated through three examples. These examples demonstrate that SGA is capable of efficiently determining the dominant failure modes with little risk of arriving to a local optimization point as compared to the most common gradient search strategies. The results obtained by SGA for these example bridges are

consistent with the experience of bridge engineers with such simple structures. The analysis can be further expanded in the future to account for the positioning of the loads on the bridge deck and for the safety assessement of more complex structural systems where the dominant failure paths are less easily identifiable.

In summary, from the examples detailed in this chapter, the following observations are made:

- SGA is a good and efficient tool for the structural reliability analysis of bridge systems.
- The live load and the M- φ curve of the main girders are the dominant random variables that control the risk to failure of typical multi-girder bridges.
- The main girder's section rigidity has significant effect only on the reliability of continuous bridges.
- Transverse beam properties (i.e. effect of slab) has some influence which can not be ignored for reliability analysis of typical multi-girder bridge systems.

CHAPTER 7

CONCLUSIONS

7.1 CONCLUSIONS

The goal of this dissertation was to develop efficient and accurate methods to obtain the reliability of bridge structural systems. Two tools were required to achieve the objectives. The first tool consisted of a new version of the program NONBAN that incorporated new models to better represent the nonlinear behavior of typical steel and concrete bridge members. In addition, the efficiency of the nonlinear program and its convergence were improved by developing a new solving algorithm that did not require the assembly of the global stiffness matrix at every load increment. The second tool was an improved genetic search algorithm to identify the dominant bridge failure modes. The main features of this study consisted of the following:

- Modeling the Nonlinear Behavior of Steel Bridges. This study reviewed the nonlinear properties of steel bridge members including the various factors that influence the performance of bridge systems such as plastic hinge lengths, mesh sizes, nonlinear moment versus curvature models for positive and negative bending... Empirically derived moment versus curvature relationships for steel sections were obtained from experimental results on typical steel girders. These models were then incorporated into the program NONBAN. The testing of the proposed models has shown excellent agreement between the predicted analysis

results with experimental results of full-scale and laboratory models of steel bridges.

- Modeling the Nonlinear Behavior of Prestressed Concrete Bridges. This task consisted of studying the nonlinear properties of prestressed concrete bridge members and analyzing the various factors that influence the performance of prestressed concrete bridge systems. A new Lp-transfer model was proposed to calculate the plastic hinge length for every beam element of a grillage discretization of bridge structures. The Lp-transfer model, which is based on the results from experiments and other empirical models, was incorporated into NONBAN. The accuracy of the models has been verified by comparing the results from NONBAN with those of laboratory and in-situ experiments of full scale and model scale prestressed concrete bridges.
- Improving the efficiency of the Program NONBAN. NONBAN was developed to perform the general nonlinear analysis of highway girder bridges by using traditional matrix structural analysis methods and solving the global stiffness equations using the classical LDL^T solver. A new solver that does not require the re-assembly of the global stiffness matrix at every load step was developed. The new solver, referred to as the pseudo-force method, was found to provide dramatic improvements in computational efficiency for structural re-design and reliability analysis and was shown to perform a nonlinear incremental analysis no harder than the inversion of the global stiffness matrix.
- Development of the Genetic Search Algorithm for identification of dominant failure modes. A modified genetic search algorithm referred to as the Shredding

Genetic Algorithm, SGA, was developed to perform the reliability analysis of structural systems. The SGA introduces a filtration operator to simulate modern breeding technology that interferes with the natural selection process and filters out the weakest and unhealthy offsprings using the principle of elitism. In comparison with classic reliability analysis techniques, SGA was not only able to identify the dominant structural failure modes, but also gave detailed information about which random variables are primary contributors to the formation of these failure modes.

- Examples and illustration on the use of the proposed models and techniques were provided throughout the Dissertation. The improvements in analysis efficiency and accuracy produced are necessary to encourage the use of reliability based simulation techniques in everyday engineering practice.

It is expected that the proposed techniques will eventually lead to better control of the safety of bridge structural systems and improvements in the reliability of structural designs.

7.2 FUTURE RESEARCH

This study developed an intelligent search strategy for the failure mode identification of nonlinear bridge systems by introducing a shredding genetic algorithm into the search process and improving the nonlinear structural analysis models. The applicability of the proposed techniques was tested on simple steel and prestressed concrete girder bridge

models. The results obtained confirmed the efficiency and accuracy of the proposed methods for application during the reliability analysis of large-scale structural systems and for bridge systems in particular. The long-term benefits of the proposed techniques will be in improving current bridge design and analysis methods to eventually design bridges with optimum levels of safety and reliability based on the 'true' behavior of the system while accounting for the uncertainties in determining the member properties and the loading conditions. More work is needed to extend the range of applicability of the techniques and to demonstrate their suitability for practical implementation in engineering practice. Specifically the following additional tasks could be performed in the future:

- Verify the validity of the proposed method through a theoretical review of the process and through additional numerical experimentation. The numerical experimentation will consist of comparing the results of the proposed method to other techniques such as the directional simulation and other advanced structural reliability and simulation methods.
- Extend the applicability of NONBAN to cover more general bridge configurations including curved bridges. Further improvements in NONBAN should account for the nonlinearity in torsion and the inclusion of possible shearing modes of failure. The inclusion of beam column elements into NONBAN would allow for the analysis of complete bridge systems that will account for the interaction between superstructures and substructures.
- To improve the efficiency of the SGA search and the accuracy of the prediction of the probability of failure, an adaptive search scheme should be

developed. Such a scheme may consist of combining SGA with the response surface method. Through a discrete search of possible directions, SGA gives the location of the failure point in the random variable space. Improved estimates of the safety index, β, and more precise identification of the failure point may be obtained through the application of the response surface method expanded around the points identified by SGA.

- Improve the SGA to also consider multiple loading conditions such as moving traffic load combinations. The model should eventually account for statistical data on rate of load arrival, headway information, and possible correlation between the applied loads. The object is to study all important failure modes that may vary widely based on load position and correlation.
- Develop a realistic probability-based model for bridge material property. The object is to investigate how material ductility, brittle or semi-brittle behavior as well as statistical correlation between member capacities and behavior may influence our estimates of the structural reliability of bridge systems.
- Apply the results of the proposed structural reliability analysis to improve the structural design process for bridges. The object is to provide design guidelines that will account for the system reliability of bridge systems and to develop reliability-based design optimization techniques.

BIBLIOGRAPHY

AASHTO, (1994). "AASHTO LRFD Bridge Design Specifications." American Association of State Highway and Transportation Officials.

AASHTO (1996), "Standard Specifications for Highway Bridges", 16th Edition, American Association of State Highway and Transportation Officials, Washington DC.

Abu Kassim, A.M., and Topping, B.H.V. (1987). "Static Reanalysis: A Review.". J. Struct. Engr., ASCE, 113(5), 1029-1045.

ACI, (1995), "Building Code Requirements for Reinforced Concrete", American Concrete Institute, Michigan.

AISC, (1994), "AISC Load and Resistance Factor Design Manual of Steel Construction", American Institute of Steel construction, Inc., 2nd Edition, Chicago, IL.

Arora, J.S. (1976). "Survey of Structural Reanalysis Techniques." J. Struct. Div., ASCE, 102(4), 782-802.

Argyris, J.H. (1956) "The Matrix Analysis of Structures with Cut-outs and Modifications," Communication to the IX International Congress of Theoretical and Applied Mechanics, University of Brussels, Brussels, Belgium, Sept. pp131-142.

Baker, A.L.L., (1956), "Ultimate Load Theory Applied to the Design of Reinforced and Prestressed Concrete Frames", Concrete Publications Ltd, London.

Bathe, K. J. (1996), "Finite Element Procedures", Prentice Hall.

Bathe, K. J., and Cimento, A. P. (1980), "Some Practical Procedures for the Solution of Nonlinear Finite Element Equations," Computer Methods in Applied Mechanics and Engineering, Vol. 22, pp 59-85.

Bazant, Z. P. and Byung, H., (1983), "Deformation of Cracked net-Reinforced Concrete Walls", Journal of Structural Engineering, ASCE, Vol. 109 No. 1, Jan., 93-108.

Bertsekas, D. P., (1982), "Constrained Optimization and Lagrange Multiplier Methods", Academic Press, New York.

Burdette E.G. and Goodpasture, D.W., (1971), "Full Scale Bridge Testing – An Evaluation of Bridge Design Criteria", University of Tennessee, December.

Corley, W.G., (1966), "Rotational Capacity of Reinforced Concrete Beams," Journal of Structural Division, ASCE, Vol. 92, ST5, October, 121-146.

Corotis, R.B., and Nafday, A. M., (1989), "Structural System Reliability Using Linear Programming and Simulation." J. Struct. Engr., ASCE, 115(10), 2435-2447.

Deng, L. and Ghosn, M. (2000), "Nonlinear Analysis of Composite Steel Girder Bridges", accepted by Engineering Journal of AISC.

Deng, L. and Ghosn, M. (2000), " Pseudoforce Method for Nonlinear Analysis and Reanalysis of Structural Systems", submitted to Journal of Structural Engineering, ASCE.

Deng, L., Ghosn, M., Znidaric, A., and Casas, J, (2000), "Nonlinear Flexural Behavior of Prestressed Concrete Girder Bridges", Submitted to Journal of Bridge Engineering, ASCE.

Deng, L., Ghosn, M., and Shao, S. (2000), "Shredding Genetic Algorithm for Reliability Analysis of Structural Systems", submitted to Journal of Structural Safety.

Dennis, J. E., JR., (1976), "A brief Survey of Convergence Results for Quasi-Newton Methods," SIAM-AMS Proceedings, Vol. 9, 185-200.

Ditlevsen, O. (1979), "Narrow Reliability Bounds for Structural Systems", Journal of Structural Mechanics, 7, 435-451.

Ditlevsen, O. (1981), "Uncertainty Modeling", McGraw Hill.

Ditlevsen, O., and Bjerager, P., (1989), "Plastic Reliability Analysis by Directional Simulation", J. Engr. Mech. ASCE. 115(6), 1347-1362.

Ellingwood, B., Galambos, T.V., MacGregor, J.G. and Cornell, C.A. (1980), "Development of Probability Based Load Criterion for American National Standard A58", National Bureau of Standards, NBS Special Publication 577, Washington, D.C.

Frangopol, D.M., (1999), "Bridge Safety and Reliability", Structural Engineering Institute of ASCE.

Ghosn, M. (1998). "Design of Highway Bridges for Extreme Events", National Cooperative Highway Research Program 12-48. In progress.

Ghosn, M. and Casas, J.R., (1996), "Evaluation of Existing Highway Bridge Systems", Monograph CIMNE No. 30, International Center for Numerical Methods in Engineering, Barcelona, Spain.

Ghosn, M. Casas, J. R. and Xu J. M. (1996). "Development of an Efficient Program for the Nonlinear Analysis of Bridge", Journal of Computers and Structures, Volume 61, No. 3, 459-470.

Ghosn, M., Deng, L., Xu, J.M., Liu, Y., and Moses, F., (1997) "Documentation of Program NONBAN", National Cooperative Highway Research Program 12-36, Transportation research board, National research council, U.S.A.

Ghosn, M. and Moses, F. (1997). "Redundancy in Highway Bridge Superstructures", Final report, National Cooperative Highway Research Program 12-36, Transportation research board, National research council, U.S.A.

Ghosn, M. and Moses, F., (1998), "Redundancy in Highway Bridge Superstructures", NCHRP Report 406, National Cooperative Highway Research Program, Washington DC.

Gierlinski, J.T., Sears, R.J., and Shetty, N.K. (1993), "Integrity Assessment of Fixed Offshore Structures: A Case Study Using RASOS Software." Proce., 12th Int. Conf., Vol. II, ASME, New York, 399-408.

Goldburg, D.E., (1989), "Genetic Algorithms in Search, Optimization and Machine Learning", Addison-Wesley Publishing Company, Inc., Massachusetts.

Goldburg, D. E. and Samtani, M. P. (1986), "Engineering Optimization via Genetic Algorithm.", Proc. Of 9th Conf. On Electronic Computation, ASCE, New York, NY, 471-482.

Golub, G.H., and Van Loan, C. F., (1996), "Matrix Computation, Third Edition", John Hopkins University Press, Baltimore, MD.

Gossbell K.B. and Stevens L.K., (1968), "Test Loading of a Full Scale Bridge", Australia Research Board, Proceedings, Vol. 4, Part 2, Page 2018-2041.

Grigoriu, M., Turkstra, C. (1979), "Safety of Structural Systems with Correlated Resistance." Applied Math. Modelling, Vol. 3, 130-136.

Hall, J.C., and Kostem, C.N., (1981). "User's Manual for Program BOVAS", Fritz Engineering Laboratory Report No. 435.3A, Lehigh University., Bethlehem, PA.

Hambly, E.C., (1991), "Bridge Deck Behavior", E & FN Spon, London.

Hawkin, N.M. and Mitchell, D., (1984), "Seismic Response of Composite Shear Connections", Journal of Structural Engineering, ASCE, Vol. 110 No. 9, Sep.

Heller, R. A. and Thangjitham, S. (1993). "A Survey of Probabilistic Service Life Prediction Methods for Structures", IUTAM Symposium San Antonio/USA 1993, Springer-Verlag, 237-266.

Hirai, I., Wang, B.P., and Pilkey, W.D., (1984). "An Efficient Zooming Method for Finite Element Analysis," International Journal for Numerical Methods in Engineering, Vol. 20, pp1671-1683.

Holnicki-Szulc, J. (1989). "Optimal Structural Remodeling: Simulation by Virtual Distortion." Communication in Appl. Numer. Methods, 5, 289-298.

Holnicki-Szulc, J. (1991). Virtual Distortion Method. Springer, Berlin.

Huria, V., Lee, K.L, Aktan, A.E. (1993), "Nonlinear Finite Element Analysis of RC Slab Bridge", Journal of Structural Engineering, ASCE, Vol. 119, No. 1, Jan.

Idriss, R.L., White, K.R., (1991), "Secondary Load Paths in Bridge Systems", Transportation Research Records No. 1290., TBR Bridge Engineering Conference March 1991.

Karamchandani, A. (1987), "Structural System Reliability Analysis Methods." Report No. 83, Department of Civil Engineering, Stanford University.

Kathol, S., Azizinamini, A. and Luedke, J., (1995), "Strength Capacity of Steel Girder Bridges", NDOR Research Project No. RES1 90099, P469, Nebraska Department of Roads, February.

Kennedy, D.J.L., (1982), "Study of Performance Factors for Section 10 Ontario Highway Bridge Design Code", Morrison, Hershfield, Burgess & Huggins, Ltd., Report No. 2805331, Toronto, Canada.

Keuser, M. and Mehlborn, G., (1987), "Finite Element Models for Bond Problem", Journal of Structural Engineering, ASCE, Vol. 113 No.10, Oct.

Kirsh, U., and Moses, F, (1995). "An Improved Reanalysis Method for Grillage-Type Structures", Cambridge, England, August.

Kirsh, U. and Rubinstein, M.F. (1970). "Modification of Structural Analysis by the Solution of a Reduced Set of Equations", UCLA paper Eng-0570, University of California, Los Angels, Calif.

Kirsh, U. and Rubinstein, M.F. (1972). "Reanalysis of Limited Structural Design Modifications," Journal of the Engineering Mechanics Division, ASCE, Vol. 98, No. 1. Feb. pp61-70.

Kohnke, P., (1997), "Ansys User's Manual: Theory", Ansys, Inc.

Komatsu, S., Moriwaki, Y., Fujino, M., and Takimoto, T., (1984), "Ultimate Strength of Girders in Combined Load," Journal of Structural Engineering, Vol. 110 No. 4. April.

Kullman, R.B., Hosain, M.U., (1985), "Shear Capacity of Stub-Girders: Full Scale Tests," Journal of Structural Engineering, ASCE, Vol. 111 No. 1, Jan. 56-75.

Lemonick, M.D. and Thompson, D, (1999), "Racing to Map Our DNA", Time Magazine, January 11, 44-50.

Livesley, R.K., (1970), "Matrix Methods of Structural Analysis", Pergamon, Oxford.

MaGuire, W., and Gallagher, R.H. (1979). Matrix Structural Analysis, Wiley, New York.

Makode, P.V., Corotis, R.B., and Ramirez, M.R. (1999) "Nonlinear Analysis of Frame Structures by Pseudodistortions", Journal of Structural Engineering, ASCE, Nov., Vol. 125 No. 11.

Matthies, H., and Strang, G., (1979), "The Solution of Nonlinear Finite Element Equations," International Journal for Numerical Methods in Engineering, vol. 14. Pp.1613-1626.

Mattock, A.H., (1965), "Rotational Capacity of Hinging Regions in Reinforced Concrete Beams", Flexural Mechanics of Reinforced Concrete, Proceedings of the ASCE-ACI International Symposium, Miami, FL.

Mattock, A.H. (1967), "Discussion of 'Rotational Capacity of Reinforced Concrete Beams' by W.G. Corley, Journal of Structural Division, ASCE, Vol. 93, ST2, April, 519-522.

Mohraz, B. and Wright, R.N. (1973), "Solving Topologically Modified Structures," Computers and Structures, Vol. 3, pp341-353.

Moses, F. (1982), "System Reliability Developments in Structural Engineering," Structural Safety, 1(1), 3-13.

Moses, F., (1990), "New Directions and Research Needs in System Reliability Research," Journal of Structural Safety, NO, 7.

Moses, F. and Ghosn, M., (1985), "A Comprehensive Study of Bridge Loads and Reliability", Report FHWA/ODOT/85-005.

Moses, F., Verma D. (1989), "Calibration of a Bridge Strength Evaluation Code", Journal of Structural Engineering, ASCE, 115, 6.

Murotsu, Y., Okada, H. and Shao, S. (1993). "Reliability-based Design of Transmission Line Structures Under Extreme Wind Loads", The 6th International Conference on Structural Safety and Reliability, Innsbruck, Austria, 9-13 August 1993. 1675-1681.

Nagarajarao, N.R., Estuar, F.R., and Tall, L., (1964), "Residual Stress in Welding Shapes," The Welding Journal, Research Supplement, Vol. 43 July, 255-306.

Nowak, A. (1993), "Calibration Report for NCHRP project 12-33", Department of Civil Engineering, University of Michigan, Ann Arbor, MI, December.

Nowak, A. (1995), "Calibration of LRFD Bridge Code", ASCE journal of Structural Engineering, Vol. 121, No.8, pp. 1245-1251.

Pail, G.H., and Buckle, I. G. April, (1970), "Computer Program for Bridge for Deck Analysis", Report No. UC SESM 70-26, University of California, Berkeley.

Park, R. and Pauley, T., (1975), "Reinforced Concrete Structures", Wiley and Sons, New York.

Razaqpur, A.G. and Nofal, M., (1988), "Transverse Load Distribution at Ultimate Limit States in Single Span Slab-on-Girder Bridges with Compact Steel Girders", Ontario Ministry of Transportation, MISC-88-01, September.

Ricles, J. M., and Popov, E. P. (1994). "Inelastic Link Element for EBF Seismic Analysis." J. Struct. Engrg., ASCE, 120(2), 441-443.

Ricles, J.M., Yang, Y.S., and Priestley, M.J., (1998), "Modeling Nonductile R/C Columns for Seismic Analysis of Bridge", Journal of Structural Engineering, April.

Robinson, D.G., and Toussaint, G., (1993), "Reliability of Unidirectional Composites Using Genetic Algorithms", Probabilistic Structural Mechanics: Advances in Structural Reliability, IUTAM Symposium San Antonio/USA, Springer-Verlag, 455-465.

Sack, R.L., Carpenter, W.C., and Hatch, G.L. (1967), "Modification of Elements in the Displacement Method," AIAA journal, Vol. 5, No.9, Sep, pp 1708-1710.

Sawyer, H.A., (1964), "Design of Concrete Frames for Two Failure States," Proceedings of the International Symposium on the Flexural mechanics of Reinforced Concrete, ASCE-ACI, Miami, November, 405-431.

Schilling, C. G. (1989), "A Unified Autostress Method", Project 51 (Development of Design Specifications for Continuous Composite Plate-Girder Bridges), American Iron and Steel Instiure.

Schilling, C.G. and Morcos S.S., "Moment-Rotation Tests of Steel Girders with Ultramacompact Flanges", Project 188 Autostress Design of Highway Bridges, American Iron and Steel Institute, 06, 1988.

Sherman, J., and Morrison, W. J. (1949). "Adjustment of an Inverse Matrix Corresponding to Changes in the Elements of a Given Column or a Given Row of the Original Matrix." Annals of Mathematical Statistics, Vol. 20, pp.621.

Sherman, J., and Morrison, W. J. (1950). "Adjustment of an Inverse Matrix Corresponding to a Change in One Element of a Given Matrix," Annals of Mathematical Statistics, Vol. 21, pp124-126.

Skogman, B.C., Tadros, M. and Grasmick, R., (1988), "Ductility of Reinforced and Prestressed Concrete Flexural Members", PCI Journal, November-December.

Shao, S., Murotsu, Y., (1996), "Approach to Failure Mode Analysis of Large Structures," Procs. Of ASCE 7th Specialty Conf. On Probabilistic Mechanics & Structural Reliability, 1996, pp 704-707.

Shao, S., Murotsu, Y., (1999), "Approach to Failure Mode Analysis of Large Structures," Probabilistic Engineering Mechanics, Vol. 14, Nos.1-2, 169-177.

Shetty, N.K., (1994), "Selective Enumeration Method for Identification of Dominant Failure Paths of Large Structures", Proc. OSME, Volume II, Safety and Reliability, 381-391.

Tabsh, S.W. and Nowak, A.S., (1991) "Reliability of Highway Girder Bridges", ASCE Journal of Structural Engineering, Vol. 117, No. 8, pp. 2373-2388.

Thoft-Christensen, P., and Baker, M., J. (1982). "Structural Reliability Theory and Its Application." Spring-Verlag Berlin Heidelberg New York.

Thoft-Christensen, P., Murotsu, Y. (1986). "Application of Structural System Reliability Theory." Spring-Verlag Berlin Heidelberg New York.

Thompson, D., (1999), "Gene Maverick", Time Magazine, January 11, 54-55.

US Dept. of Energy, (1997), "Human Genome Program Report, www.ornl.gov/hgmis/publicat/97pr/index.html", Progress Report from 1994-1997.

Vasseghi, A., and Frank, K.H., (1987), "Static Shear and Bending Strength of Composite Plate Girders," Final Reprot AISI Laboratory Report N. 87-4, University of Texas, Austin, TX, June.

Wang, W., Crotis, R. and Ramirez, M.R., (1995) "Dominant Failure Modes for Structures with Stochastic Load Processes," Journal of Engineering Mechanics, ASCE, Vol. 121, No. 11, November, 1995, pp. 1252-1260

Wang, B.P. and Pilkey, W.D. (1980), "Efficient Reanalysis of Locally Modified Structures,", Department of Mechanical and Aerospace Engineering, Virginia University, Charlottesville, Va. 1980.

Wang, B.P. and Pilkey, W.D. (1981), "Parameterization in Finite Element Analysis," Proceedings of International Symposium on Optimum Structural Design, Tuscon, Ariz., pp7.1-7.7.

Wang, B.P. Pilkey, W.D. and Palazzola, A.R. (1983). "Reanalysis, Modal Synthesis and Dynamic Design", State-of-the-art Surveys on Finite Element Technology, A.K. Noor, and W.D. Pilkey, Eds., American Society of Mechanical Engineers, New York, New York, pp225-295.

Xiao, Q., and Mahadevan, S., (1994), "Fast Failure Mode Identification for Ductile Structural System Reliability". Structural Safety, 12(4), 207-226.

Zienkiewicz, O.C. & Taylor R.L., (1994), "The Finite Element Method", Fourth Edition, McGraw-Hall Book Company, London

Zokaie T., Osterkamp, T.A., and Imbsen, R.A., (1991), "Distribution of Wheel Loads on Highway Bridges", Final Report, NCHRP project 12-2/1, March.

Znidaric A., Moses F. (1997), "Structural Safety of Existing Road Bridges", 7th International Conference on Structural Safety and Reliability ICOSSAR '97, 1843-1850, Kyoto.

Znidaric A., Moses F. (1998), "Resistance of Deteriorated Post-Tensioned Concrete Beams: An Ongoing Research", 8th IFIP WG 7.5 Working Conference on Reliability and Optimization of Structural Systems, 339-346, Krakow.